Master's thesis

NTNU
Norwegian University of Science and Technology
Faculty of Information Technology and Electrical Engineering
Department of Engineering Cybernetics

Anne Willkommen Eiken

Position Alignment and Geographical Location Determination of Railway Track Condition Monitoring Data

Master's thesis in Cybernetics and Robotics
Supervisor: Adil Rasheed
Co-supervisor: Albert Lau
June 2022

NTNU
Norwegian University of
Science and Technology

Anne Willkommen Eiken

Position Alignment and Geographical Location Determination of Railway Track Condition Monitoring Data

Master's thesis in Cybernetics and Robotics
Supervisor: Adil Rasheed
Co-supervisor: Albert Lau
June 2022

Norwegian University of Science and Technology
Faculty of Information Technology and Electrical Engineering
Department of Engineering Cybernetics

NTNU

Kunnskap for en bedre verden

Abstract

Using readily available track geometry inspection data, condition monitoring may contribute to reliable and cost-efficient maintenance strategies. However, recorded track geometry data suffers from substantial uncertainty in the assigned positional value. This entails that time series recorded along the same tracks during different measurement runs, cannot easily be compared, making fault predictions challenging. Further, it is essential to determine the absolute position of the recorded measurements to locate the corresponding track part in the field to conduct physical inspection and/or maintenance activity. Although several studies have been completed to minimize this relative positional error between time series, no study has addressed data recorded in complex terrain. Several studies have utilized GPS coordinates and continuous track records to determine absolute position, but no study has extensively compared different position determination methods and estimated uncertainties through conducting field measurements. Hence, this paper identifies the lack of research on these topics as an issue and explores approaches for preprocessing, aligning, and determining the absolute position of measurement data recorded in complex Nordic terrain. The result is a more robust relative alignment and absolute position determination. Relative alignment methods, including Cross-Correlation Function (CFF), Recursive Alignment by Fast Fourier Transform (RAFFT), Dynamic Time Warping (DTW), Correlation Optimized Warping (COW), and a combined method consisting of both RAFFT and COW are tested on preprocessed and further pre-aligned input data. Results presented in this study show that the pre-alignment utilizing CCF can reduce the initial shift between the measurement series. Alignments produced with pre-aligned measurement series achieved a higher warping effect independent of the alignment method utilized, compared with only preprocessed input data. Further, the study shows that COW is the most suited algorithm to align the utilized data set. This study is able to determine the absolute position of the recorded measurement series with an expected upper limit for inaccuracy equal to 1.43 meters. With an additional verification scheme proposed, utilizing high voltage mast records, the absolute position can be determined where GPS signal is missing, e.g., in tunnels. This verification scheme also allows for positions to be sporadically verified, reducing the risk of unexpected errors. Combining these methods, this study proposes a pipeline that enables the utilization of track geometry inspection data in predictive maintenance in complex terrain.

Sammendrag

Gjennom bruk av tilgjengelige sporgeometriske inspeksjonsdata kan tilstandsovervåking bidra til pålitelige og kostnadseffektive vedlikeholdsstrategier. Imidlertid er det knyttet stor usikkerhet til posisjonsnøyaktighet til disse sporgeometridataene. Dette innebærer at tidsserier registrert langs de samme sporene under forskjellige målekjøringer ikke uten videre kan sammenlignes, noe som gjør feilprediksjon utfordrende. Videre er det viktig å kunne fastslå den absolutte posisjonen til de registrerte målepunktene for å kunne lokalisere den tilsvarende spordelen i virkeligheten for deretter å kunne utføre fysisk inspeksjon og/eller vedlikeholdsaktivitet. Selv om flere studier har vurdert metoder for å minimere den relative posisjonsfeilen mellom tidsserier, har ingen studie adressert data registrert i komplekst terreng. Flere studier har brukt GPS-koordinater og kontinuerlige sporregistere for bestemmelse av absolutt posisjon, men ingen studie har sammenlignet forskjellige posisjonsbestemmelsesmetoder og estimert usikkerheten ved å utføre GPS feltmålinger langs jernbanespor. Denne oppgaven identifiserer mangelen på forskning på disse temaene som et problem og utforsker tilnærminger for forbehandling, relativ justering og bestemmelse av den absolutte posisjonen til måledata registrert i komplekst nordisk terreng. Resultatet er en mer robust, relativ justeringsmetode og absolutt posisjonsbestemmelse. Relative justeringsmetoder, inkludert Cross-Correlation Function (CFF), Rekursiv Alignment by Fast Fourier Transform (RAFFT), Dynamic Time Warping (DTW), Correlation Optimized Warping (COW), og en kombinert metode bestående av både RAFFT og COW testes på forhåndsbehandlede og ytterligere forhåndsjusterte data. Resultatene som presenteres i denne oppgaven, viser at forhåndsjustering ved bruk av CCF kan redusere forskyvning mellom tidsseriene. Justeringer utført på forhåndsjusterte måleserier oppnådde et bedre resultat, uavhengig av justeringsmetoden som ble brukt, sammenlignet med justeringer på kun forhåndsbehandlede data. Videre viser arbeidet at COW er den mest egnede algoritmen for å justere det brukte datasettet. Denne oppgaven er i stand til å bestemme den absolutte posisjonen til de registrerte måleseriene med en forventet øvre grense for unøyaktighet lik 1,43 meter. Med det foreslåtte verifikasjonsskjemaet som benytter seg av høyspentmastregister, kan den absolutte posisjonen bestemmes også der hvor GPS-signal ikke er tilgjengelig, f.eks. i tunneler. Denne verifiseringsmetoden gjør det også mulig å verifisere posisjoner sporadisk, noe som reduserer risikoen for uventede feil. Ved å kombinere disse metodene foreslår denne oppgaven en prosess som muliggjør bruk av sporgeometriinspeksjonsdata i prediktivt vedlikehold i komplekst terreng.

Preface

This thesis concludes my Master of Science degree in Cybernetics and Robotics at the Norwegian University of Science and Technology (NTNU). Working on this thesis has been exciting, challenging and rewarding, and I have especially appreciated the possibility of working with a real industry problem. I am especially contempt with my thesis topic as I believe in the saying *"the world's most valuable resource is no longer oil, but data"*. I hope that the work presented through this thesis can contribute to the premise for predictive modeling deployment at Bane NOR and other enterprises, enabling the transition into predictive maintenance.

During my thesis work, I have been supervised by Professor Adil Rasheed (Department of Engineering Cybernetics, NTNU) and Associate Professor Albert Lau (Department of Civil and Environmental Engineering, NTNU), and I would like to thank them for their contributions to my thesis. I am very grateful for Adil's work and dedication to the supplementary article, for helping me shaping the overall direction of this thesis, and for providing feedback on my writing. I am also highly appreciative of the domain knowledge provided by Albert, leading to key discussions on railway-specific issues faced during working on this thesis. Further, I want to praise Albert for setting aside a day to guide me during my field experiments, facilitate by prearranging the necessary equipment, and work out the formalities of the field excursion with the department.

I would like to thank Bane NOR for providing all the data utilized in this project and their willingness to contribute with their extensive expertise and knowledge. Especially I would like to thank Anna Gjerstad, Yme Asgeir Kvistedal, Frank Woldsund, and Arturo Opsetmoen Amador for their help and guidance.

The work conducted in this thesis is the continuation of a specialization project finished the fall of 2021. In the parts where this thesis builds directly on work done in the specialization project, subsections are copied directly from the previous work. This applies to major parts of Section 2.2.1, 2.3, 3.1 and the specific code implementation of each algorithm in Section 4.1.3. Where applicable, the connection to the specialization project is cited. Further, in parallel to this thesis, my supervisors and I have shaped a supplementary article mainly based on the findings from the specialization project. During the process of submitting this article to IEEE Access, valuable feedback from peer-reviewers was received. Based on the received feedback, improvements have been made that form parts of this thesis, stated explicitly where applicable.

All code used to produce the results in this study, where not explicitly stated otherwise, was written by the author in Python 3.8.

Trondheim, June 2022
Anne Willkommen Eiken

Contents

List of Figures

List of Tables

List of Algorithms

Nomenclature

Abbreviations

CCF	Cross-Correlation Function
COW	Correlation Optimized Warping
DD	Decimal Degrees
DDM	Degrees-Decimal-Minutes
DMS	Degrees-Minutes-Seconds
DTW	Dynamic Time Warping
ECEF	Earth-Centered Earth-Fixed
FFT	Fast Fourier Transform
GNSS	Global Navigation Satellite Systems
GPS	Global Positioning Systems
MSE	Mean Square Error
RAFFT	Recursive Alignment by Fast Fourier Transform
RPE	Relative Position Error
SVD	Singular Value Decomposition

1. Introduction

With greater focus than ever on zero emissions and lower carbon footprints, more travelers look for environment-friendly means of transportation. Today's railway is characterized by growing maintenance backlogs and struggles to meet expectations regarding punctuality. With strict performance requirements, it is apparent that more effective maintenance strategies are demanded. The current work aims to enable track data recorded in complex terrain to be used as input to data-driven track defect detection models. Made possible, such detection models can form the basis for effective maintenance strategies.

1.1. Background and Motivation

Across Europe, nine billion passengers and 1.6 billion tons of freight travel yearly on the existing railway network [4]. This railway network consists of more than 201000 kilometers of track line, with spending for maintaining and renewing infrastructure making up 53% of the total expenditures for the responsible enterprises [5]. Despite these high spendings, operators are struggling to sufficiently maintain all assets, resulting in frequent delays and cancellations [6].

In Norway, the state-owned enterprise Bane NOR is responsible for all the railway infrastructure. This infrastructure has over several years suffered from high wear and tear, resulting in an estimated maintenance backlog summing up to 2.3 billion USD [7]. The Norwegian National Budget does not include a sufficient amount for yearly maintenance [8]. Hence, this backlog will grow if maintenance activities cannot be optimized at a reduced cost. Today Bane NOR executes preventive maintenance, which is mainly based upon time intervals, in combination with condition monitoring for some types of assets. The preventive maintenance does not consider the actual condition of the asset, often resulting in the execution of unnecessary maintenance and thereby generating avoidable costs [9, 10].

Bane NOR, as other operators, periodically collect a large amount of data to monitor the condition of the railway tracks [1]. This data includes measurement recordings of the track geometry, i.e., longitudinal level, gauge, cross-level, and twist. Traditionally, and in Bane NOR today, the data is utilized in computing statistical indices over a certain length of track (often 200 meters) to represent the track state [11]. However, to detect location-specific single defects, predictive modeling techniques are prominent. By harnessing historical data in machine learning models, not only the location-specific state of the railway assets can be monitored, but future defects can also be predicted. Several approaches for predicting geometry defects have been presented in recent years [12, 13, 14]. However, a prerequisite for applying such methods is achieving alignment between subsequent track measurements. The recorded data by Bane NOR suffers from substantial uncertainty in the assigned positional value due to frequently induced errors

in the utilized position determination scheme. Further, to conduct maintenance activities, the absolute position of the track measurements needs to be determined.

The author in [15] utilizes the Cross-Correlation Function (CCF) to determine the shift between subsequently measured track geometry and a selected reference measurement series for constant track segments. The geometric data used to achieve alignment is either one or a combination of curvature, cross-level, twist, and sporadic location information. In [13] the measurement series are instead divided into segments with varying lengths based on track attributes, as an alternative to the fixed length of typically one kilometer. The segments are then aligned using CCF on three different measurement channels [16]. The first channel roughly aligns the measurement series, and then the other channels adjust this initial alignment. The method decreased positional errors from deviations up to 30 meters down to variations below 3 meters.

Applying CCF yields one linear shift to be applied to the whole segment. However, the authors in [17] consider shifts to be non-linearly varying and propose therefore to employ Dynamic Time Warping (DTW) as an alignment method. By comparing the average and standard deviation of absolute variation sums for data processed by DTW and CCF, the paper concludes that it achieves better alignments by employing DTW. [18] effectively combines CCF and DTW by applying either CCF or DTW, based on the presence of stretched data to align the track inspection data. Big-data fusion and incremental learning algorithms are utilized by [19] to synchronize track geometry inspection data. This is done by utilizing all the sensor channels in the measurement data. The study decreases the Relative Position Error (RPE) to be within 0.15 meters at a 99% confidence level, despite measurements being sampled every 0.25 meters.

However, applying DTW, Big-data fusion, and incremental learning algorithms alternates the shape of the measurement series, an undesirable trait when utilizing the aligned data in defect prediction. Therefore, [1] evaluates the efficiency of five alignment methods, including CCF and DTW, but also Recursive Alignment by Fast Fourier Transform (RAFFT), Correlation Optimized Warping (COW), and a combined method. The efficiency is evaluated based on the alignment's preciseness and ability to maintain the original shape of the time series, utilizing simplicity value and peak factor combined as a metric. The paper concludes that the combination of RAFFT and COW achieves the most accurate results, with positional errors decreasing from up to 15 meters to below 0.25 meters on 90% of the track. Although [1] minimizes positional errors while conserving the shape of the measurement series, no research has yet addressed similar alignment analysis for data recorded in complex terrain, as present in Norway. Complex terrain consists of tight curves, frequent low-speed limits, and tunnels, resulting in severe positional shifts. Investigation into more robust alignment methods and preprocessing techniques that can tackle the challenges of complex terrain would benefit Norway and simultaneously be applicable on all other railways.

Absolute position information, for a recorded measurement, is according to [17] most often determined utilizing Global Positioning Systems (GPS). The position accuracy relies then on the accuracy of the GPS sensor, system update and calibration frequency. The authors in [18] find that comparing subsequent measurement series directly, where the position is adjusted based on GPS data, does not yield sufficient accuracy for degradation analyses. The GPS utilized in their study suffered from a lag of up to 2 meters. In

complex terrain, GPS positioning is affected by multiple tunnels and less coverage due to deep valleys blocking signal. In [15] the use of GPS to determine geographic position was considered to not be reasonably accurate for exact pinpointing recorded measurements. Hence, the authors propose to obtain absolute geographic position through intelligently comparing measurements with track geography data available in records. The geography data, including values for both curvature and cross-level, is reconstructed to match in format and track length to the measured track data. The proposed reconstruction does not include interpolation, or other preprocessing steps, necessary to pair vehicle measured data and records storing object information. Further, to the extent of the author's knowledge, no research has been conducted to compare various methods to detect best practice for determining absolute position in the railway domain.

1.2. Contribution, Research Objectives and Research Questions

1.2.1. Contribution

The present work's main contribution is a processing pipeline that takes recorded measurement data as input and produces aligned measurements series with corresponding absolute positions as output. The proposed pipeline consists of three parts: preprocessing, relative alignment, and absolute positioning. This study evaluates a broad selection of methods for all consecutive parts, thereby making it possible to conclude on best practice based of the Bane NOR provided data set.

Although preprocessing has been covered in works by others, as well as in the underlying specialization project, [13, 15, 20, 21], these are to the extent of the author's knowledge only related to track geometry data and do not include track geometry data gathered in complex terrain. The inventor of [15] aligns track measurements and records to obtain absolute position by utilizing curvature and cross-level, where the records are reformatted to match in format and track length. However, records with object-related data demand more complex processing, including interpolation or other construction methods. This study tightens this gap by proposing and evaluating a broad set of preprocessing steps applicable to superstructure and high voltage mast records. Further, the set of relative alignment methods evaluated in this study is adapted from [1]. However, the work presented here can be viewed as a generalization to achieve higher robustness. The presented evaluation builds on the work conducted in the underlying specialization project [21], where improvements in method combination, selection of reference series, and measurement channels are made. Although several studies determine absolute positioning utilizing GPS [17], to the extent of the author's knowledge, no study has verified the accuracy of collecting GPS coordinates along railway tracks by comparing obtained positions with field measurements. This study goes even further in covering the knowledge gap in absolute positioning by evaluating absolute position determination utilizing measured and recorded stagger.

1.2.2. Objectives

To guide this study, a set of research objectives are formulated. In addition, research questions leading to the research objective are presented.

Primary Objective: Obtain a robust approach for determining relative alignment and absolute position of Bane NOR recorded track geometry data.

Secondary Objectives:

- Find and evaluate suitable relative alignment methods.
- Find and evaluate suitable methods for determining absolute position.
- Explore preprocessing steps needed to meet the primary objective.

1.2.3. Research Questions

To the extent of the authors' knowledge, no extensive research has been conducted into alignment and absolute position determination of track geometry data and track records provided by Bane NOR. To this end, the following research questions govern the research produced by this study:

- Are there aspects in the Bane NOR data sets that need to be corrected through preprocessing?
- Can relative alignment methods used by other studies be utilized on data gathered in complex terrain?
- Can absolute position be determined for track geometry data and what uncertainty can be expected?

1.3. Structure of the Thesis

This thesis consists of six chapters, the first of which is the current introduction, Chapter 1. Here, the motivation and research questions governing this study are presented, together with relevant studies performed by others. Based on the latter, the knowledge gap is identified and the most important contributions by this studied outlined. In Chapter 2, theory related to the railway track, relative alignment and absolute positioning are presented. In addition, evaluation metrics and utilized data engineering principles are included. Chapter 3 presents all available data sets and evaluates preprocessing steps applicable, resulting in a proposed preprocessing setup. Section 3.1 covers the track geometry data set, while Section 3.2 deals with both superstructure and high voltage mast records. The proposed methods to achieve relative alignment and absolute positioning are presented in Chapter 4. In Section 4.1 reference data set and measurement channel for alignment are selected, followed by a proposed implementation and layout for evaluating the proposed alignment methods. Thereafter, in Section 4.2, methods for determining absolute position utilizing GPS position data and track object records are proposed. Results obtained by following the proposed methods are presented in Chapter 5, in which the aspects of the obtained results are discussed and the applied methods evaluated. Section 5.1 addresses relative position alignment, while the results obtained for absolute positioning are presented in Section 5.2. Finally, in Chapter 6, the work is concluded. Here, the proposed pipeline is presented while in Section 6.1, the most important directions for further research are suggested.

2. Theory

2.1. Measurement diagnostic vehicle

Enterprises utilize diagnostic vehicles to gather data regarding the railway track infrastructure [1]. Bane NOR's measurement vehicle, Roger 1000, is developed with MERMEC S.p.A of Italy [22]. Self-propelled, Roger 1000 has a top speed of 160 km/h, and while hauled, it can reach speeds up to 200 km/h. The vehicle is equipped with automatic train protection[1], anti-skid brakes, cruise control, and full GPS location equipment. The placement of the GPS sensors on the Roger 1000 train vehicle is detailed in Figure 2.1. The Pantograph labeled in this figure is covered in Section 2.2.2. With its onboard equipment, Roger 1000 can measure:

- Loaded track geometry
- Overhead contact line
- Rail profile
- Integrated track
- Integrated overhead

All parameters are sampled by Roger 1000 each half meter and are measured based on contact-less measurement methods.

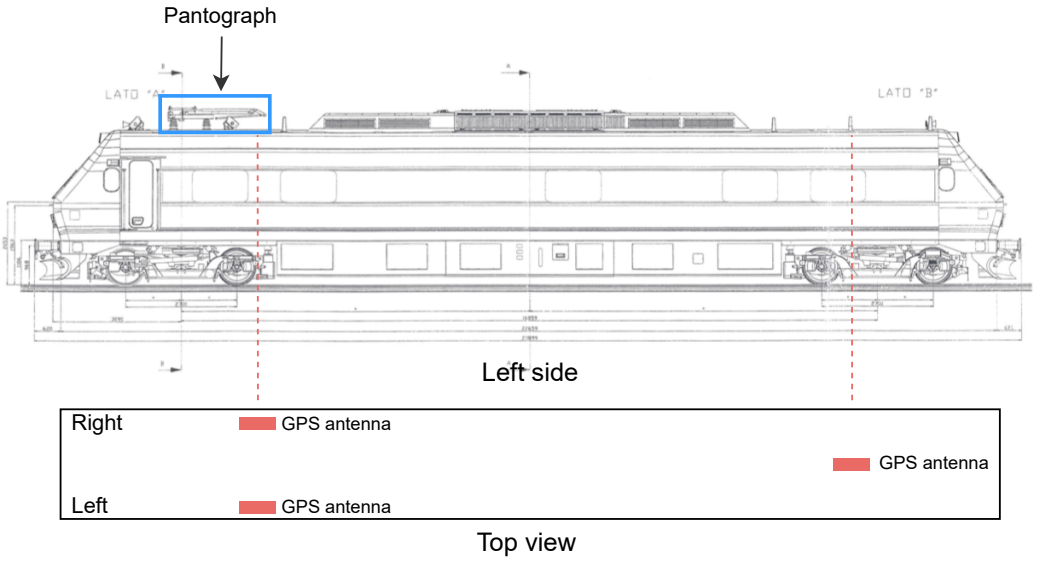

Figure 2.1.: Roger 1000 layout, including placement of GPS sensor and Pantograph.

[1]System that continually checks if the speed of a train agrees with the speed allowed by the signaling system.

2.2. Railway track outline

2.2.1. Track geometry - displacement

Track geometry is the three-dimensional layout of the railway tracks. Deformations in track geometry is a deviation in track location compared to initial track placement. These displacements can have a variety of forms and are therefore often divided into five subcategories: longitudinal level, alignment, gauge, cross-level, and twist. Each of these displacements can cause irregular rolling stock movement and will be described relative to the coordinate system depicted in Figure 2.2.

In Norway, track sections are divided into quality classes with respect to the speed limit on that specific track section. A track section with a high speed limit poses higher demands on track quality than a track section with a low speed limit. Depending on the quality class, each geometric measurement of track placement is categorized as new track, alert limit, intervention limit, or immediate limit. Today, Bane NOR labels measurements surpassing intervention limit as defects and these are included in planned maintenance, while measurements surpassing immediate limit are given instant attention.

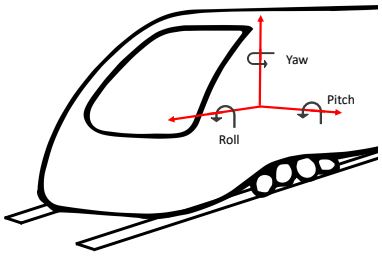

Figure 2.2.: Rotation axis relative to train body.

Longitudinal level

Longitudinal level irregularities occur when a rail deviates from initial placement in vertical direction as illustrated in Figure 2.3a. Such deviation can cause a passing rolling stock body to experience rotation around pitch, felt as a form of bounce by train passengers. Longitudinal level is the displacement parameter that is most associated with the condition of the track bed [23] and hence in research papers [1, 13, 24] often utilized without regarding other track geometry parameters to determine track deterioration. Table A.1 lists deviation limits utilized by Bane NOR for longitudinal level irregularities, given track category.

Alignment

Alignment irregularities occur when the rails are displaced sideways in horizontal direction, see Figure 2.3b, while the distance between the left and right rail remains constant. A rolling stock body passing an alignment irregularity would possibly experience yaw or sway. Bane NOR has no direct limits related to this type of deviation.

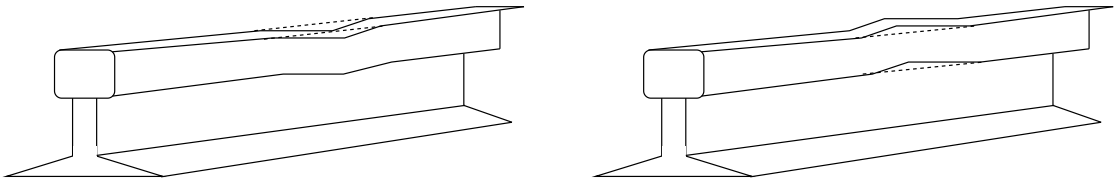

(a) Longitudinal level irregularity.

(b) Alignment irregularity.

Figure 2.3.: Track deviation from original placement in respectively vertical and horizontal direction.

Gauge

Gauge is the perpendicular distance between two rails, in Norway measured 14 mm beneath the track plan, see Figure 2.4a. The nominal gauge value for tracks in Norway is 1435 mm. Gauge irregularities are any deviations from this initial distance. Correct gauge extends the life of both track components and train wheelsets as the forces between track and train are minimized [25]. In addition, according to [25], gauge defects are the most common cause of derailment. Gauge can be measured statically or dynamically. Static gauge measurements are recorded without the influence of a passing train, while dynamic gauge measurements are taken when the rail is subject to train load. Under force, the rails tend to move further apart, and hence static and dynamic gauge values deviate. Roger 1000 measures dynamic gauge. Table A.2 lists deviation limits in dynamic gauge, for the different track categories.

In addition, Bane NOR poses limits on the average deviation from nominal gauge over a 10 meter long track section. These limits are listed in table A.3.

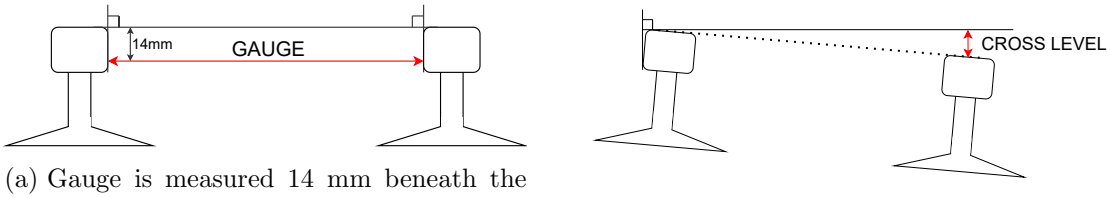

(a) Gauge is measured 14 mm beneath the track plan.

(b) Cross-level irregularity.

Figure 2.4.: Definition of gauge and cross-level measurement between two rails.

Cross-level

Cross-level, also named cant, superelevation, cross-slope or cross-fall, occurs when left and right rails are not leveled, see Figure 2.4b. This height difference can either be intentional or unintentional. Intentional cross-level is present in conjunction with curves to contribute to passenger comfort. Cross-level irregularities occur when the height difference is unintentional. These irregularities can cause a passing train to experience roll or sway. Table A.4 lists deviation limits for unintentional cross-level for the different track categories.

Twist

Twist irregularities occur when the variation in cross-level measured over a specific distance, often over 2 and 9 meters, is above a given limit. As for cross-level, twist

irregularities can cause a passing train to experience roll or sway. Table A.5 and A.6 list deviation limits for twist over a distance of 2 and 9 meters respectively.

2.2.2. Catenary System

The catenary system supplies passing electric trains with electricity through contact wires which are in contact with the pantograph mechanism mounted on the roof of the trains, depict in Figure 2.1 [26]. Poles or gantry[2] placed alongside the railway track are equipped with cantilever used to support the contact wire. Poles or gantry, hereafter collected under the term mast, span the contact wire between adjacent masts with a typical span length in the range of 50 to 70 meters under normal conditions [27]. The catenary system is a complex system not covered fully by this study. However, specific parts of the system relevant to this study are in the following covered in detail.

To each mast the contact wire is mounted with a fixed lateral displacement with respect to the track center line [27]. This displacement is called stagger and reduces the wear on the pantograph by shifting the contact point between the pantograph and the contact wire. The described setup from a top view is depicted in Figure 2.5.

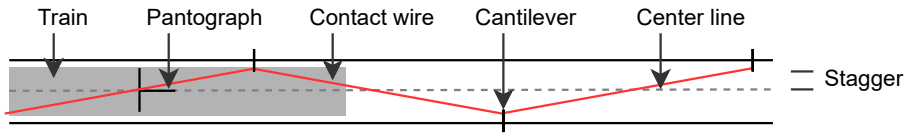

Figure 2.5.: Schematic overview from a top perspective of induced stagger through cantilevers and interaction with pantograph.

The lateral displacement is induced by a steady arm connected to the registration arm and cantilever, which depending on both the mast position and desired displacement relative to the track center line, either can be push-off or pull-off type. Figure 2.6 illustrate an example of both push-off and pull-off steady arms. In Figure 2.6 the cantilever is connected to the pole at the top horizontally with a supporting beam across, however this structure varies. Nevertheless, for other cantilever to pole and cantilever to gantry structures, the steady arm principle remains the same.

Poles can be placed on either side of the track, where the topography of the track line and geographical constraint affect the placement. For example, on curved track, curvature and cross-level will induces natural shifts of the contact point. Combination of different cantilever and registration arm beam length, pull- or push-off steady arm and pole placement relative to track side are parameters that under the design of the catenary system are decided to induce desired stagger.

In addition, parameters including environmental condition and wheel to rail contact influence the contact point between the pantograph and contact wire. For example the presence of cross-winds can cause lateral displacement of the contact wire, largest in the middle of the span. The wheels on a train vehicle have cone shaped treads which steers the train on both tangent and curved track. In curves, acting forces press the outer

[2]Bridge-like overhead structure supporting cantilever.

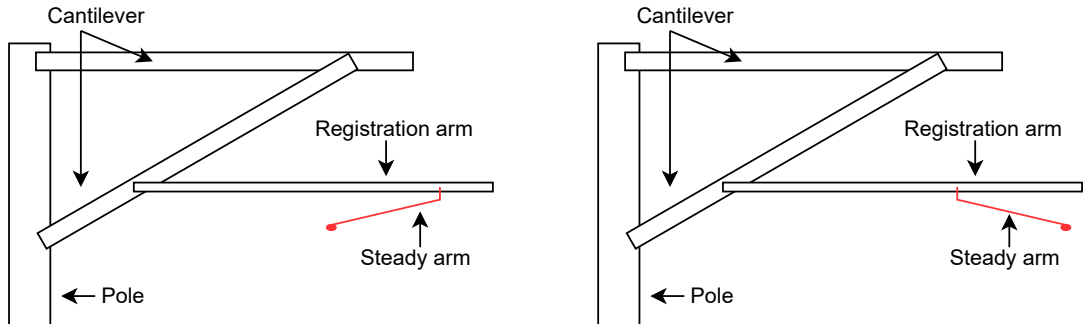

(a) Push-off steady arm.

(b) Pull-off steady arm.

Figure 2.6.: Cantilever connected to pole with registration and steady arm setup.

wheel outwards, causing a slight, constant displacement between the rail and wheel contact point in the same direction. On straight track however, there is no constant force creating a stable contact point. Hence, this creates small sinusoidal motions in the search for a stable contact point. This motion can propagate and slightly influence the contact point between the pantograph and contact wire, observed as noise.

2.3. Relative position alignment

Alignment methods can be classified based on distinguishing characteristics [28]. These classifications give insight into the properties of the different alignment methods. One such characteristic is profile-based versus feature-based. Profile-based methods look at the whole data set when performing the alignment, while feature-based methods only evaluate based on extracted features from the original data set. Another characteristic is piece-wise methods versus segment-wise methods. Piece-wise methods consider the whole data set, while segment-wise methods look at a data window at the time. In addition, alignment methods can be distinguished based on whether they are pair-wise or inter-sample methods. Pair-wise alignment methods perform the alignment by comparing to a reference, while inter-sample methods align the data without a reference.

Several alignment methods have been employed in literature with varying results. As this paper aims to conduct a targeted investigation to find the most encouraging alignment method, the selection of methods to be evaluated is based on previous results in literature. [1] evaluates five alignment methods based on criteria that align with the objective of this paper. Therefore, this paper aims to reproduce an evaluation of this set of methods utilized on Norway-specific measurement data. The same set of methods were evaluated in the related specialization project [21]. However, in hindsight, improvements to this evaluation are proposed. For more detail, see Section 4.1. The set includes three methods that have shown great capacity in aligning different data sets in various fields, namely Dynamic Time Warping (DTW), Correlation Optimized Warping (COW), and Recursive Alignment by Fast Fourier Transform (RAFFT). In addition, [1] proposes a combined method, a combination of RAFFT and COW, which exploits the individual strengths of the respective methods. The Cross-Correlation Function (CCF) is widely utilized to align track geometry data today and is hence also included.

A complete overview of the different alignment methods selected and how they fit into

the presented classification is given in table 2.1.

Table 2.1.: Classification of utilized alignment methods (adapted from [1]).

Alignment Method	Abbreviation	Profile-based/Feature-based	Piece-wise/Segment-wise	Pair-wise/Inter-sample
Cross-Correlation Function	CCF	Profile-based	Piece-wise	Pair-wise
Dynamic Time Warping	DTW	Profile-based	Piece-wise	Pair-wise
Correlation Optimized Warping	COW	Profile-based	Segment-wise	Pair-wise
Recursive Alignment by Fast Fourier Transform	RAFFT	Profile-based	Segment-wise	Pair-wise

Following is an in-depth description of the theory behind the utilized methods. Assume there are two series of equal length, i.e. sub-samples of the original measurement series,

$$\begin{aligned} X &= \{x_1, x_2..., x_N\} \\ Y &= \{y_1, y_2, ..., y_N\} \end{aligned} \tag{2.1}$$

where X is the reference series and Y the series that is desired to be aligned to X. Since X and Y are sub-samples, they can be selected to have equal lengths. However, the following described alignment methods would equally apply for series with different lengths.

Cross-Correlation Function

CCF is a method that determines the similarity between two series [29]. This similarity is found utilizing the fact that the relationship between two seriess can be quantified by summing the products obtained through point-by-point multiplication. This is expressed in Equation 2.2 [29],

$$r_{XY} = \sum_{i=0}^{N-1} X_i Y_i \tag{2.2}$$

where X and Y are defined by Equation 2.1 and N is the number of data-points in the respective series.

Equation 2.2 is not normalized. Normalization is desirable to avoid reduced cross-correlation with increasing shift, i.e. when fewer data points are evaluated. With normalization, cross-correlation values are independent of the number of data points evaluated. Normalization can be achieved by dividing r_{XY} by the product of the square roots of each series squared when not shifted, as expressed in Equation 2.3 [29]. Here s represents the number of data points shifted.

$$p_{XY}(s) = \frac{r_{XY}(s)}{\sqrt{r_{XX}(0)}\sqrt{r_{YY}(0)}} \tag{2.3}$$

Since the denominator represents perfect cross-correlation, Equation 2.3 will never be greater than one. Equation 2.3 can be modified by subtracting the mean value of each series from each data point such that negative correlation only occurs when the series have an inverse relationship. This results in Equation 2.4 [29],

$$p_{XY}(s) = \frac{\sum_{i=0}^{N-1}(X_i - \bar{X}) \cdot (Y_{i-s} - \bar{Y})}{\sqrt{\sum_{i=0}^{N-1}(X_i - \bar{X})^2}\sqrt{\sum_{i=0}^{N-1}(Y_{i-s} - \bar{Y})^2}} \tag{2.4}$$

known as the Pearson product-moment correlation. X and Y are defined by Equation 2.1, $\bar{X}$ and $\bar{Y}$ are the mean of the respective series, s the number of data points shifted and N the number of data-points in the respective series.
By shifting one time series, Y, relative to the reference, X, and computing the Pearson product-moment correlation for each shift s, the optimal shift can be determined. Then, applying the found shift to time series Y, results in an alignment between the two time series.

Alignment by cross-correlation applies a constant shift to the whole time series Y. This can pose as a weakness if measurements, in reality, are stretched or compressed, which would require a varying shift. Concurrently, the shape of the series is with CCF never alternated. Hence if no or little stretching or compressing is present in the original series, a constant shift is optimal as alternation of the shape of the series is avoided.

The larger the shift applied, the higher the amount of unmatched data. In addition, the larger the shift, the fewer data points are included in the correlation computation. Hence, only a small subset of the series is considered for a large shift. If this small subset matches well in a given scenario, a high cross-correlation value can be achieved, regardless of the mismatch in the rest of the series. To avoid this, a max shift can be imposed. [29] proposes a max shift of $\frac{N}{2}$. For railway-specific data, as suggested by [1], it is possible to observe the max shift present in the data and rather utilize this as an upper shift limit.

Recursive Alignment by Fast Fourier Transform

RAFFT [30] performs recursive alignment, from first aligning X and Y (defined by Equation 2.1) on a global scale to progressively aligning smaller sub-segments of X and Y. The optimal shift is determined at each step by applying Fast Fourier Transform (FFT) cross-correlation. Utilizing FFT, rather than computing the cross-correlation in state space, results in a more rapid computation of the correlation between two series [1, 31]. This is a desirable property when the correlation is computed repetitively, as is the case for RAFFT.

The pseudocode for the RAFFT alignment method is detailed in Algorithm 1 [30]. The method utilizes a minimum segment length equal to ten to prevent the method from overfitting to noise. If the series to be aligned has a length greater than ten, the optimal shift is determined by utilizing FFT cross-correlation, as described. If the optimal shift is zero, the input series will be returned directly, and no further local alignment is performed. Else, the series Y is shifted according to the found optimal shift, and the next position for splitting, p, is determined such that $p = min(Y(x)) \;\; x \in [N/4, 3N/4]$. The found position p is then utilized to divide the series to be aligned and references into two sub-segments, and a new recursive call to the RAFFT algorithm is made. This procedure is repeated until either the remaining series has a length below ten or the optimal shift is zero.

Algorithm 1: RAFFT

```
Result: Y_aligned
input: Y - series to be aligned, X - reference series ;
if length(Y) ¡ 10 then
    return Y
end
shift = max(FFTCorr(Y,X)) ;
if shift == 0 then
    return Y
end
MOVE(Y,shift);
p=findMin(Y);
leftY = Y[0:p-1];
leftX = X[0:p-1];
rightY = Y[p:N-1];
rightY = Y[p:N-1];
RAFFT(leftY,leftX);
RAFFT(rightY,rightX);
```

An advantage with this approach compared to CCF is that since recursive local alignments are conducted, the method can compensate for compression and stretching present in the series. However, if no compression and stretching is present, this method may overfit by finding false local optimal alignments. This can occur as there exists no one-to-one mapping between the series. Hence, the difference in amplitude can cause the alignment method to select a specific false alignment that exhibits a higher correlation value.

Dynamic Time Warping

DTW [32, 33] aligns two time series through warping, thereby creating a match between the series. The alignment method comes in two different forms, symmetric and asymmetric. The latter warps only along one series, allowing alignment of one series relative to a reference. This is the desired behavior in this project, making it possible to compare DTW alignment to the other methods presented. Hence it is asymmetric DTW which is presented here.

To align Y to X, both with length N, a N x N cost matrix, D is constructed. The values in D represent the euclidean distance between the data points in Y and X. For example, let the two time series Y and X be given by $Y = [1, 3, 5, 2, 1]$ and $X = [3, 1, 2, 5, 1]$, plotted in Figure 2.7. The corresponding 5 x 5 D matrix for these two time series is given in Figure 2.8a.
Then, based on the cost matrix D, a N x N cumulative distance matrix, δ, is computed based on Equation 2.5 [33]. For the D matrix found in the example utilized above, the δ matrix is given by Figure 2.8b.

$$\delta(i,j) = \begin{cases} D(i,j) + min[\delta(i-1,j), \quad \delta(i-1,j-1), \quad \delta(i,j-1)] \quad i,j \geq 2 \\ 0 \quad i,j = 1 \end{cases} \tag{2.5}$$

The optimal warping path, W_{min}, is the minimal accumulated distance found in the δ matrix from $\delta(N,N)$ to $\delta(1,1)$. W_{min} can be computed utilizing Equation 2.6 [33],

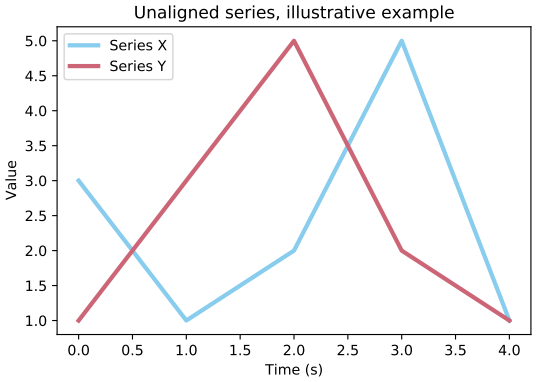

Figure 2.7.: Time series $Y = [1, 3, 5, 2, 1]$ and reference series $X = [3, 1, 2, 5, 1]$ utilized to explain Dynamic Time Warping.

X \ Y	1	3	5	2	1
1	0	2	4	1	0
5	4	2	0	3	4
2	1	1	3	0	1
1	0	2	4	1	0
3	2	0	2	1	2

(a) Cost matrix D. Euclidean distance between each data point in X and Y.

X \ Y	1	3	5	2	1
1	7	7	7	4	4
5	7	5	3	6	9
2	3	3	6	5	6
1	2	4	6	5	5
3	2	2	4	5	7

(b) Cumulative distance matrix δ. Computed utilizing Equation 2.5.

X \ Y	1	3	5	2	1
1	7	7	7	4	4
5	7	5	3	6	9
2	3	3	6	5	6
1	2	4	6	5	5
3	2	2	4	5	7

(c) Optimal warping path. Computed utilizing Equation 2.6.

Figure 2.8.: Example of cost matrix, cumulative distance matrix, and optimal warping path found by DTW.

$$W_{min} = Arg_W min \left(\frac{1}{k} \sqrt{\sum_{i=1}^{k} w_i} \right) \tag{2.6}$$

where w_i denotes the cumulative distance at point i and k refers to the length of W under the condition $max(n, n) \leq k \leq n + n + 1$. This is easier to grasp visually, see Figure 2.8c for the optimal warping path for the utilized example.

By warping along the found path, an alignment is achieved. For the utilized example, warping along the path visualized in Figure 2.8c yields $Y_{aligned} = [1, 1, 3, 5, 1.5]$. In Figure 2.9, $Y_{aligned}$ is compared to the reference X. Observe that DTW has altered the initial shape of Y by averaging the last two points in Y. This can become problematic and is discussed in the following paragraph.

DTW has achieved superior results in aligning time series in previous work, such as [34]. However, in this study, the warping may impose a weakness as it is desirable to preserve the shape of the original series as much as possible, especially the amplitude, to detect irregularities. The results obtained by [1] support these concerns, showing that although

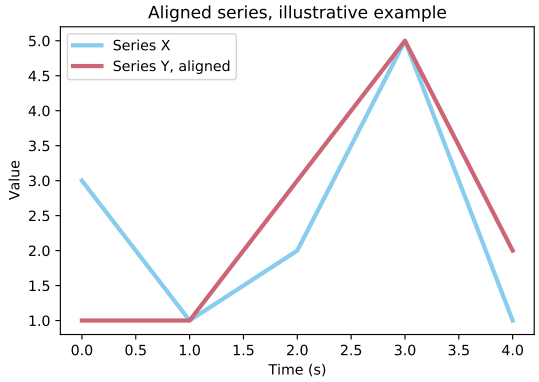

Figure 2.9.: Time series $Y_{aligned} = [1, 1, 3, 5, 1.5]$ aligned to the reference series $X = [3, 1, 2, 5, 1]$ by utilizing Dynamic Time Warping.

DTW achieved the highest degree of similarity between the aligned time series, this is at the expense of conserving the series shape.

Correlation Optimized Warping

Correlation Optimized Warping (COW) was first proposed by [35]. COW achieves alignment by dividing X and Y (defined by Equation 2.1) into sub-samples with equal length and aligning each sub-segment through stretching or compressing. The number of segments, N_{seg}, is given as input to the algorithm.

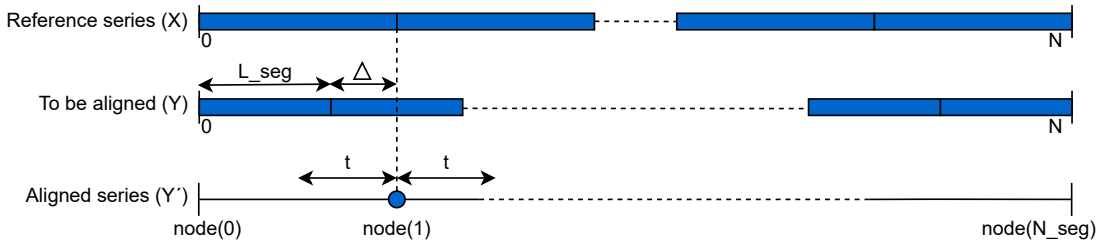

Figure 2.10.: Visualization of COW alignment method structure (adapted based on [1]).

Let y be a sub-sample of Y with length L_{seg} and x a sub-sample of X with length $L_{seg} + \Delta$, where $\Delta = (n/N_{seg}) - L_{seg}$. In addition, let nodes bound each sub-segment. The structure is visualized in Figure 2.10. Let the range z be determined based on Δ and a slack variable t, given as input, such that $z = (\Delta - t; \Delta + t)$. Each segment y is then stretched or compressed with all the values in the range z. For each value in the range z, linear interpolation is utilized to make the length of the stretched or compressed segment y' equal to the length of the corresponding reference segment x. Thereupon corresponding correlation coefficients are computed. The obtained correlation coefficients are compared to find the optimal level of stretching and compression. The mentioned bounding nodes, In_i, are placed in an interval determined by Equation 2.7 [35].

$$
\begin{aligned}
In_{i,1} &= [i \times (L_{seg} + \Delta - t); i \times (L_{seg} + \Delta + t)], i = 0, ..., N_{seg} \\
In_{i,2} &= [n - (N_{seg} - i) \times (L_{seg} + \Delta + t); n - (N_{seg} - i) \times (L_{seg} + \Delta - t)], i = 0, ..., N_{seg} \\
In_i &= In_{i,1} \cap In_{i,2}
\end{aligned}
\tag{2.7}
$$

As stated, the N_{seg} and slack parameter t are given as input. In [1] the slack parameter is set equal to the max shift observed in the series while N_{seg}, is set equal to twice the slack. Since the series are segmented, this imposes a limitation in either selected segment length or selected slack value, as the value for N_{seg} cannot be greater than the segment length.

Similar to DTW, COW produces alignment through stretching and compressing. However, as pointed out by [1], COW exhibits no flexibility in aligning the first and last points in a segment, as it aims to connect the first and last points of the series to be aligned with the reference. This will be a disadvantage if the series to be aligned is subject to a high initial shift, i.e. there is no common first or last data point. Therefore, [1] proposes a combined method that eliminates this weakness.

Combined method

The combined method is proposed by [1] and performs alignment by utilizing both RAFFT and COW. As mentioned, COW exhibits no flexibility in aligning the first and last points of a segment, which is problematic when no common first and last point exists between the segments. Therefore, the combined method utilizes RAFFT to remove the parts that are not common. RAFFT compares the segment to be aligned with the reference and determines the shift between these. If the shift is positive, data points equal to the length of the found shift will be removed from the start of the segment to be aligned. Equal amount of data points with value zero will be added at the end of the segment. Conversely, if the found shift is negative, data points with zero value will be added to the segment's start, and an equal amount of points will be removed from the end of the segment. The pre-aligned segment is thereupon used as input to the COW alignment method.

The combined approach can utilize a smaller slack variable for the COW algorithm due to the pre-alignment [1]. Not only does this lower the computational time required for computing the alignment, but it also solves the trade-off between the N_{seg} parameter and segment width described above.

2.3.1. Reference data set

All pair-wise alignment methods are dependent on selecting a reference measurement series. In literature, several methods are proposed regarding how the reference series can be selected [36, 37, 38]. [36] utilizes a random series as references while [37] argues that the series collected under the most favorable circumstances is the logical choice for the reference. The latter would imply a measurement series recorded close to initial track placement. [38] proposes to utilize the series with the highest mean correlation value when correlated with all the other measurement series as reference.

[1] evaluates these approaches for alignment of measurement series collected within the railway domain and concludes that if historical measurements are available, the oldest measurement series will be a good reference as it is most equal to the desired state. Else, selecting the series with the highest mean correlation coefficient with respect to the other measurement series as reference is a reasonable method. To compute correlation coefficients [1] utilizes longitudinal level measurements.

2.3.2. Measurement channel

Alignment methods are dependent on track measurements to perform the alignment. In literature [1, 13, 19, 39] these measurements are often either values for longitudinal level or gauge, however, in theory, any track measurement can be utilized. [1] tests alignment with cross-level, gauge, alignment, and longitudinal level measurements and achieves the highest accuracy utilizing gauge. The paper states that gauge measurements are less affected by factors like degradation between inspections, which may explain the result. [13] performs alignment using three different measurement channels, short and medium wavelength longitudinal level and gauge. If two or more alignments produce a shift within the same range, the shift is applied. [40] suggests utilizing curvature measurements as it can be assumed that these measurements do not vary between track recordings.

2.3.3. Evaluation metrics

An evaluation metric is proposed to evaluate the success of the proposed alignment methods. The metric is chosen based on the objective to achieve precise alignment while keeping the original shape of the measurement series.

A common metric used to evaluate time series alignment is Mean Square Error (MSE). However, due to degradation between measurement recordings, an amplitude difference that is desirable to preserve will be present between the series evaluated. Hence, this metric is not suited to evaluate the achieved alignments.

Simplicity value

The simplicity value is a metric proposed by [41] and utilized by among other [1, 42, 43, 44] to measure how well-aligned a set of data is. The principle of simplicity value is related to Singular Value Decomposition (SVD), where the singular values state how much of the variance can be explained. Well-aligned time series will have more variance that the first component can explain. The simplicity value is calculated utilizing Equation 2.8 [41],

$$\text{Simplicity value} = \sum \left(\text{SVD} \left(\frac{[X; Y']}{\sqrt{\sum_{i=1}^{N} X^2(i) + Y'^2(i)}} \right) \right)^4 \tag{2.8}$$

where $X = \{x_1, x_2, ..., x_N\}$ is the reference series and $Y' = \{y'_1, y'_2, ..., y'_N\}$ is a series aligned to X. The simplicity value ranges from 0 to 1, with a more accurate alignment achieved the closer the value is to one.

Simplicity value alone will award undesirable change in both shape and area of the aligned series if it contributes to similarity. Hence, an additional metric is included, which penalizes change in shape.

Peak factor

Preservation of shape throughout the alignment is desirable as the variation in amplitude is an essential attribute for detecting defect development. The peak factor is computed utilizing Equation 2.9 [41],

$$\text{Peak Factor} = \frac{\sum_{i=1}^{N}(1 - min(|\frac{\|Y'(i)\| - \|Y(i)\|}{\|Y(i)\|}|, 1)^2)}{N} \tag{2.9}$$

where $Y = \{y_1, y_2, ..., y_N\}$ is the series before alignment and $Y' = \{y'_1, y'_2, ..., y'_N\}$ the same series after alignment.

A higher value for peak factor (between 0 and 1) indicates better preservation of peak area and shape. This formula utilizes the fact that if the norm stays the same post alignment, the absolute term will be equal to zero, and thereby the overall contribution of that specific point will be one. A partly warped point has an absolute term between zero and one, thereby contributing with a value smaller than one. If the point is been warped extensively, the absolute term will grow bigger than one, and hence the overall contribution for that specific point will be zero.

Since the euclidean length is utilized here, distortion of peaks with higher amplitude has a more significant influence on the peak factor. This is consistent with the objective to preserve the amplitude of defects.

Warping effect

Warping effect [41] is equal to the sum of simplicity value and peak factor, thereby evaluating both preciseness and preservation of the alignment. Hence warping effect is an overall measure of how well the alignment meats the objective.

2.4. Absolute position determination

In the scope of this study, absolute positioning is the determination of the position at which a measurement has been conducted. This section covers the theory that constitutes the background knowledge needed to determine absolute position and associated uncertainty when utilizing coordinate measurements and records.

2.4.1. Satellite-based positioning

Satellite-based positioning is the determination of positions using satellites [45]. A receiver measures its distance to several satellites to compute its position, where known positions of the satellites are utilized in the computation. This distance is computed by measuring the time required for the satellite signal to reach the receiver, where the accuracy realizes on precisely set clocks. Therefore, modern receivers utilizing inexpensive clocks require a connection to four satellites to compute an accurate position. The four unknown parameters, latitude, longitude, height, and clock bias, can be computed with a connection to four satellites. Several different global navigation satellite systems (GNSS) exist, all based on the described principle but deviating in implementation and utilized satellites. Global Positioning System (GPS) is one such system. Due to its broad usage in Europe today, it is the system referred to in this study.

Coordinate systems

The GPS receiver computes position utilizing a coordinate system that rotates with the Earth, namely the Earth-Centered Earth-Fixed (ECEF) coordinate system [46]. The coordinate system's xy-plane coincides with the Earth's equatorial plane. The +x-axis

points in the direction of 0 degrees longitude, and the +y-axis points towards 90 degrees latitude. The +z-axis points in the direction of the geographical North Pole.

Further, different models of the Earth's shape can be utilized to compute latitude, longitude, and height. Common are spherical and ellipsoidal models. For spherical models the cross-sections parallel to the equatorial plane are circular, while for ellipsoidal models cross-sections normal to the equatorial plane are ellipsoidal. Fixing the ECEF coordinate system to the center of the chosen model, latitude, longitude, and height can be defined, respectively. GPS utilizes WGS-84 as a reference scheme, which is based on an ellipsoidal model [47]. For further details, the reader is referred to [46] and [47].

To formulate coordinates, three formats are commonly utilized, namely Decimal Degrees (DD), Degrees-Minutes-Seconds (DMS), and Degrees-Decimal-Minutes (DDM). Equation 2.10 details conversion from the DMS and DDM formats into the DD format.

$$\text{Decimal Degrees} = \text{Degrees} + \text{Minutes}/60 + \text{Seconds}/3600 \tag{2.10a}$$

$$\text{Decimal Degrees} = \text{Degrees} + \text{Decimal minutes} \ / \ 60 \tag{2.10b}$$

For example, the latitude 63° 04' 38.03394" N given in DMS format would converted to DD equal to DD = 63 + 04/60 + 38.03394/3600 = 63.07723165° N.

To convert coordinates in the DD format into the DMS or DDM format, the following steps are necessary,

1. The integer part of the latitude or longitude coordinate equals the degrees
2. Multiply the decimal part by 60 to obtain DDM
3. Further, to convert into DMS, minutes are the integer part of the product found in step 2.
4. Multiply the decimal part found in 2 by 60 to obtain seconds

Take the longitude 10.38329524° E in DD format as an example. Following the given steps, conversion into DDM format gives DDM = 10° (0.38329524x60)' E = 10° 22.9977144' E. Conversion into DMS yields DMS = 10° 22' (0.9977144x60)" E = 10° 22' 59.862864" E.

Distance between coordinates

Common in literature, as done by [48, 49, 50], is to assume the Earth is spherical, which eases distance computation. Although this is a simplification, the accuracy only decreases with increasing distance due to the shape of the Earth then becoming more significant. As this paper deals with the computation of small-scale distances, this simplification is acceptable. Three commonly proposed spherical distance formulas are the Equirectangular approximation, the Spherical Law of Cosines, and the Haversine Formula. A variable utilized in all formulas is the Earth's mean circumference, equal to 6371000.0 meters [51].

Equirectangular approximation

Equirectangular distance approximation is based on the Pythagoras theorem and the equirectangular map projection [52]. The projection converts the globe into a Cartesian rectangular grid [53]. Each grid cell has the same size, shape and area. The following formula yields equirectangular distance approximation [52],

$$x = |-\lambda_2 + \lambda_1| cos\left(\frac{1}{2}\phi_1 + \frac{1}{2}\phi_2\right) \tag{2.11a}$$

$$y = |-\phi_2 + \phi_1| \tag{2.11b}$$

$$d = r \cdot \sqrt{x^2 + y^2} \tag{2.11c}$$

where (ϕ_1, λ_1) and (ϕ_2, λ_2) are latitude and longitude of coordinates one and two respectively (in radians) and r the earth mean radius.

Spherical Law of Cosines

The spherical law of cosine is a theorem based on spherical trigonometry [48, 52], and utilizes the classical law of cosine [54]. The formula is rearranged from the canonical form into the geodetic form to allow expression utilizing latitude,

$$d = r \cdot arccos(sin(\phi_1)sin(\phi_2) + cos(\phi_1)cos(\phi_2)cos(-\lambda_2 + \lambda_1)) \tag{2.12}$$

where (ϕ_1, λ_1) and (ϕ_2, λ_2) are latitude and longitude of coordinates one and two respectively (in radians) and r the earth mean radius.
When (ϕ_1, λ_1) and (ϕ_2, λ_2) are within a few kilometers, the spherical law of cosine becomes unstable due to the inverse cosine of a number very close to one giving numerical instability. With the focus of the paper being small-scale distances, this instability is critical [48].

Haversine Formula

The Haversine Formula computes the shortest distance between two coordinates on a sphare, ignoring any obstacles and hills. This is also known as great-circle distance [48, 49, 52]. By avoiding the inverse cosine, the formula is well defined also for small distances. Due to the relation between the inverse tangent and inverse sinus, there exists two versions of the formula. Equation 2.13 utilizes arcsin [52],

$$d = 2r \cdot arcsin\left(\sqrt{sin^2\left(\frac{\phi_2 - \phi_1}{2}\right) + cos(\phi_1)cos(\phi_2)sin^2\left(\frac{\lambda_2 - \lambda_1}{2}\right)}\right) \tag{2.13}$$

where (ϕ_1, λ_1) and (ϕ_2, λ_2) are latitude and longitude of coordinates one and two respectively (in radians) and r the earth mean radius.

[55] compares Spherical Law of Cosines and Equirectangular approximation in computing the geographical distance between two trace locations, where the average distance between the locations is 253.27 meters. This comparison showed that more accurate distances were found with the Spherical Law of Cosines, while faster computations were achieved with Equirectangular approximation. [56] states that mathematically, the Haversine formula is equivalent to the Spherical Law of Cosines. However, due to the Haversine formula addressing the computational limitations raised with the Spherical Law of Cosine, the Haversine formula can more precisely compute distances.

Bearing

The bearing, ϕ, is the angel between a line connecting two points and a line through the North Pole (reference), measured clockwise [57]. This is illustrated in Figure 2.11, where the bearing is marked with ψ. The bearing is computed based on Equation 2.14 [50, 57],

$$x = cos(\phi_2)sin(\lambda_2 - \lambda_1) \tag{2.14a}$$
$$y = cos(\phi_1)sin(\phi_2) - sin(\phi_1)cos(\phi_2)cos(\lambda_2 - \lambda_1) \tag{2.14b}$$
$$\psi = arctan(x, y) \tag{2.14c}$$

where (ϕ_1, λ_1) and (ϕ_2, λ_2) are latitude and longitude of two coordinates (in radians).

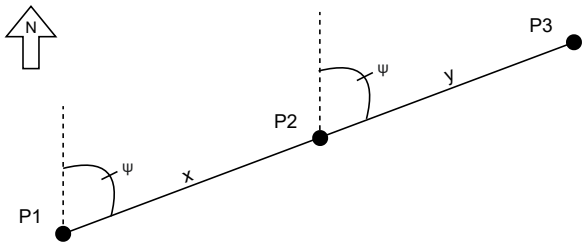

Figure 2.11.: Bearing is equivalent between two lines which are parallel.

Deriving coordinate position method

An unknown position can be derived given a known position and the bearing and distance from the known to the unknown position. Let the position P3 in Figure 2.11 be an unknown position desired to be derived from position P2. Further, assume the distance between the two points, y, is known, while the bearing, ψ, is unknown. Utilizing Equation 2.14, the bearing can be computed between the line connecting to known positions and a line through the North Pole. However, since P3 is unknown, a third coordinate position is necessary. Let this be P1. If the line between P1 and P2 is parallel to the line between P2 and P3, the bearing between both lines and the lines through the North Pole will be equal. Hence, with P2 and y known and the bearing ψ commutable utilizing P1, the position of P3 can be derived [58].

Let (ϕ_3, λ_3) be the latitude and longitude of the unknown position P3, then the position can be derived by Equation 2.15 [58],

$$\phi_3 = arcsin(sin(\phi_2)cos(\frac{y}{r}) + cos(\phi_2)sin(\frac{y}{r})cos(\psi)) \tag{2.15a}$$
$$\lambda_3 = \lambda_2 + atan2(sin(\psi)sin(\frac{y}{r})cos(\phi_2), cos(\frac{y}{r}) - sin(\phi_2)sin(\phi_3)) \tag{2.15b}$$

where (ϕ_2, λ_2) are the latitude and longitude of P2 (in radians), ψ the bearing, r the earth mean radius and y the distance between P2 and P3.

2.5. Data preprocessing

Applying preprocessing techniques to raw data transforms the data into a format more feasible to manage. Such techniques may ease the detection of patterns and comparison between data. Many preprocessing techniques exist to facilitate different data types and goals. This section describes key concepts utilized in this study. A reader familiar with the topics may find this section redundant and is advised to skip this part. Readers interested in a broader understanding of data preprocessing techniques may refer to [59].

2.5.1. Data normalization

Normalization removes the variation between attributes by transforming the data to fall within a common range. There are numerous data normalization methods, including the commonly used min-max and z-score normalizations, described in the following.

Min-max normalization

Min-max normalization transforms the data linearly [59]. Suppose x_{min} and x_{max} are the minimum and maximum values of the time series X. Min-max normalization than maps a value x_n of X to x'_n in the range [new x_{min},new x_{max}] by applying Equation 2.16 [59].

$$x'_n = \frac{x_n - x_{min}}{x_{max} - x_{min}}(\text{new } x_{max} - \text{new } x_{min}) + \text{new } x_{min} \tag{2.16}$$

Since min-max normalization preserves the relationship among the original values in the time series, the method is affected by outlier values [60].

Z-score normalization

Z-score normalization transforms the values in a time series X based on the mean and standard deviation of X. The z-score normalized value of x_n, denoted x'_n, is computed by applying Equation 2.17 [59],

$$x'_n = \frac{x_n - \bar{X}}{\sigma_x} \tag{2.17}$$

where $\bar{X}$ is the mean value of X and σ_X the standard deviation of X.

Due to its z-score normalization utilizing mean and standard deviation, the method is less affected by the potential presence of outliers.

2.5.2. Interpolation

Given a set of variables $x_1, x_2, x_3, ...$ with corresponding values $f(x_1), f(x_2), f(x_3)...$, interpolation is approximating the function f such that unknown variables x_n can be estimated [61]. There are numerous methods for approximating the function f, where the methods deviate in the degree they generalize on the provided variables. This section covers common methods that are characterized by having low complexity, due to the observed characteristics of the utilized data records. A low complexity implies that the approximation often generalizes well but lacks expressiveness.

Nearest value interpolation

With interpolation based on nearest value, a missing value inherits its value from the the closest neighbouring value. This is illustrated in Figure 2.12a, where the values A, B and C are known, while the pink line represents the function f(x) for all x between A and C.

Linear interpolation

In the case of linear interpolation, a line $y = ax + b$ [62] is fitted such that the line passes through the points A, B and C, illustrated in 2.12b.

Polynomial interpolation

Polynomial interpolation is fitting a polynomial of selected order to the provided data [62]. Hence, linear interpolation is equivalent to first-degree polynomial interpolation. When applying interpolation by polynomial of second-degree, the polynomial $y = ax^2 + bx + c$ is fitted such that the second-degree polynomial passes through the points A, B and C as illustrated in 2.12c.

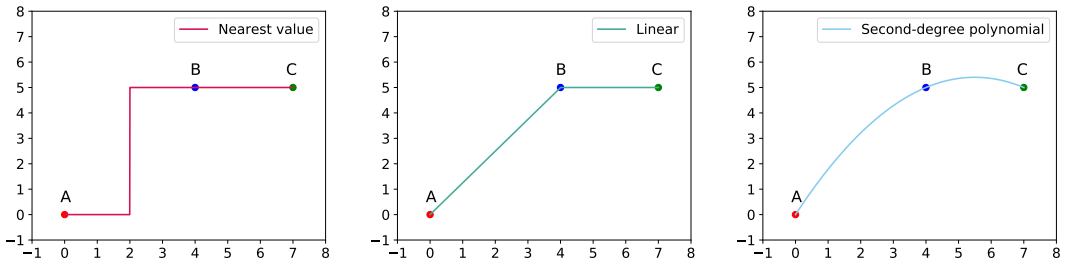

(a) Nearest value (b) Linear (c) Second-degree polynomial

Figure 2.12.: The principal behind nearest value, linear and second-degree polynomial interpolation.

3. Data

To confine the scope of this study, a subsection of the railway track is addressed. The chosen track section is located between Støren and Trondheim, a 51.65-kilometer-long track section on Dovrebanen, Norway. The track section consists mainly of a single track line, except at the stations present along the track. Figure 3.1a gives a schematic overview of the number of track lines along the studied track section. Due to the complex structure in close proximity to Trondheim station, Figure 3.1b depicts a detailed overview of this area. The studied track section includes five tunnels and follows the speed limits specified in Figure 3.1c, applicable to the main track line.

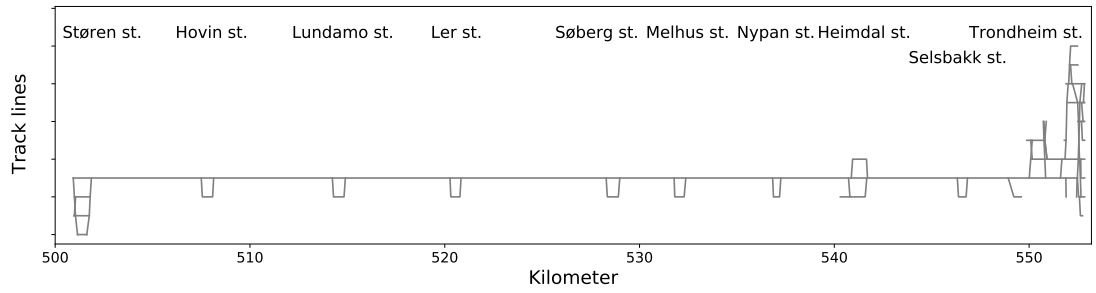

(a) Track line structure between Støren and Trondheim station.

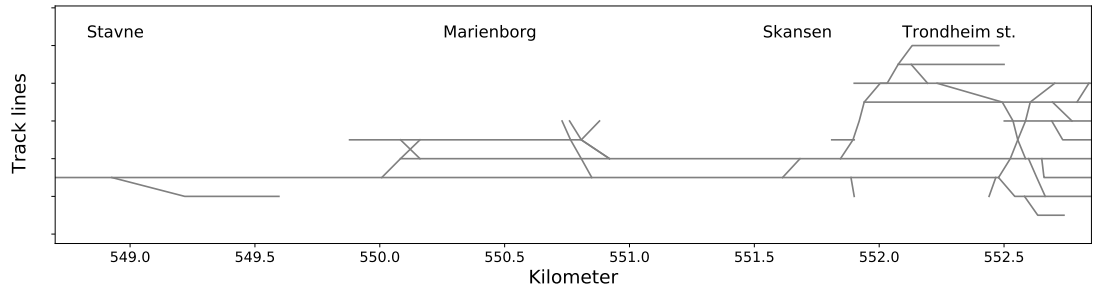

(b) Track line structure near Trondheim station, between Stavne and Trondheim station.

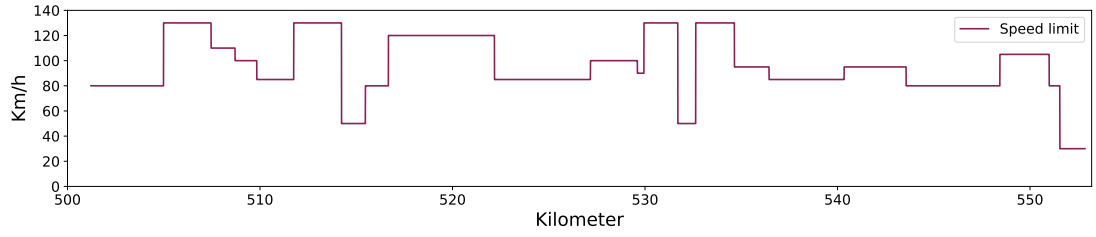

(c) Speed limits applicable along the main track line between Støren and Trondheim station.

Figure 3.1.: Track line structure and speed limit applicable on the studied track section between Støren station (501.2 km) and Trondheim station (552.850 km).

The data utilized in this study resides in three different types of data sets. This includes one data set containing track geometry measurements and two data sets storing track

objects. In the following, these data sets are presented, and the preprocessing steps applied are justified and explained. Bane NOR has provided all utilized data.

3.1. Track geometry data set

The track geometry data set contains measurement series collected by the Roger 1000 inspection train. The data set contains historical data from spring 2016 until autumn 2020, and as two measurement recordings were conducted every year, the data set consists of ten measurement series in total. Data is collected each half meter, resulting in 1 044 937 recorded positions, all with corresponding track geometry measurements. An overview of the data structure with the corresponding naming is given in Figure 3.2. A subset of the different track measurement sensor values, hereafter referred to as measurement channels, is listed and described in Table 3.1. The subset includes all measurement channels that are utilized in this project.

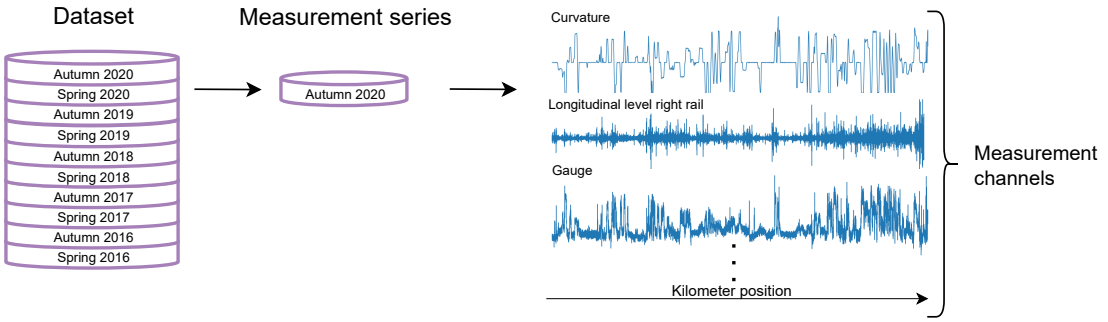

Figure 3.2.: Overview of the structure of the track geometry data set. The data set consists of ten measurement series, where each measurement series consists of multiple measurement channels.

Position data

All collected measurement series have a mileage value corresponding to each recorded measurement, i.e., a distance from Oslo central station. This mileage value is computed based on the number of train wheel revolutions and is therefore highly exposed to errors. For example, slipping and sliding of the train wheel relative to track rails will cause over- or undersized recorded mileage value [19, 63]. Calibration before and during measurement recordings also affects assigned mileage value, where the magnitude of this error is studied in Section 3.1.1. Due to the high risk of inaccurate kilometer values, mileage cannot be regarded as a piece of reliable position information.

Measurement series collected autumn 2018 and later contain coordinate position for each conducted measurement, i.e., a value for respectively latitude and longitude. These coordinate positions utilize the WGS-84 reference system. In the period autumn 2018 to autumn 2019, a unknown[1] GPS sensor was utilized. On the train section between Støren and Trondheim, this sensor gave on average a position update every 9.8 meters and a max distance with no position update equal to 33 meters. Measurements with missing GPS signal, for example due to tunnels, are disregarded.

[1]It has not been possible to obtain the specific sensor type from Bane NOR.

Table 3.1.: Overview over available measurement data.

Variable	Description
SurveyID	Measurement series ID, unique number for each series
SpaceSync	Unique ID number within a measurement series, increasing within series
Km	Distance from Oslo central station
Speed	Speed of measurement vehicle
Latitude (recorded autumn 18 and later)	Position north relative to equator
Longitude (recorded autumn 18 and later)	Position east relative to prime meridian
RF_3_25_RX_LongitudinalLevel	Longitudinal level displacement, right rail
RF_3_25_LX_LongitudinalLevel	Longitudinal level displacement, left rail
RF_3_25_RX_Alignment	Horizontal alignment displacement, right rail
RF_3_25_LX_Alignment	Horizontal alignment displacement, left rail
TwistOnABaseOf2Metre	Twist over a 2-meter distance
TwistOnABaseOf9Metre	Twist over a 9-meter distance
Cant	Deviation in cross-level
Curvature	Rail curvature
Gauge	Deviation in gauge
Stagger	Measured stagger of overhead contact lines
Height	Measured height of overhead contact lines
Inclination	Degrees of deviation from the horizontal track

In 2020 the until then utilized GPS sensor was replaced by a new[2] GPS sensor to improve positioning. On the studied track section, the new sensor gave on average a position update every 0.5 meters and a max distance with no position update equal to 8.5 meters, also here disregarding measurements for which GPS signal was missing. Notice that the average distance between each position update for the new sensor was near equal to the sampling rate, recalling that measurements were conducted each half meter. Figure 2.1 depicts the placement of the GPS sensors onboard the Roger 1000 measurement vehicle. It is unknown which of the three GPS sensors onboard, or if it is a combination of the three sensors, which provide the coordinates in the track geometry data set utilized.

3.1.1. Preprocessing

The measurement series are preprocessed to enhance alignment accuracy before aligning the data set. The proposed preprocessing steps are depicted in Figure 3.3. These steps and descriptions are based on work done in the specialization project [21]. New is a third proposed segmentation method that aims to ease later implementation in conjunction with absolute positioning. Additionally, manual position updates are handled and track data from different data sets combined. In the following, these preprocessing steps are presented and evaluated in detail.

[2]Specific sensor type of the new sensor is also unknown, but because of its more frequent updates, it is assumed to be a new sensor.

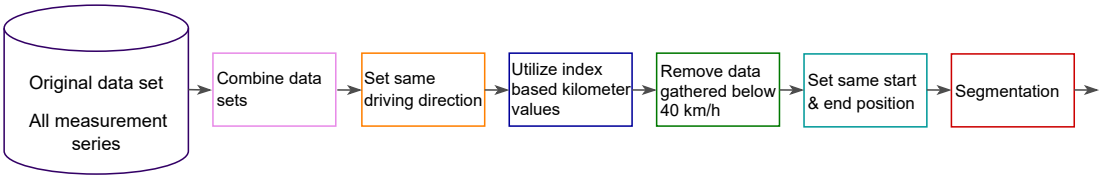

Figure 3.3.: Proposed preprocessing setup.

Combination of data sets

The measurement channels stagger, height, and inclination reside in a different data set than the track geometry measurement channels listed in Table 3.1. As measurements in both data sets have a spaceSync variable associated with each measurement, this variable can be utilized to merge the two data sets. With a variation in start and end position between the data sets, data associated with spaceSync variables that are not present in both data sets are disregarded. Although this applies to 2548 measurements, i.e., 1274.0 meters of recorded track data, the speed at which these measurements are recorded is below 40km/h and hence invalid by definition anyhow, please refer to the section below regarding invalid data.

Direction

The measurements are recorded in different directions, with the majority being recorded from Støren to Trondheim. To compare the measurement series, Støren to Trondheim is set as the desired direction, and hence measurement series recorded in the opposite direction are reversed. The impacted (reversed) measurement series were collected autumn 2017 and autumn 2019.

Due to this direction modification, the sign of inclination for the reversed measurement channels is multiplied by minus one. This is necessary to interpret driving downhill and uphill correctly after modifying train driving direction.

Non-incremental kilometer position data

Roger 1000 has manually corrected its kilometer position in all of the ten measurement series, i.e., distance from Oslo central station. However, the number and magnitude of corrections vary for each measurement series. To perform a distance correction, personnel on board the measurement vehicle use known position information of places the train passes. The recorded position is either adjusted forwards or backwards based on the deviation between the recorded and known positions. These corrections are performed at high and low speed and thereby with varying accuracy. A complete overview of all corrections and their length is given in Table A.7 in the Appendix, while Table 3.2 contains the same information related to the spring 2020 measurement recording.

Position adjustments contribute to the recorded mileage value not being incremental, as mentioned under position data at the beginning of this chapter. An example of the effect on the recorded data is visualized in Figure 3.4 for the forward adjustment at 540.00 kilometers, spring 2020. In Figure 3.4a recorded cross-level is mapped to recorded kilometer position while in Figure 3.4b recorded cross-level is mapped to the index-based kilometer position. The latter is derived by initially utilizing the recorded

Table 3.2.: Manual position corrections during measurement recording spring 2020. For an overview of all performed corrections, see table A.7 in the Appendix.

Year	Season	Position of correction	Length of correction, in meters	Direction of correction
2020	Spring	502.0000	3.0	Backwards
2020	Spring	510.0000	18.0	Forwards
2020	Spring	520.0000	18.0	Forwards
2020	Spring	530.0000	5.0	Forwards
2020	Spring	540.0000	23.5	Forwards
2020	Spring	550.0000	24.0	Forwards

kilometer start position and thereupon continuously incriminating this value by half a meter, i.e., the recording distance. From Figure 3.4a, it can be observed how the position correction induces a constant shift in the middle of the series. Even with the correction being spot on regarding the accuracy, it is unrealistic that the shift in recorded mileage value has occurred in such great magnitude at one place. For the spring 2020 recording, mileage is corrected every 10 kilometers, and hence the correction resembles accumulated shifts since the last correction. Therefore, it is desirable to preserve the shape of the measurement series and let later alignment methods induce shifts to compensate for compression and stretching in the data. It is assumed that such corrections can be more targeted than these low-frequency corrections performed manually. Hence, index-derived kilometer position is utilized throughout this study when referring to kilometer position, when not specified otherwise.

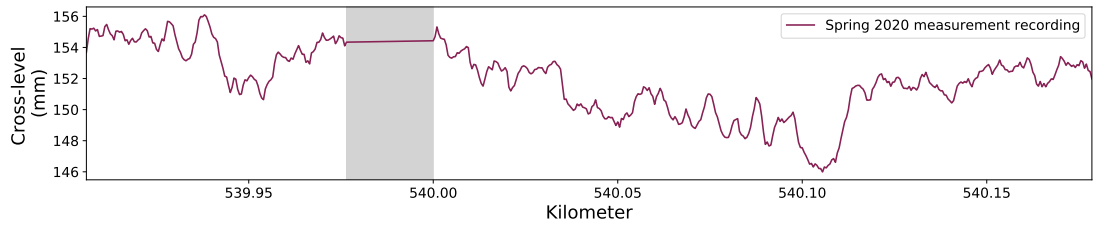

(a) Cross-level measurements mapped to recorded kilometer position spring 2020. Position update during recording cause constant shift in the recorded values.

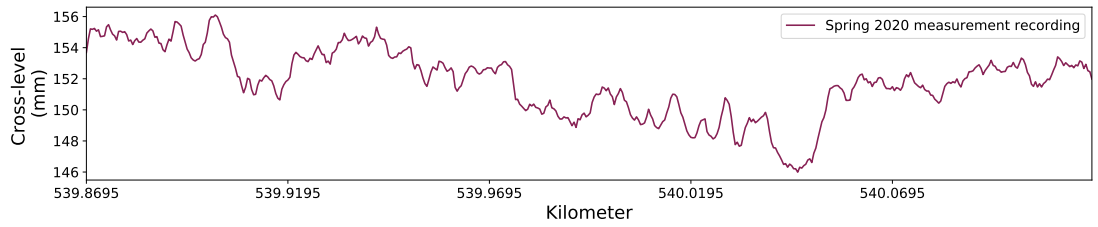

(b) Cross-level measurements mapped to index derived kilometer position spring 2020. The method preserves the shape of the measured signal.

Figure 3.4.: Comparison of utilizing recorded kilometer position and index derived position. Utilizing recorded kilometer position effects the shape perseverance of the measured signal.

Invalid data

According to [64], measurements recorded under the speed of 40 km/h are inaccurate. Figure 3.5 gives an overview of the percentage of the data, for each respective measurement series, collected at a speed below 40 km/h. The average percentage of data below 40 km/h is 9.6%, equivalent to 4.96 km of track. The measurement series from spring 2019 shows a particularly high percentage of low-speed measurements. Figure 3.6 details the speed recorded spring 2019, showing how repeated intervals of data are collected below 40 km/h, not just at the start and end of the measurement series. This pattern is present in all measurement series, however, with different lengths and numbers of low-speed intervals. Figure 3.7 gives a complete overview over numbers of low-speed intervals for each respective measurement series. [1] and [64] remove measurements below 40 km/h completely, an approach adopted by this paper. However, because of the described high number of low-speed intervals, this deletion will introduce new, additional positional shifts between the measurement series. It is unknown if this has been a problem in similar studies such as [1] and [64], or if this applies only specifically to the Bane NOR collected data set. This paper proposes an alternative segmentation procedure to minimize the effects of this introduced shift.

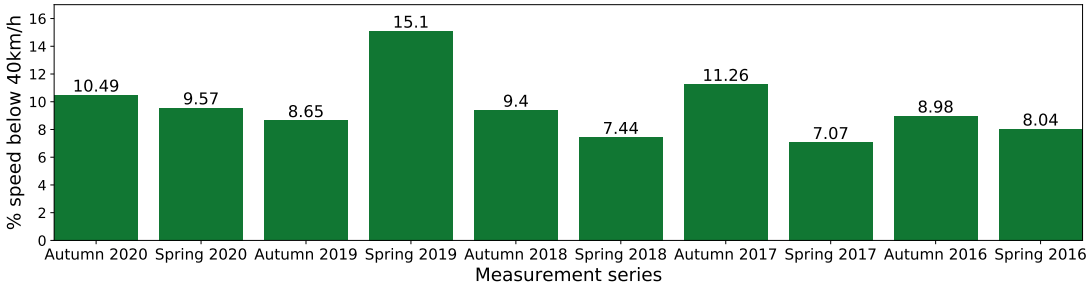

Figure 3.5.: Overview over percentage of data collected below 40km/h for the respective measurement series.

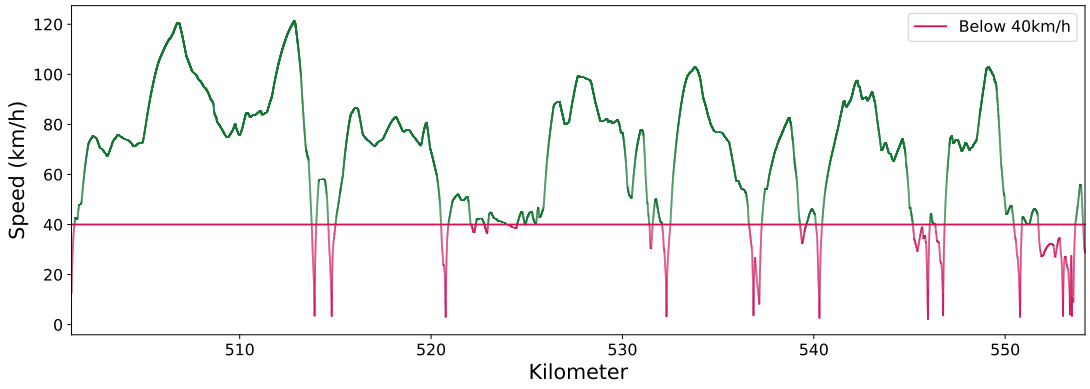

Figure 3.6.: Speed of measurement vehicle under data collection spring 2019. Measurements below 40km/h are highlighted.

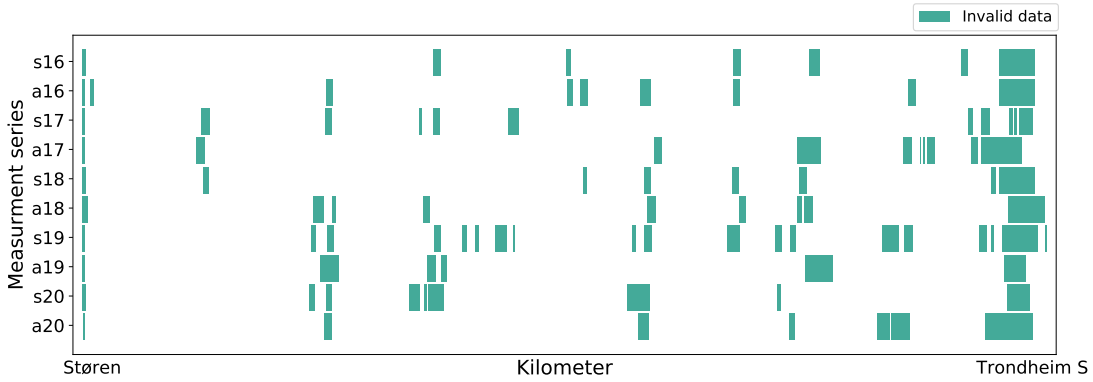

Figure 3.7.: Overview of all intervals where data is collected below 40km/h for the respective measurement series, between Støren and Trondheim.

Start and end position

The exact start and end positions, given in kilometers from Oslo central station, vary. An overview is given in Figure 3.8. Note that measurements collected at a speed below 40km/h have already been disregarded, as discussed above. There are two main approaches for handling the differences in start and end position. One approach is to keep the measurement series as is. As the series undergo alignment, this approach keeps all data based on the assumption that potential position differences imposed by different start and end positions are removed through alignment. By not removing any data, loss of valuable information is avoided. However, when later aligning the measurement series to a reference series, a data reduction can still occur if the chosen reference contains fewer data points compared to the measurement series being aligned.

The alternative approach proposed is to use a common start and end position for all measurement series. This is at the cost of reducing the amount of available data by 2.56%. However, the benefit of this second approach is a minimized initial shift between the series, increasing the likelihood of a successful alignment.

As the objective of this paper is to determine if a shift can be applied to align the different measurement series, the second approach is more favorable, and the data loss can be accepted.

Segmentation

It is common in research papers [1, 13, 20, 65] to segment the measurement series in smaller windows, however different lengths, both constant and varying, are utilized by different papers. This paper proposes three different segmentation methods, where method one utilizes constant segmentation windows, while method two and three utilize adaptive segmentation windows. The properties of the different segmentation methods are discussed and compared, resulting in a preferred selected segmentation procedure.

Method 1
Authors in [1] propose segmenting all measurement series in windows with constant length equal to 1 km, a value adopted by this method. Data points at the end of the measurement series not filling a whole 1 km window are disregarded. Note that disconti-

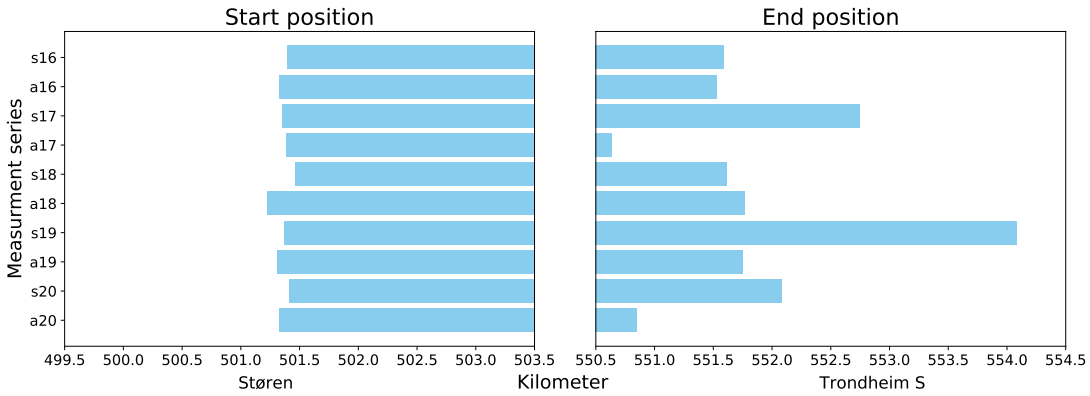

Figure 3.8.: Visualization of start and end position for the different measurement series after removal of all data recorded at a speed below 40 km/h. Here "a" and "s" denote measurement series collected in autumn and spring, respectively. Distances are given as kilometers from Oslo central station.

nuities due to deletion of invalid data will reside within the 1 km segment when utilizing this segmentation method. Measurements are not placed in segments with regard to assigned positional kilometer value, but instead based on the number of valid subsequently measurements such that in total, 2000 valid measurements (one measurement each half meter) are included in each segment.

Method 2

Figure 3.7 provides an overview of the number of intervals present in each measurement series where the speed is below 40km/h. Utilizing this information, an alternative segmentation procedure is proposed. The measurement series are segmented in smaller windows, however, not with constant length, but rather a max length of 1 km. When encountering an interval of data collected at a speed below 40km/h, the current segment is ended, and a new segment started. This applies both for the segment to be aligned and the reference segment, i.e., a new segment is started if there is a discontinuity in either the reference or the series to be aligned. This contributes to the equivalent data residing in a specific measurement series segment and the corresponding references segment, which is necessary to achieve alignment. In addition, the segments are constrained to have a minimum length corresponding to twice the highest shift[3] observed in the data set. This constraint avoids small segmentation windows where no optimal shift can be determined. Figure 3.9 illustrates the obtained segments (in pink) for the measurement series recorded autumn 2019. Notice how both the autumn 2019 and the spring 2020 recording, the latter utilized as reference, need to have valid measurements for a distance longer than the mentioned constraint for the data to be utilized. Figure 3.10 illustrates the same segmentation procedure, however for the measurement series recorded autumn 2020. Notice how the resulting segments for autumn 2020 are not equivalent to the autumn 2019 obtained segments, as expected.

Method 3

Each measurement series utilizes an uniquely adapted segmentation scheme in segmenta-

[3]For illustration purposes, this chapter utilizes the max shift constraint applied in the specialization project [21], namely 250 meters. This constraint is revised in Chapter 4.

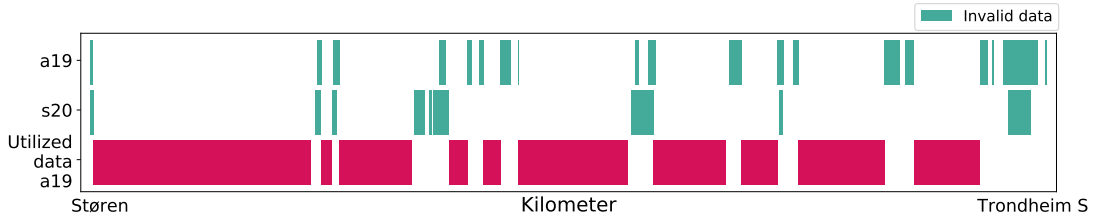

Figure 3.9.: Utilized data (pink) to produce unique segments, following segmentation method 2, for measurement series recorded autumn 2019 compared with reference spring 2020.

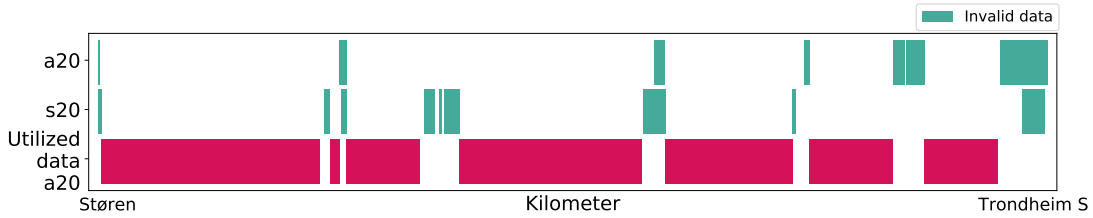

Figure 3.10.: Utilized data (pink) to produce unique segments, following segmentation method 2, for measurement series recorded autumn 2020 compared with reference spring 2020.

tion method two. This, however, becomes problematic when desiring to compare values from all measurement series, as different subsections of the references are utilized. Therefore, this paper proposes an extension to the proposed segmentation method, where this is taken into account. The extension ensures that all measurement series have valid data for a given position, not only the given measurement series and the reference. This is illustrated in Figure 3.11. However, such procedure comes at the cost of high data loss. Compared to method two, where 80.92% of the valid data is utilized, this extension only utilizes 62.46% percent of the data for alignment.
To avoid such high data loss, other methods can be applied to achieve the same property. An alternative is to apply segmentation method two under alignment and thereupon compare all segments to valid data in the reference, adding `None` values where a given measurement series is encountering invalid data.

The proposed adaptive segmentation methods have to the extent of the authors knowledge not been implemented by any other study, except in the related specialization project [21]. The advantage of these approaches is the avoidance of known discontinuities. However, this is at the cost of reducing the amount of available data.

As part of the specialization project [21] underlying this study, alignment with segmentation method one and segmentation method two was tested on gauge measurements, utilizing spring 2016 recording as reference. Independent of the alignment method utilized, segmentation method two produced more accurate results, i.e., scoring a higher warping effect. Hence, applying segmentation method one is not favorable. Further, as the objective of this study is to investigate whether an absolute position mapping between all measurement series is feasible, utilizing segmentation method three is preferred. Although the data loss is higher, simplified implementation is beneficial to determine

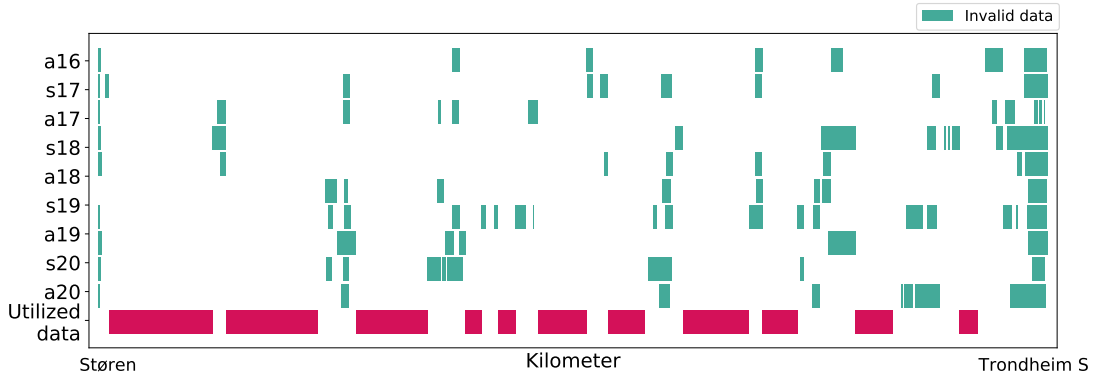

Figure 3.11.: Utilized data (pink) to produce common segments, following segmentation method 3, for all measurement series.

if such mapping can be applied successfully. If this study achieves the desired absolute position mapping, optimization could be proposed as future work.

3.2. Track object records

Information regarding objects along the track is stored in databases. In Bane NOR, the master database for railway infrastructure data is Banedata, and it functions as a centralized system for the whole business. Information from Banedata is utilized throughout the value chain, from planning and building to operation and maintenance. Objects in Banedata can be categorized into six different classes, high voltage, low voltage, superstructure, substructure, signal, and telecommunications.
Today, the location of objects in Banedata is determined based on mileage, which has led to inaccurate positions and misinterpretations of position in some situations. However, in an ongoing project, Bane NOR aims to register the railway track's absolute position based on landscape measurements and thereby increase the accuracy of objects' positions. Due to the ongoing improvements, it is relevant to investigate the possibility of mapping track object records to measurements from the diagnostic train. Such mapping is desirable because it would enable direct connection between objects in Banedata and track data measured by Roger 1000.

The current version of the data in the master database is utilized to conduct the proposed investigation. This is viable because the primary goal is to determine if it is possible to utilize this type of data to achieve absolute alignment.

3.2.1. Superstructure record

Between Støren and Trondheim, there are in total 780 registered fixed points related to superstructure. These points include, among others, built objects such as bridges, tunnels, and level crossings. Objects are either labeled as one point, or with start and end kilometer positions as two separate points. For example, bridges where the train passes underneath are registered as a single bridge point. In contrast, bridges crossed by the train are registered as two separate bridge points, with the bridge's start and end kilometer positions separate. In addition, transition curves are registered as points with corresponding radius, cross-level, and length. A transition curve is used between strait

track and circle curves or between circle curves with different radius and is characterized by a continuous change of radius and cross-level. Transition curves are utilized to achieve smooth transitions, improving passenger comfort, contributing to safety, and lowering wear and tear on the track and the trains. The start and end positions are marked as separate points for each transition curve. The start of the transition curve is the point in the transition where it goes from straight track to transition curve and is named OB [66]. The end of the transition curve is the point where the transition curve has reached the same radius as the circle curve and is named OE. For transition curves between two circle curves, the smallest exhibited radius is labeled as OB, while OE is used for the largest radius that the transition curve exhibits. Counter curves[4] with no straight track between the curves are named FOB and represent a shared OB. Figure 3.12 displays all OB, OE and FOB points between Støren and Trondheim with corresponding curvature value, where $curvature = \frac{1}{radius}$. Notice that cross-level could equivalently have been selected to display the OB, OE, and FOB points and would only deviate from curvature in Figure 3.12 with different values along the y axis.

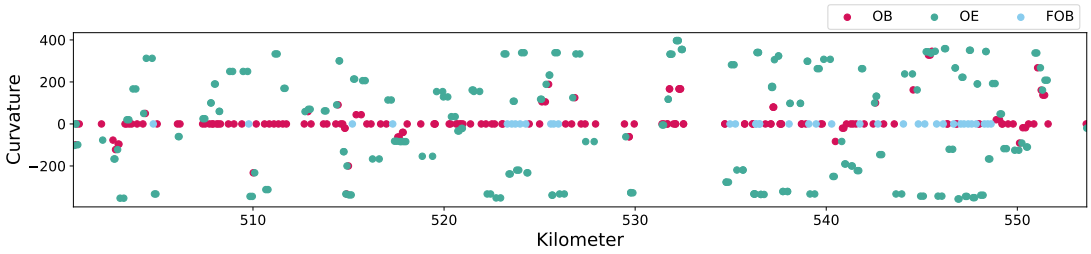

Figure 3.12.: Transition curve points between Støren and Trondheim. OB: start of transition curve, where track transition from straight track to curved or from a smaller curve to curve with greater radius. OE: end of transition curve, where the transition curve has reached the same radius as the (largest) circle curve. FOB: shared OB, occurs with counter curves.

Preprocessing

As curvature and cross-level also are measured by Roger 1000 and therefore present in the track geometry data set, the goal is to investigate the possibility to achieve a mapping between these two data sets. In the following section, preprocessing steps are proposed to enable such mapping.

Interpolation

As the data type is point data, an interpolation method can be applied to construct a continuous version of the same data. The goal is to construct a continuous version that is as equal as possible to the measured data to enable alignment. Based on the characteristics of the measurement data, three simple, low order interpolation methods are proposed, namely interpolation based on nearest value, linear, and second-degree polynomial. The theory behind these methods are covered in Section 2.5.2.

To determine which interpolation method is best suited, each method is compared with measured curvature and cross-level by the Roger 1000 measurement vehicle. These

[4]Two connected circle curves in opposite direction with equal radius.

comparisons are visualized in Figure 3.13 and Figure 3.14 for curvature and cross-level respectively. In Figure 3.14 the absolute value of measured cross-level spring 2020 is utilized due to a difference in definition of cross-level between the measurement vehicle recorded data and the track object record. The track object record does not distinguish upon whether the cross-level is due to left or right rail having the highest position, while measurements from Roger 1000 have a negative sign if the right rail is positioned lowest. Hence, this additional absolute value preprocessing step is necessary to enable alignment between measured and stored cross-level values. Note that although the constructed signal and the measurement vehicle recorded data align well in Figure 3.13 and Figure 3.14, the segment displayed resides close to Støren and hence greater shifts are excepted during recording.

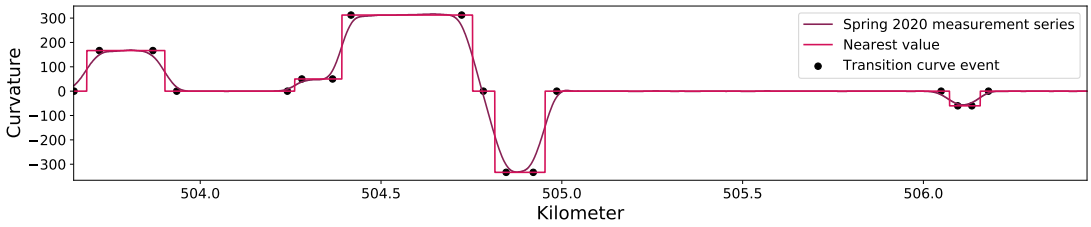

(a) Interpolation based on nearest value between transition curve points with known curvature values compared to measured values spring 2020.

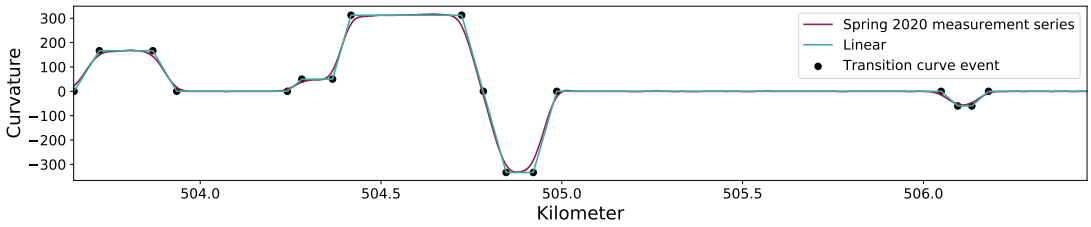

(b) Linear interpolation between transition curve points with known curvature values compared to measured values spring 2020.

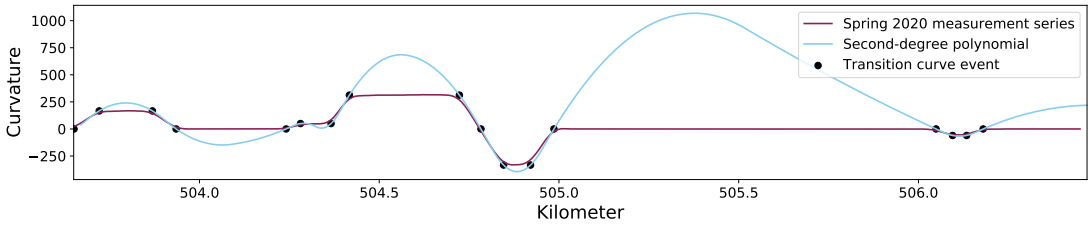

(c) Interpolation with second-degree polynomial between transition curve points with known curvature values compared to measured values spring 2020.

Figure 3.13.: Nearest value, linear and polynomial interpolation methods between transition curve points with curvature values compared to measured values spring 2020 on a subsection of track between Støren and Trondheim.

Visual analysis indicates that the the best match is achieved when utilizing linear interpolation for both measurement channels. To quantify this visual result, euclidean distance is computed between the z-score normalization of the constructed signals and the measured values spring 2020 for the whole studied track section, i.e., between Støren and Trondheim. As covered in Section 2.5.1, z-score normalization removes the difference

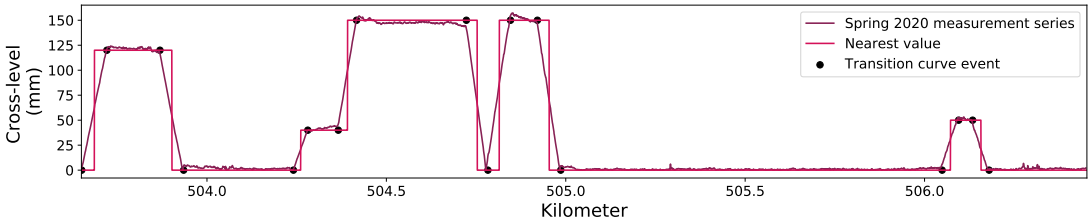

(a) Interpolation based on nearest value between transition curve points with known cross-level values compared to measured values spring 2020.

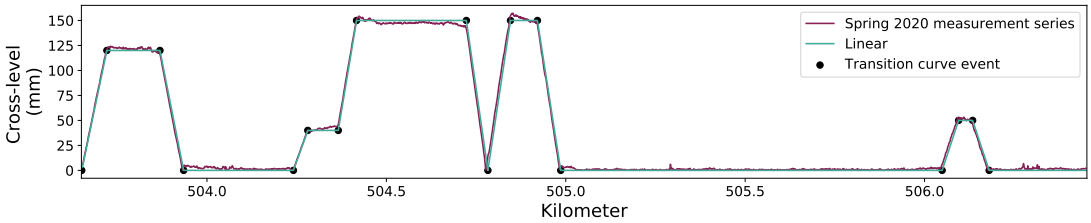

(b) Linear interpolation between transition curve points with known cross-level values compared to measured values spring 2020.

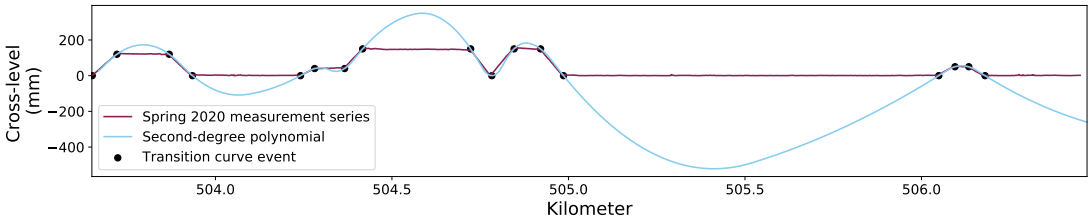

(c) Interpolation with second-degree polynomial between transition curve points with known cross-level values compared to measured values spring 2020.

Figure 3.14.: Nearest value, linear and polynomial interpolation methods between transition curve points with cross-level values compared to measured values spring 2020, on a subsection of track between Støren and Trondheim.

in magnitude, making it possible to compare euclidean distance for the different measurement channels. Euclidean distance is utilized rather than simplicity value as the goal is to achieve minimum distance between each measurement value in the measurement recording and the corresponding measurement value in the constructed signal. For curvature, euclidean distance is respectively 173.7216, 154.3810, and 300.7612 for interpolation based on nearest value, linear interpolation, and second-degree polynomial. Similar for cross-level, euclidean distance is measured to 294.9080, 279.4165, and 330.3409 for the different interpolation methods. Hence, based on the computed euclidean distance, linear interpolation yields the most similar result between the constructed and recorded measurements and is, therefore, the proposed interpolation method to be utilized on this data.

Lowest euclidean distance when comparing measurement channels is achieved for curvature, i.e., the deviation in distance between the constructed curvature signal and the measured curvature is smaller then for the constructed cross-level signal and measured cross-level. However, as stated in the introduction, this study aims to determine if it is possible to utilize this type of data to achieve absolute alignment, not to determine

each method's accuracy. Therefore alignment is proposed tested with both measurement channels.

3.2.2. High voltage mast record

Between Støren and Trondheim, there are in total 1602 registered masts. Every mast is labeled with detailed information including, among other, kilometer position, placement relative to track (right or left), which railway track the mast belongs to (main track, train track, side track or other track), height, material, stagger, curvature and cross-level. For the studied section, right- and left-hand side in record correspond to right- and left-hand side when traveling towards Trondheim.

Preprocessing

Stagger, height, curvature, and cross-level are all measured by Roger 1000, and hence a mapping similar to that proposed for the superstructure record is relevant to investigate. A prerequisite for such mapping is determining which track lines the measurement vehicle has used such that only the corresponding pole or gantry are selected from record.

Detection of driven track line
As each pole and gantry characteristic is unique, it is essential to ensure comparison between equivalent masts, i.e., between the mast passed by the measurement vehicle and the corresponding mast in record. As depicted in Figure 3.1a, the majority of track between Støren and Trondheim consists only of a single track line, and hence extracting correct masts from record is trivial. However, in close proximity to stations, two or more track lines are present. Since no data exists stating which of these tracks Roger 1000 used, an alternative detection method needs to be derived. This study investigates three approaches for detecting driven track line, namely based on measured stagger, assumptions linked to train speed, and GPS. These methods are presented through examples utilizing data recorded spring 2020 by Roger 1000, hence residing in the track geometry data set covered in Section 3.1.

A subsection of track is selected where only one or two track lines are present in parallel to simplify this investigation. This constraint applies to track lines in close proximity to Trondheim, and hence all data is disregarded after 548.927 kilometers from Oslo central station, i.e., between Stavne and Trondheim station. In addition, this applies to Støren and Heimdal stations. Hence, due to the applied boundaries, the studied subsection of track consists of six locations where two track lines reside in parallel, namely at Hovin, Lundamo, Ler, Søberg, Melhus, Nypan, and Selsbakk stations.

The first proposed approach creates a mast characteristic pattern of stagger and corresponding kilometer value for the different track types at the named locations where two track lines reside in parallel. The aim is to compare these characteristics with the stagger measured by the measurement vehicle and thereby determine which track line the measurement vehicle has utilized. Figure 3.15 visualizes an example of how such a characteristics looks like for the train track and main track at Hovin station.

Unfortunately, stagger values cannot blindly be extracted based on its label in the record to create such characteristics. Due to irregularities and errors in the record, both human manual check and rule based manipulation is necessary. In the mast record, the sign

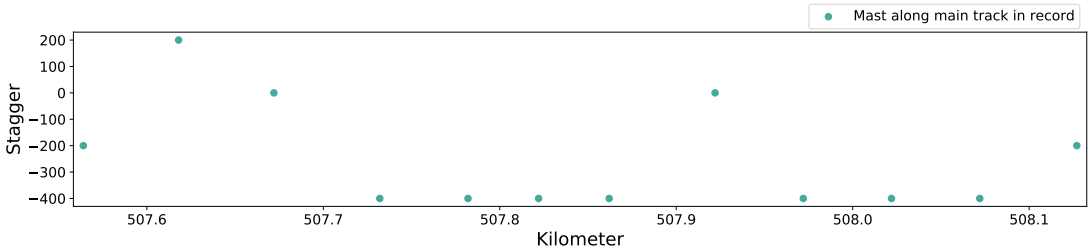

(a) Stagger at corresponding kilometer position for mast along the main track at Hovin station.

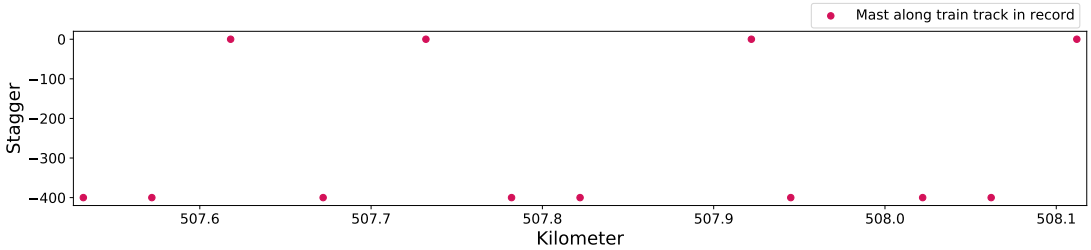

(b) Stagger at corresponding kilometer position for mast along the train track at Hovin station.

Figure 3.15.: Mast characteristics at Hovin station for the two track lines residing in parallel. Notice that the kilometer position and induced stagger vary for some of the masts along the main track and train track. These differences can be utilized when compared with measured stagger to determine which track the measurement vehicle has utilized.

in front of stagger is based on whether the steady arm is of type pull- or push-off (see Section 2.2.2), not regarding whether the pole is placed on the left- or right-hand side of the track. This creates a mismatch between the measured stagger by the measurement vehicle and the stagger registered in record. A solution is changing the sign of all stagger measurements in the record for poles placed on the right-hand side of the track. In situations where the cantilever is connected to gantry, irregularities between utilized sign and the type of steady arm are discovered. Additional errors are also discovered for specific masts constructions, handled in a later section.

For Hovin station, which is studied in Figure 3.15, stagger values have been modified based on registered side of track position. Additionally, after a manual check, the side position of masts located at 507.732, 507.783 and 507.822 kilometers have been corrected. For the illustrated mast characteristics in Figure 3.15, these modifications have already been applied. The detected anomalies raise suspicions towards the quality of the data set, discussed in the next section.

Stagger measurements from record are utilized rather than height, curvature, or cross-level as the listed measurements are less unique for a specific mast. Tracks in parallel often have masts at the same kilometer position and hence share curvature and cross-level. Height varies little between masts, especially when the cantilevers are mounted to gantry, where mast height is equal. The same justification applies for matching positions of maxima and minima in measured stagger with mast kilometer position, as the masts often have the same kilometers position for both track lines in parallel. Notice that these remarks only apply to detect driven track lines. In other utilization of the data set, these

remarks do not apply.

To determine which characteristic matches with the recorded stagger spring 2020, the characteristics and measured stagger are compared in Figure 3.16. It can be observed that the best match is achieved for the masts along the main track, and hence for Hovin station, it can be concluded that the measurement vehicle utilized the main track. It cannot be expected to achieve a complete overlap due to inaccurate kilometer positions for both data sets and environmental effects impacting measured stagger, covered in Section 2.2.2. Performing the described matching analysis for all six stations concludes that the measurement vehicle has used the main track at all stations.

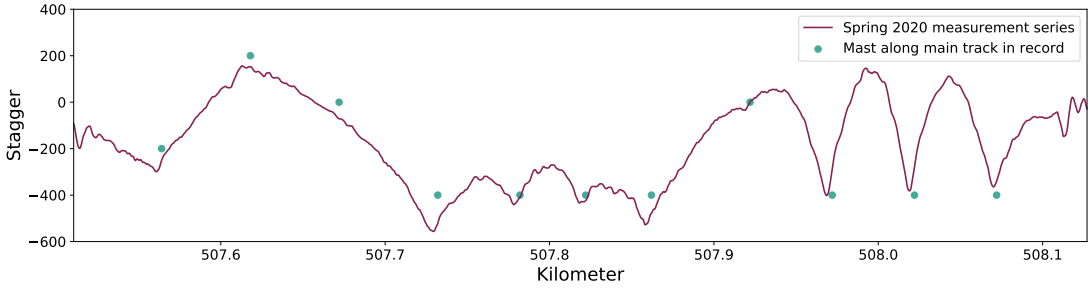

(a) Mast characteristics along the main track.

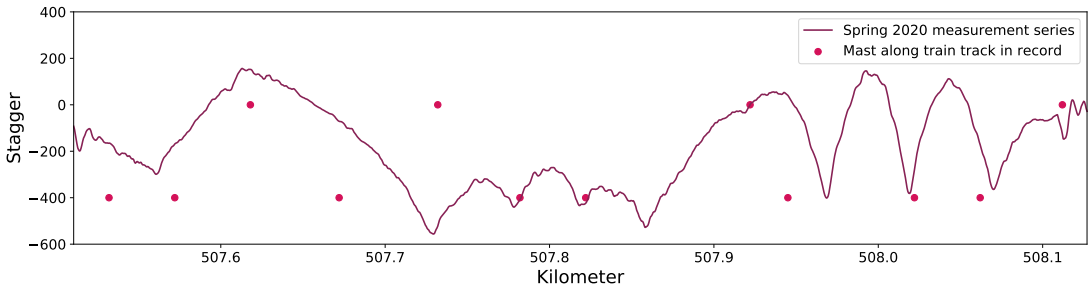

(b) Mast characteristic along the train track.

Figure 3.16.: Comparison of mast characteristics and measured stagger spring 2020. Mast are differentiated based on residing on the track's left- or right-hand side.

Alternatively, a method based on the speed of the measurement vehicle is proposed. This method compares the recorded speed of the measurement vehicle with locations along the track where more than one track line is present. It is assumed that if the speed of the measurement vehicle is below 20 km/h, the measurement vehicle has used side tracks at these locations. Knowing that the track section is subject to frequent traffic, it is realistic to assume that the measurement vehicle has had to use side tracks to give priority to trains driving in the opposite direction.

In the high voltage pole record, the track type for each mast is recorded as either main track, train track, side track, or other track. In sections with only one track line, the masts have track-type main track. Hence, this yields selecting masts along the train track when the measurement vehicle passes stations below the described speed assumption and main track masts if passing stations at higher speeds. Figure 3.17 depicts the

described analysis for the measurements collected spring 2020. Based on the described assumption, it is assumed that under the measurement recording spring 2020, Roger 1000 has used train tracks at Lundamo, Ler, and Melhus stations, otherwise the main track.

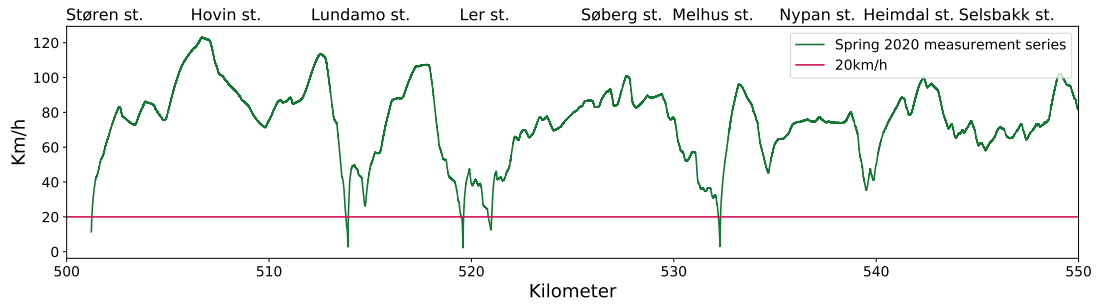

Figure 3.17.: Speed of measurement vehicle spring 2020 between Støren station and Selsbakk station, compared to locations with parallel track lines.

The third proposed method utilizes the GPS coordinates recorded by the measurement vehicle spring 2020. Plotting all extracted coordinates and visually evaluating driven passage at stations determines utilized track. By comparing driven track with the definition of track-types in record, it can be concluded on driven track. Figure 3.18 illustrates such visual analysis at Hovin station, where the GPS coordinates follow the outermost track. Conducting the same evaluation at all stations leads to the conclusion that the main track has been utilized at all stations.

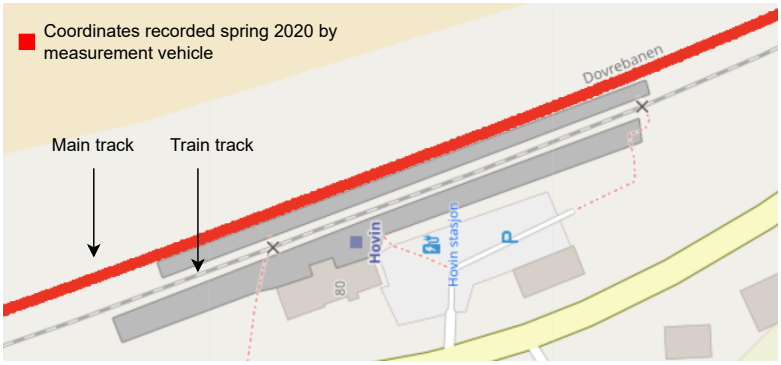

Figure 3.18.: Visual analysis of utilized track line at Hovin station, based on coordinates from measurement vehicle spring 2020. It can be observed that the coordinates from the measurement vehicle are located along the main track and hence concluded that the main track line was utilized at this station.

The three proposed detection methods are evaluated and compared to determine best practice. Comparing the results from the three methods, selecting driven track based on measured stagger and GPS yields the same result. As both methods produce the same result and do not rely on any assumptions, contrary to the method based on measured speed, it is assumed that these methods' result is correct. Initially, a constraint was set on the number of parallel track lines and hence the stations Støren, Heimdal, and the track between Stavne and Trondheim station were not included in the evaluation.

Both methods are however capable of detecting driven track lines independent of the number of lines present, contrary to the method based on speed. However, the record is shortcoming, and it is impossible to sufficiently distinguish the tracks in record based on track type and track number. Hence, improvements to the record is necessary to be able to utilize the high voltage record at the named sections. The uncertainty in environmental conditions when measuring stagger and the detected anomalies in record make selecting driven track based on stagger error-prone and time-consuming. Hence, with GPS available, detecting driven tracks based on coordinate data is preferred. In addition, due to the high update frequency of the GPS, if an anomaly coordinate was to occur, the method is more robust and thereby less affected by such data. A disadvantage with GPS-based track line detection is when the GPS signal is missing, i.e., in tunnels. If driven track line needs to be detected and GPS signal is missing, it is possible to revert to the procedure based on stagger measurements. The latter is not a scenario present on the studied track section.

Anomaly and missing data detection

Although procedures detailed above successfully detect the driven track line, several anomalies and situations with missing data were observed. Hence, blindly selecting mast based on track type will induce undesired errors. Therefore, this section proposes a method to limit errors due to falsely classified masts. Records are created through human input and hence subject to error. In addition, specific mast construction create exceptions to the defined labeling convention, resulting in anomalies or missing data.

Two such constructions are selected from the studied track section as examples, depicted in Figure 3.19. In Figure 3.19a mast EH-MAS-023298 at Søberg station is shown. The cantilever for both tracks is mounted to a single-pole placed along the train track. In record, this mast is only registered once, with track-type train track. Hence data for the cantilever positioned above the main track is missing from the record. In Figure 3.19b masts EH-MAS-023371 (left) and EH-MAS-023370 (right) at Melhus station are depict. Both masts are labeled along the main track, respectively on the track's left- and right-hand side. It can be visually observed that the main track has cantilever both from the left and right mast and that the left mast also carries cantilevers for the train track. Hence in this situation, it can neither be determined data for the train track cantilever nor determined which of the entered data for the main track is applicable.

This study proposes utilizing the length between succeeding poles to compare with specified span length in record to flag the described anomalies. An exception is raised if deviations between specified span length and kilometer position are above ten meters. This slack is utilized to filter out minor errors in registration of position or span length, as the goal is to detect missing or duplicated masts, not verify the accuracy of the data set. Flagged exceptions require a manual check to conclude the error's cause and appropriate action.

For the masts along the driven track spring 2020, the proposed detection method flags 34 out of 964 masts. A manual review of all these raised exceptions, results in detecting nine falsely selected masts and six missing masts. The rest, the majority of the raised exceptions, are after manual checking assumed to be due to errors in either recorded position or span length value. Both mast constructions studied in Figure 3.19 were detected as anomalies with the proposed method. In seven of the nine cases of falsely selected masts, it is possible, based on cantilever type, to remove the assumed duplicate

(a) EH-MAS-023298 mast at Søberg station. One pole supplies both tracks with cantilever.

(b) EH-MAS-023371 (left) and EH-MAS-023370 (right) masts at Melhus station. Two masts supply the right track line with cantilever.

Figure 3.19.: Examples of mast constructions that cause error in record. Pictures extracted from Gule Sider [2].

masts. This is due to one of the duplicate masts having cantilever type undefined, and is therefore assumed to be a redundant mast. For all six missing masts, it is possible to add the kilometer position, height, curvature, and cross-level of the detected missing mast due to the assumption that these values are shared with the mast present in parallel, supplying the other track. However, other data regarding the detected missing mast, e.g., stagger, cannot be determined.

Data construction

As in Section 3.2.1, it is desirable to create a continuous version of the mast values from the record. The utilized masts are extracted based on the detected driven track line and adjusted using the described anomaly detection procedure. This section investigates which interpolation method yields the most similar mapping between a constructed signal based on the mast record and measured values from the track geometry data set. Other data construction methods are explored in situations where interpolation methods are insufficient. As mentioned initially, stagger, height, curvature, and cross-level are all measured by Roger 1000 and are relevant to consider in these mappings.

Figure 3.20 depicts a comparison between respectively cross-level and height values from the high voltage mast record and measured cross-level and height by the measurement vehicle passing the corresponding masts. When comparing recorded and measured cross-level, Figure 3.20a shows high deviation in amplitude between measured and recorded values. This high deviation is present across the studied track section, i.e., between Støren and Trondheim, although some masts are recorded with a cross-level value unequal to zero. For contact wire height, Figure 3.20b shows a constant height for the majority of the masts in the record, making a mapping unfeasible. Hence, due to the characteristics of this data, neither interpolation methods nor other construction methods are possible to apply to enable alignment utilizing these measurement channels.

For curvature, Figure 3.21 compares interpolation based on nearest value, linear interpolation and second-degree polynomial. This is the same selection of methods as analyzed in Section 3.2.1, and as the characteristics of the data are similar, the same methods are proposed here. The absolute values of measured curvature spring 2020 and curvature in the high voltage mast records are utilized due to the difference in the definition of

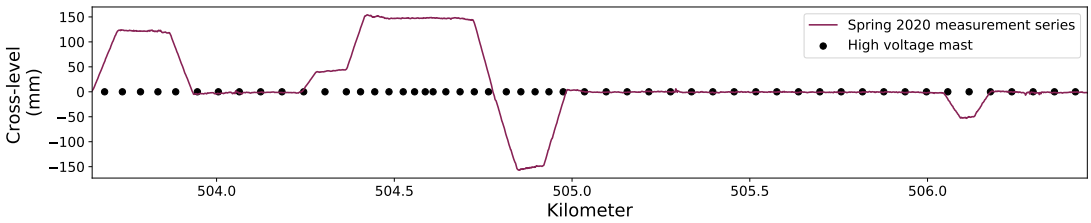

(a) High voltage masts with recorded cross-level compared to measured values spring 2020.

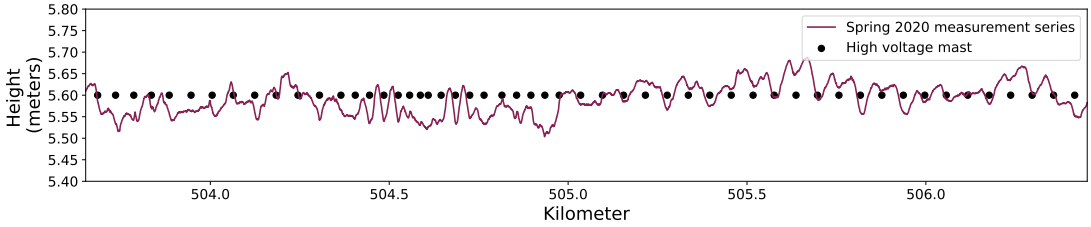

(b) High voltage masts with recorded contact wire height compared to measured values spring 2020.

Figure 3.20.: Comparison between measured cross-level and height of contact wire with values in the high voltage mast record. Figures displaying data for a subsection of track between Støren and Trondheim.

curvature between the data from the measurement vehicle and the high voltage mast record. The high voltage mast record sporadically varies between distinguishing and not distinguishing if the track curves left or right. In contrast, Roger 1000 distinguishes between curving directions utilizing positive and negative signs. Hence, this additional absolute value preprocessing step is necessary to enable alignment between measured and stored curvature values.

Visual analysis yields best match between recorded and constructed data when linear interpolation is utilized. Euclidean distance between the z-score normalization of the constructed signal and measured values results in distances 333.7480, 325.2568, and 336.1348 for interpolation based on nearest value, linear interpolation, and second-degree polynomial, respectively. Hence, linear interpolation is most suited to construct a signal similar to the measured curvature data.

In Figure 3.22, stagger from the record is compared with stagger measured by the measurement vehicle while passing the corresponding masts. As discussed under detection of driven track line, the sign of stagger for mast placed on the right-hand side of the track is inverted. Due to the studied subsection of track in Figure 3.22 residing between stations, only one track line is present. Hence, no cantilever is connected to gantry, reducing the possibility of falsely labeled mast side information in the record.

Two distinguishable patterns between stagger from the record and measured stagger can be observed in Figure 3.22. As discussed in Section 2.2.2, on curved track, curvature and cross-level will naturally induce stagger. As expected, when comparing measured stagger with measured curvature in Figure 3.22, a correlation between the observed patterns and curvature can be observed. On straight track i.e., zero curvature, stagger closely resembles a triangular pulse. While on curved track, a second-degree polynomial

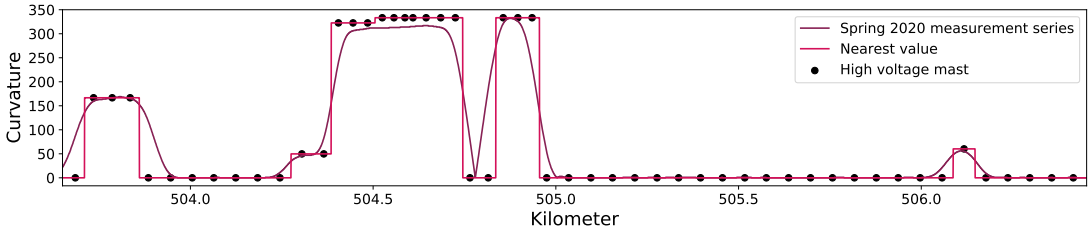

(a) Interpolation based on nearest value between high voltage masts with known curvature values compared to measured values spring 2020.

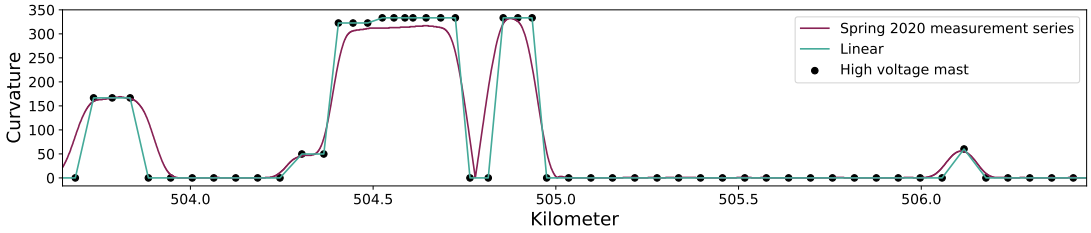

(b) Linear interpolation between high voltage masts with known curvature values compared to measured values spring 2020.

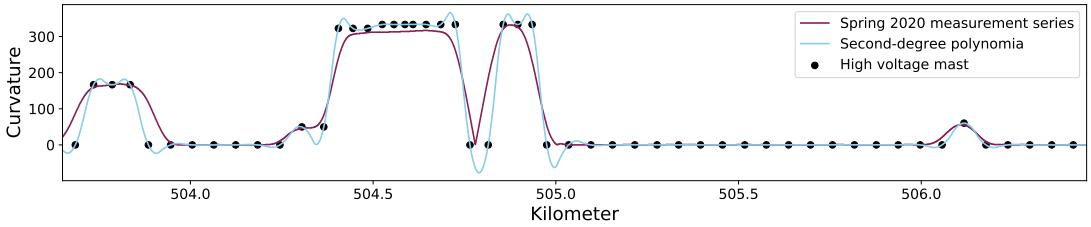

(c) Interpolation with second-degree polynomial between high voltage masts with known curvature values compared to measured values spring 2020.

Figure 3.21.: Nearest value, linear and polynomial interpolation methods between high voltage masts with curvature values compared to measured values spring 2020. Figures display a subsection of track between Støren and Trondheim.

between high voltage masts resembles measured stagger by the measurement vehicle. Due to these different characteristics, an alternative approach to interpolation to facilitate matching between the data sets is proposed.

In Figure 3.22 it can be observed that where there is a mast in record, measured stagger is either at a maxima, minima or equal to zero, in line with the theory presented in Section 2.2.2. Masts in record with stagger equal to zero occur on strait track. However, there are exceptions, for example at ca. 505.5 kilometers in Figure 3.22. Due to these exceptions, only local minima and maxima are extracted as assumed mast positions from the measurement vehicle recorded stagger, see Figure 3.23. As inaccuracies in measured stagger occur due to vibrations caused by wheel-rail interaction, see Section 2.2.2, local minima and maxima are extracted on a selected interval length. Selecting a too short interval length increases the chance of incorrect selection due to noise, while selecting a too wide interval length increases the chance of not detecting masts. Although the theoretical standard span length between two adjacent masts is between 50 and 70 meters [27], the deviation from this range in the studied data set is high. Figure 3.24

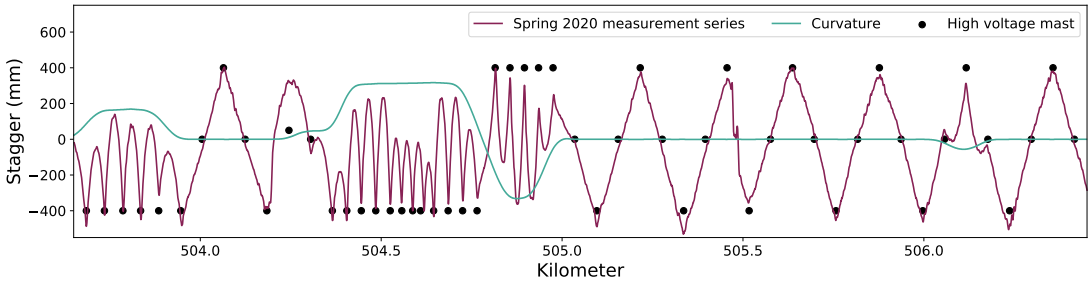

Figure 3.22.: High voltage mast with recorded stagger compared to measured stagger and curvature spring 2020.

depicts a histogram over span lengths between all adjacent masts, showing that 95% of all span lengths are between 24 and 64 meters. Based on this, local minima and maxima are extracted with a minimum distance requirement to the neighboring local minima or maxima equal to 24-meters. This requirement is enforced by utilizing the order parameter in conjunction with the argrelextrema function, provided by scipy [67], for extracting assumed mast positions.

On curved track, it can be observed in Figure 3.22 that for positive curvature, representing a right-hand curve, the masts are located where stagger is at a minimum, while in a left-hand curve, the masts are located at maximum stagger. This observation is applied to the extracted minima and maxima, yielding in the assumed high voltage mast position depicted in Figure 3.25. Although this procedure does not detect all the masts in the record, for example masts where stagger is equal to zero, the extracted position enables an investigation into whether matching algorithms can be applied between the high voltage masts in record and the extracted positions from the measured stagger, see Section 4.2.2.

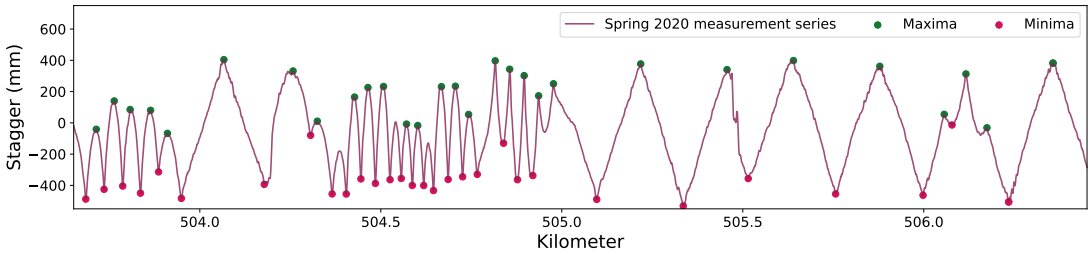

Figure 3.23.: Local minima and maxima in measured stagger spring 2020 with a minimum distance requirement to neighbouring minima/maxima equal to 24 meters. The studied track section in this figure is a subsection of the track between Støren and Trondheim.

To conclude, with the proposed data construction methods, investigation into mapping between measured and recorded stagger and curvature is enabled. This section has found that data for cross-level and contact wire height is not appropriate to use for such mappings.

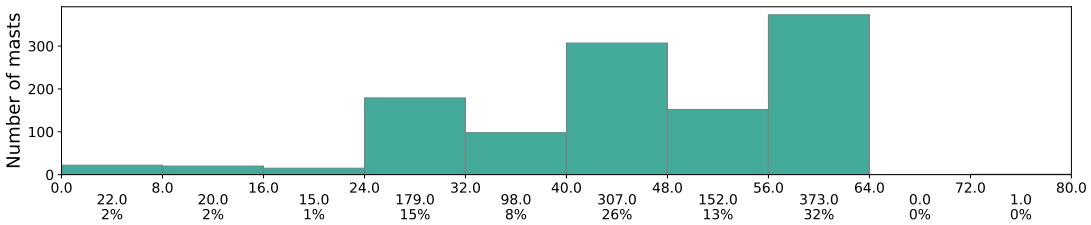

Figure 3.24.: Histogram of span length between adjacent mast. 95% of the masts along the driven track spring 2020 have a span length between 24 and 64 meters.

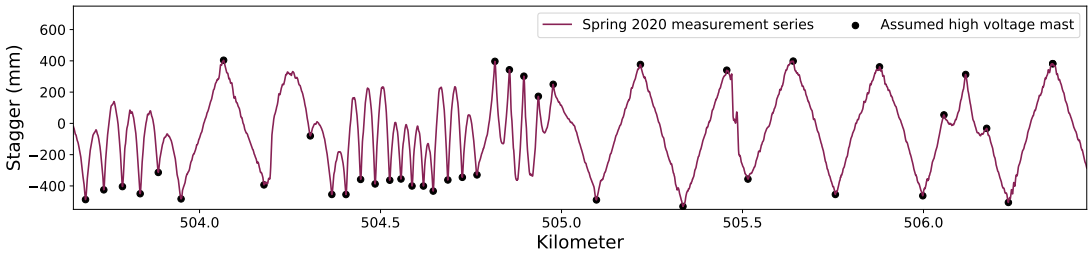

Figure 3.25.: Assumed high voltage mast position and stagger based on minimum and maximum measured stagger and curvature recorded spring 2020. The Figure displaying a subsection of track between Støren and Trondheim.

4. Method

The aim is to develop a method that takes the preprocessed track geometry data and track object records from Chapter 3 as input and generates aligned measurement data mapped to its true absolute position. To simplify, the development of this method is split into two consecutive steps. First, methods are proposed for relative positioning between recorded measurement series and, thereupon, for mapping the relative aligned measurement series to its true position. This setup is depicted in Figure 4.1. The optimal method is obtained by evaluating the results from all proposed methods in Chapter 5. The data utilized in this chapter, if not stated otherwise, is preprocessed according to the procedure presented in Chapter 3.

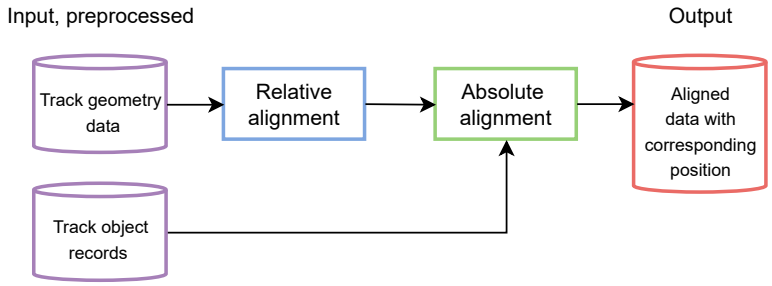

Figure 4.1.: Proposed structure of method to achieve aligned measurement series with corresponding absolute position. Pre-processed track geometry data and track object records are utilized as input.

4.1. Relative position alignment

As part of the specialization project [21] completed prior to this master thesis, relative position adjustment on the same sub-section of track was investigated. However, the feedback from reviewers on this work and an increased time frame have resulted in improvements to the original work, detailed in this section.

4.1.1. Reference data set

In the related specialization project [21], measurements collected spring 2016 were utilized as reference in line with the selection procedure proposed by [1], covered in Section 2.3.1. The procedure entails comparing mean correlation coefficients for the left rail longitudinal level measurements, utilizing each measurement series separately as reference. However, a reviewer highlighted that aligning two respective input series with too low correlation coefficient is unreliable. As longitudinal level measurements are highly impacted by degradation, values vary noticeably between measurement recordings. The reviewer proposed utilizing gauge, curvature, or cross-level measurement channels, as

these measurements are less exposed to degradation. This proposal is taken into account, and an improved reference series selection procedure is applied.

Mean correlation coefficients are computed segment-wise on the preprocessed data. This is beneficial as it uses the same data format as for alignment, thereby avoiding inducing bias. As stated in Section 3.1, GPS sensor signals from the utilized measurement vehicle were updated before 2020 recordings, increasing the GPS accuracy. To benefit from this updated positioning, it is desirable to align the other measurement series as accurately as possible to either spring or autumn 2020 recordings. Therefore, mean correlation coefficients are computed where both these recordings are utilized as reference for cross-level, curvature, and gauge measurement channels, respectively. An overview of the resulting mean correlation coefficients is given in Figure 4.2. It can be observed that mean correlation coefficients are higher when utilizing the spring 2020 recording as reference, independent of the measurement channel utilized. Therefore, spring 2020 is utilized as reference series.

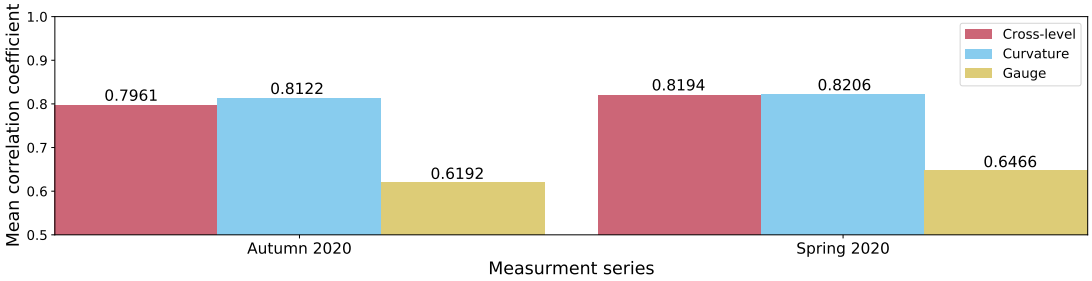

Figure 4.2.: Mean correlation coefficient when correlating measurements recorded spring and autumn 2020 with all other conducted recordings. The highest mean correlation coefficient was achieved with spring 2020 measurements, and hence this recording is proposed utilized as reference.

4.1.2. Measurement channel

As discussed in Section 2.3.2, previous studies have performed alignment based on a variety of different track measurement channels. In the related specialization project [21], gauge measurement data was utilized based on the findings in [1]. However, as the success of the alignment methods strongly depends on the choice of measurement channel, this section aims to select the most suited measurement channel based on a thorough evaluation.

There are twelve measurement channels for which measurements have been recorded for all ten available measurement series and hence relevant channels to utilize under alignment. This includes deviation in longitudinal level for right and left rail, deviation in alignment for right and left rail, twist on a basis of two and nine meters, cross-level, gauge, curvature, stagger, height, and inclination. To evaluate the performance of these measurement channels, alignment is conducted, and the resulting shifts are compared. To simplify the investigation, only the Cross-Correlation Function with a max shift constraint equal to 250 meters is utilized under alignment. CCF and the max shift constraint are chosen both based on the results obtained in the related specialization project [21] and due to the method finding a constant shift, making comparison of shifts feasible.

The mentioned method and constraint, and the found optimal reference series recorded spring 2020 are utilized throughout this subsection to detect the optimal measurement channel(s). Shift is unfeasible to compute for the height of overhead contact lines due to their constant height and is therefore excluded from the evaluation. Figure 4.3 shows a comparison of detected shifts when aligning the measurement series recorded autumn 2019 with the chosen reference series, utilizing all the different measurement channels. It can be observed that the detected shift is not identical for the different measurement channels. The root cause of these deviations is the lack of a true mapping between the compared recordings. For example, high degradation can impact the measurements series to such a degree that the alignment algorithm fails to locate the actual shift present. The nature of the measured variable can also create complications for alignment. For example, in theory, curvature is a well-suited measurement channel for alignment due to the low degradation present between recordings. However, in situations with no curvature within a segment, shift will be impossible to detect.

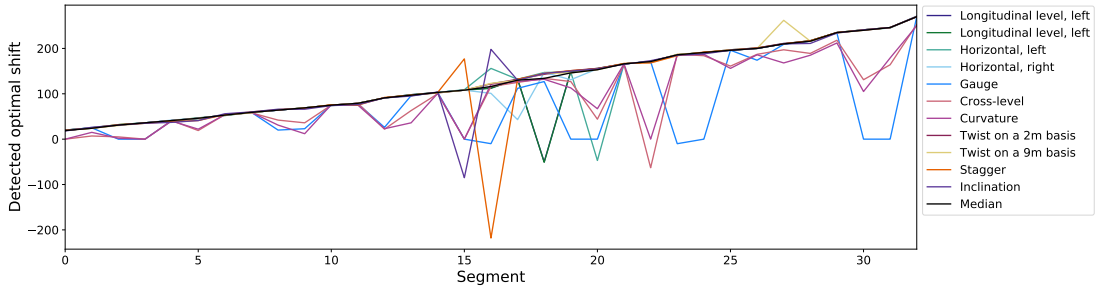

Figure 4.3.: Detected shifts for all available measurement channels for data recorded autumn 2019, computed utilizing CCF.

The statistical median computed based on all detected shifts is included in Figure 4.3. It can be observed that the median shift is increasing almost linearly with the recorded position from Støren to Trondheim. Assuming that the statistical median represents the overall ideal shift, a measurement channel can be selected based on the minimum deviation from the statistical median. This assumption is based on the fact that the statistical median is computed based on results from all eleven different measurement channels, thereby achieving robustness towards outliers. However, to further substantiate this assumption, the detected shifts are applied, and the resulting alignment is evaluated utilizing warping effect.

With the proposed assumption, it is expected that the highest warping effect is achieved when applying the median shift. As the measurement channels are also used in the warping effect computation, all the detected shifts, including median shift, are evaluated separately based on the eleven available measurement channels, see Figure 4.4. Notice here that achieved value for warping effect when utilizing different measurement channels in the evaluation metric cannot be compared, as factors like degradation will impact achieved value. However, values can be compared when utilizing the same measurement channel in the evaluation metric while determining shifts with various measurement channels. Hence, although evaluating alignment on curvature, cant, and gauge results in a high warping effect, this suggests only that these channels are less affected by degradation. Accumulating the achieved warping effect for each found shift in Figure 4.4 yields a marginally higher score in total for median shift compared to shifts detected with the various individual channels, strengthening the proposed assumption.

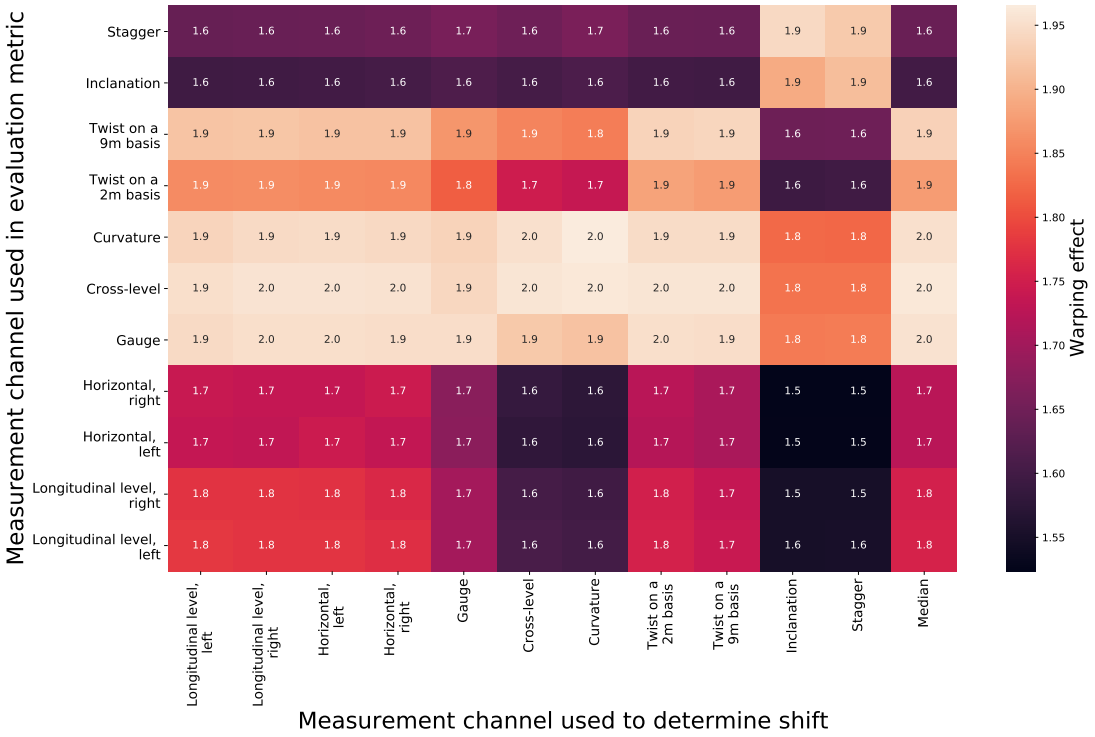

Figure 4.4.: Heat map displaying achieved warping effect evaluated on all available measurement channels compared to which measurement channel (including median of all) has been utilized to determine shift.

Comparing each alignment only with the warping effect obtained from the measurement channel it was aligned with, yields accumulated the highest total warping effect. However, this does not consider the induced bias that arises when both aligning and evaluating on the same measurement channel. The high warping effect comes at the expense of robustness.

Further, Figure 4.4 shows a mismatch between alignment with track geometry and contact wire geometry parameters (stagger and inclination). Shifts found with track geometry parameters score low warping effect when evaluated on stagger and inclination compared to the other track parameters, and vice versa. Although contact wire geometry parameters reside in a separate data set, the measurements are recorded simultaneously and mapped utilizing the Spacesync parameter that both data sets utilize namely for this purpose. A plausible explanation for this observation could be the sensor placement on the measurement vehicle. As Roger 1000 is 23.9 meters long, differences in sensor location would induce a positional shift. If this is the case, it is expected that the deviation in found shift has a constant length in the same direction. To verify this explanation, shift is computed utilizing gauge measurement channel and visualized on stagger measurements for verification. Figure 4.5a shows recorded stagger autumn 2020 compared to the reference prior to alignment, while in Figure 4.5b the detected shift of 11 meters in direction left is applied. In Figure 4.5b a deviation is observed between the recorded measurement series autumn 2020 and reference, where it would be expected that for an optimal match, the applied shift should be smaller.

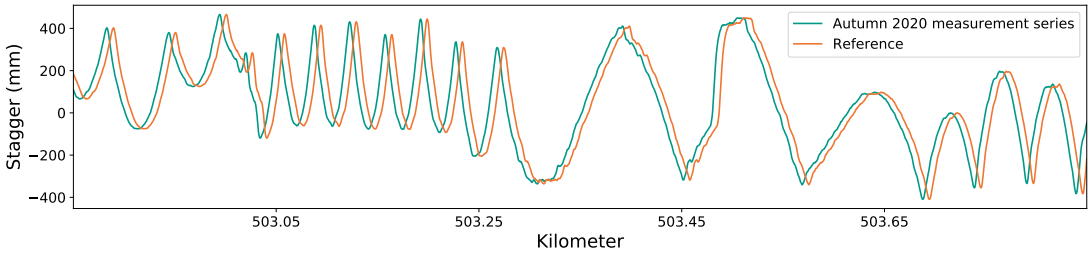

(a) Measured stagger autumn 2020, compared to the reference.

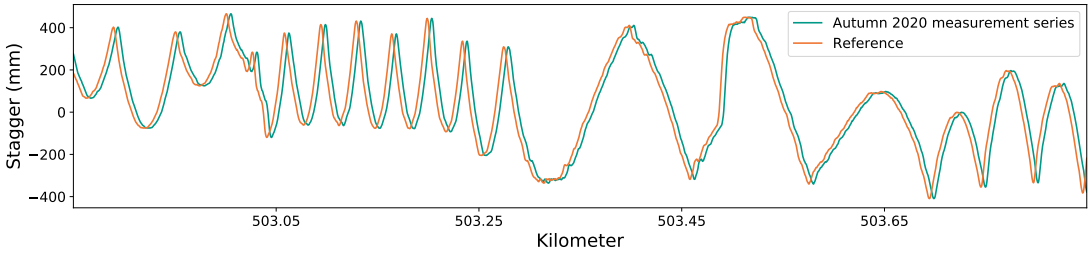

(b) Measured stagger autumn 2020 after applying shift, compared to the reference.

Figure 4.5.: Shift found for gauge measurement channel applied to measured stagger for a subsection of track between Støren and Trondheim. The applied shift should be smaller to achieve optimal match.

For comparison, Figure 4.6 displays the same segment, but rather comparing the references with the measurement series recorded spring 2017. In Figure 4.6b the detected shift of 5 meters in left direction is applied. However, it would be expected that for an optimal match, the applied shift should be greater. Hence, it has been shown that the necessary correction shift that needs to be applied, has the opposite direction. Assuming that the actual placement of the sensor itself on the measurement vehicle has not changed and knowing that the measurements have been recorded in the same driving direction, ensured in Section 3.1, it can be concluded that sensor placement is not the cause of the observed mismatch and hence no constant shift can be utilized for correction.

Measured stagger will vary between measurement recordings in small sections of the track due to variation in driven track line, see Section 3.2.2. In addition, environmental conditions impact measured stagger, see Section 2.2.2. Due to these uncertainties and the observed mismatch between track geometry parameters and contact wire geometry parameters, it is concluded that it is neither desirable to detect alignment solely based on stagger nor on inclination. In addition, the median shift is computed based on all measurement channels, including stagger and inclination, and compared with the median shift computed on all measurement channels, excluding stagger and inclination. Independently of measurement channel evaluated on, a higher average warping effect is achieved for median shift computed without stagger and inclination. Based on these findings, stagger and inclination are not suited to determine shift and hence excluded from further evaluation.

Revisiting the strengthened assumption that the statistical median (excluding stagger and inclination) represents the overall ideal shift, the measurement channel most similar to the statistical median can be selected based on minimum deviation from the statis-

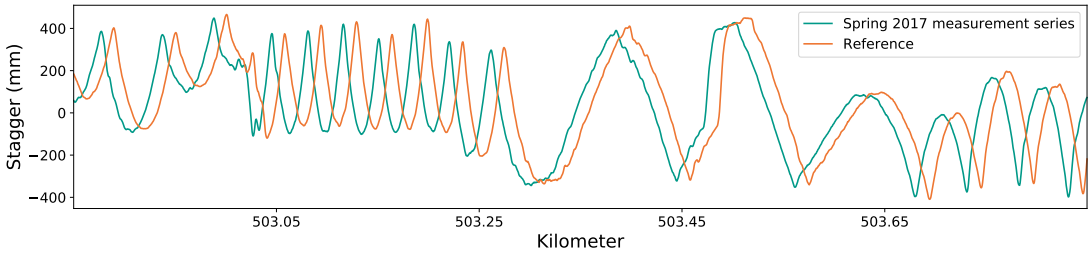

(a) Measured stagger spring 2017, compared to the reference.

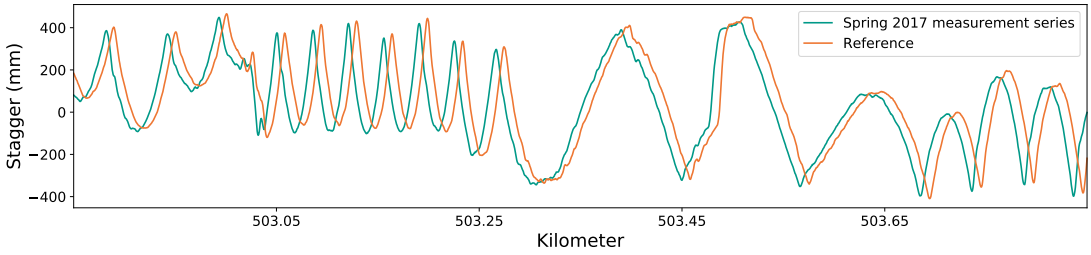

(b) Measured stagger spring 2017 after applying shift, compared to the reference.

Figure 4.6.: Shift found for gauge measurement channel applied to measured stagger for a subsection of track between Støren and Trondheim. The applied shift should be greater to achieve an optimal match, still in the same direction.

tical median. This is done to evaluate a single measurement channel as an alternative to aligning with median shift, as computing median shift is time expensive and only feasible for the CCF alignment method. The latter is due the other alignment methods performing local warping.

To conduct this evaluation, deviation in detected shift compared to median shift is computed for all measurement channels, as shown in Figure 4.7. This evaluation shows, that the by far lowest deviation is achieved with twist on a 2-meter basis, with a deviation equal to 345.5 meters in total, followed by twist on a 9-meter measurement basis with a deviation equal to 781.5 meters in total. Studying deviations for twist on a 2-meter basis in greater detail, it is found that 54.85% of the deviation occurred during the spring 2018 measurement recording. Deviations for the spring 2018 measurement series are relatively high independent of the measurement channel used for alignment compared with other measurement series, indicating either high degradation or outlier behavior within the series.

Further, it has to be determined whether the found deviation in shift for twist on a 2-meter basis, although lowest, is acceptable. Recall that deviations are computed by comparing with the median found shift, based on the assumption that the latter represents the ideal shift, as there exists no ground truth. With the main deviation residing within one of the nine aligned measurement series, the deviation mainly affects only this series. Comparing with the results for warping effect obtained in Figure 4.4, the alignment obtained with twist on a 2-meter basis scores overall high when evaluated on all measurement channels, only surpassed by the median shift.
Hence, the results indicate that twist on a 2-meter basis is a robust choice of measurement channel when the requirement is to compute alignment based on a single measurement

channel.

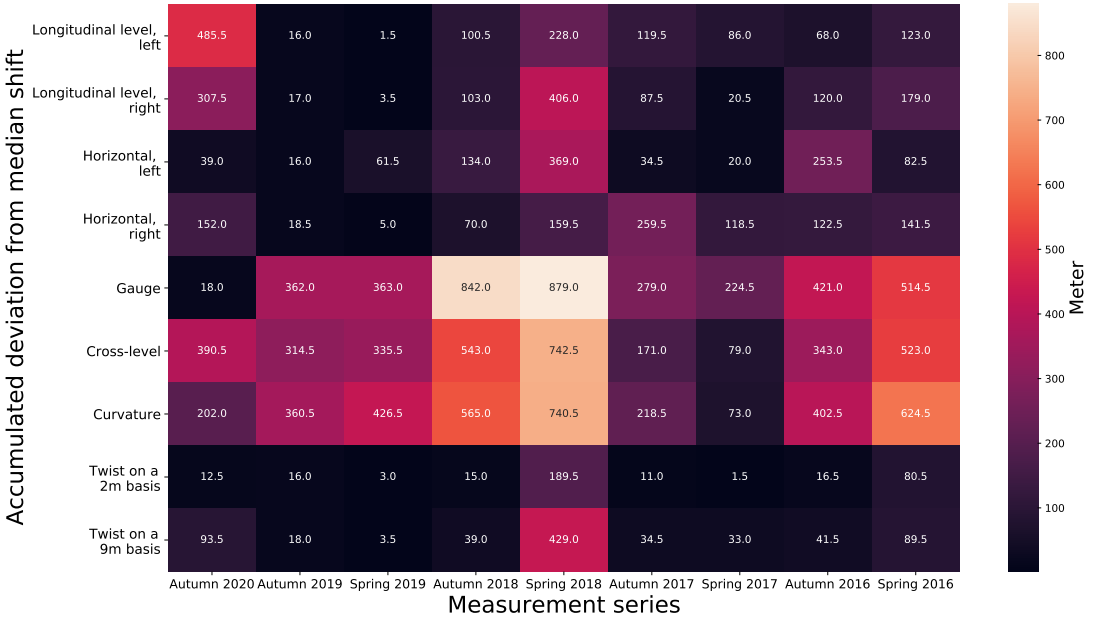

Figure 4.7.: Heat map displaying deviation in found shift for each measurement channel when compared to the median shift. Each measurement series is evaluated separately.

To conclude, this section has proposed two best practices for selecting measurement channel, where the prioritized method depends on the area of use. The median shift is the optimal choice for limited track section lengths and with alignment methods producing a constant shift. The median shift could also be computed on a subset of measurement channels to reduce time overhead. However, as this study aims to compare various alignment methods, utilizing median shift is not feasible and therefore, twist on a basis of 2 meters is selected.

4.1.3. Implementation of alignment method

In the referenced specialization project [21] executed prior to this study, considerable initial shifts were observed between the measurement series to be aligned and the reference series. It was concluded that the high initial shift was a potential contributor to the obtained warping effect results, based on which CCF was evaluated to be utilized as alignment method. Despite efforts to remove the initial shift in Section 3.1, these shifts are still present in smaller magnitude. To test and potentially minimize the effect of the initial shift, this study proposes utilizing CCF as a prepossessing step before aligning with RAFFT, COW, DTW, and the combined method. In practice, this modification resembles the principle behind the combined method, recalling that RAFFT pre-aligns the measurement series to enhance the alignment performance of COW. Similar to the combined method being proposed by [1] to cope with COW's lack of flexibility in aligning the first and last points, pre-alignment with CCF is proposed to cope with the high initial shifts present.

As alignment is conducted on segmented data, data equaling the shifted amount can

be extracted from neighboring segments and included instead of for example filling the segment with zero values. Therefore, CCF is utilized rather than RAFFT, as the constant shift found by CCF allows for such extraction. The benefit of inclusions from neighboring segments is that higher shifts are not penalized in the simplicity value utilized as part of the evaluation metric. This is the case with for example zero values, as they will seldom resemble the reference data. In addition, a greater percentage of similar data will reside within each segment, easing alignment. However, recalling the segment structure depicted in Figure 3.11, not all segments have neighboring segments with valid data, i.e., data recorded above 40km/h, and it thus becomes a trade-off between either utilizing zero values or potentially invalid data. In line with the goal of this study, it is more desirable to enhance alignment, accepting potential invalid data. In cases where detected shifts are greater then the data available, zero values will still be utilized.

Further, pre-alignment with CCF and data inclusion from neighboring segments will also impact the peak factor. As discussed, these steps are proposed to achieve a higher similarity between measurement series and reference, expecting a higher simplicity value to be achieved. However, as extracting data from neighboring segments post-determining shift with CCF induces a change in the measurement series to be aligned, this can negatively impact the peak factor. Hence a distinction is necessary between desirable change in peak factor due to data inclusion and undesirable change in peak factor due to too much customization. Therefore, it is proposed to utilize the pre-aligned series with CCF to represent the series before alignment, i.e., Y in Equation 2.9, when evaluating the data inclusion feature.

The proposed evaluation scheme is depicted in Figure 4.8. Here the input is preprocessed track geometry data following Section 3.1, and selected reference measurement series and measurement channel for alignment. Additionally, a max shift constraint equal to 150 meters is given as input. This is a reduction from the max shift constraint equal to 250 meters utilized in the specialization project [21], however feasible due to an observed reduction in the initial shift due to improved preprocessing. Recall that the segments obtained are constrained to have a minimum length corresponding to twice the highest shift observed. Hence, to maximize the amount of data utilized, it is desirable to use a small value for the max shift constraint. The scheme outputs all series aligned to the reference, based on the most favorable alignment method. The latter is determined utilizing the evaluation metric proposed in Section 2.3 with the modifications proposed above. All alignments will be evaluated on the measurement channel utilized under alignment, namely twist on a 2-meter basis. The evaluation to determine the best practice to achieve relative alignment is conducted in Chapter 5.

The proposed alignment methods were separately implemented in the related specialization project [21]. Following is a description covering how these algorithms are implemented to attain reproducibility.

Cross-Correlation Function

The Cross-Correlation Function is implemented utilizing correlate, a function from the NumPy library in Python. The correlate function cross-correlates two N-dimensional arrays and returns a 2xN-dimensional array containing cross-correlation values obtained by shifting one array relatively to the other. Utilizing np.argmax(), the optimal shift is obtained for each segment. If np.argmax() returns a shift greater than the max shift,

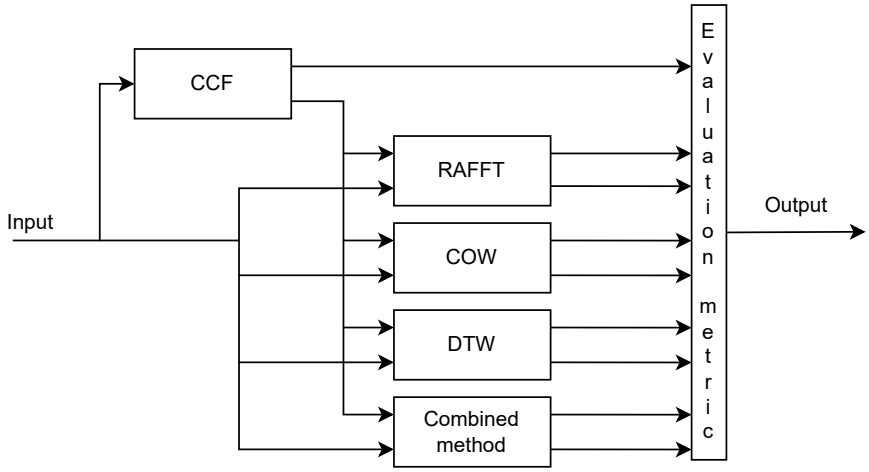

Figure 4.8.: Proposed scheme to determine best practice to achieve relative alignment.

the next most optimal shift is found. This procedure is repeated until a shift is found that satisfies the max shift constraint. The slack variable is selected equal to the max shift constraint utilized by the other methods, i.e., 150 meters and hence the segment length variable utilizes is equal to 300 meters (twice the slack).

Recursive Alignment by Fast Fourier Transform

RAFFT is implemented utilizing Matlab code downloaded from [68]. As all data processing is implemented in Python, the Matlab function is called from Python.

Dynamic Time Warping

To implement Dynamic Time Warping, the Python library dtw from dtwalign is utilized. The dtw function returns an alignment object based on an input series (to be aligned) and a reference series. Additionally, the function allows specifying window type and size utilized to enforce the max shift constraint. The Sakoe-Chiba band, which is a constant diagonal band parallel to the diagonal in the cumulative distance matrix in Section 2.3, is selected as the window type to ensure comparable enforcement of the constraint to the other methods. The library has a get_warping_path function used to extract the indexes of the aligned series from the alignment object.

Correlation Optimized Warping

COW is implemented utilizing available Matlab code created in [69], based on the work inn [35]. The utilized code is downloaded from [70] and the Matlab function is called from Python.

Combined method

Recall that the combined method is a combination of RAFFT and COW. Hence the combined method is implemented by first aligning the segment with RAFFT (see the implementation of RAFFT above) and then utilizing the obtained alignment as input to COW (see the implementation of COW above).

4.2. Absolute position determination

In Section 4.1 methods were proposed to align all historical track geometry measurement series to the chosen reference series collected spring 2020. This section investigates methods for determining the absolute position of this reference series, thereby achieving a mapping between all measurement series and absolute positions.

4.2.1. Measurement vehicle GPS position data

Recall from Section 3.1 that measurement series collected autumn 2018 and later contain coordinate position of recorded measurements. However, there are considerable deviations between what the measurement series regard as their actual position after relative alignment. An example of these deviations is depicted in Figure 4.9, where despite successful relative alignment, there are severe disagreements in the corresponding absolute position of the selected measurement.

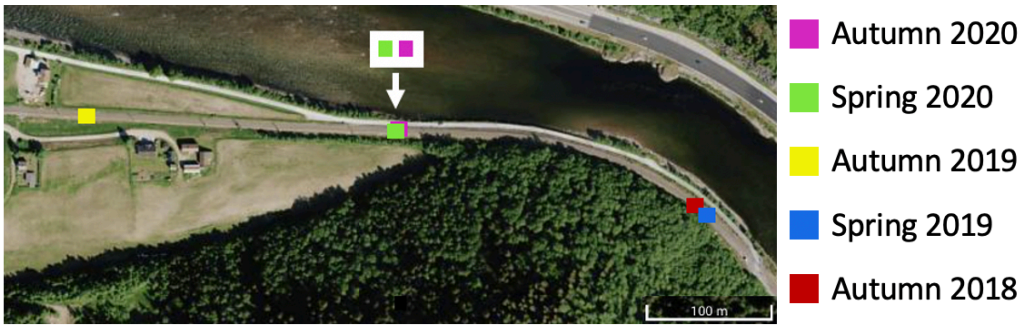

Figure 4.9.: Deviations in absolute position for a specific measurement, retrieved from the different measurement recordings equipped with GPS, despite relative alignment.

In Section 3.1 different update frequencies were detected for the GPS utilized in the period 2018 and 2019 compared to 2020. As the update frequency increased in 2020 and therefore is assumed to be more precise, this section proposes a method to determine the accuracy of the 2020 recorded GPS coordinates. Carrying out the proposed method, Chapter 5 evaluates the obtained results to determine if utilizing GPS coordinates from the measurement vehicle is sufficient to attain the absolute position.

Comparing location of known objects

To validate the GPS coordinates from the measurement vehicle, a known object or fixed point needs to be extracted from the measurement series such that the associated GPS value can be verified through field measurements. Minima and maxima in measured stagger value are examples of an object that can be extracted, as these values occur when passing high voltage masts. Other fixed points, such as transition curves, are more challenging to locate in the field and are therefore less suitable. Superstructure objects, although easily located in the field, are challenging to detect in the recorded measurements and hence also less suitable.

This yields the following proposed GPS verification setup. First, masts are located

in the high voltage mast record that are accessible along the track, such that it is possible to access the mast without moving onto the track itself, and with appropriate access from close-by roads. These requirements are set for safety reasons and to simply access. Thereupon, minima and maxima of measured stagger are compared with the selected masts from the high voltage mast record. This enables locating the selected mast in the measurement series such that the coordinates from the measurement vehicle can be extracted.

Five masts are selected from the studied track section that meet the safety and accessibility criteria. The measurement vehicle must also pass these masts at a speed above the induced speed limit for valid data, i.e., 40 km/h, and the masts should be evenly spread along the studied track section. The latter ensures a better validation of the whole track section compared to selecting adjacent masts. However, the flexibility in selection is limited by the safety, accessibility, and speed criteria. The selected mast and their extracted coordinates based on minima and maxima stagger from the measurement data recorded spring 2020 and autumn 2020 respectively are detailed in Table 4.1. Although spring 2020 is chosen as the reference, the accuracy of the autumn 2020 coordinates are equally evaluated due to the possibility to utilize these coordinates interchangeably after relative alignment, assuming the alignment is successful.

Table 4.1.: Selected mast from record with the corresponding coordinate position assigned by measurements recorded spring 2020 and autumn 2020 respectively.

Mast object in record	Kilometer position in recorded	Distance from track center line (m)	Obtained coordinates from measurement series Spring 2020	Autumn 2020
EH-MAS-022783	505.216	2.85	63.07721667° N, 10.25288754° E	63.07722146° N, 10.25288949° E
EH-MAS-023069	517.595	3.13	63.17346202° N, 10.30532359° E	63.17347016° N, 10.30533444° E
EH-MAS-023226	525.262	3.09	63.23295538° N, 10.28045131° E	63.23295884° N, 10.28043427° E
EH-MAS-023281	527.822	3.19	63.25415533° N, 10.28476041° E	63.25415056° N, 10.28474538° E
EH-MAS-023826	549.055	3.22	63.41060810° N, 10.38329524° E	63.41062906° N, 10.38330008° E

Extracted GPS coordinates from the measurement vehicle can visually be validated utilizing satellite images as illustrated in Figure 4.10. The figure depicts a satellite image of the selected mast EH-MAS-023826 and GPS coordinates of the mast extracted from measurements collected spring and autumn 2020. Visually, position accuracy seems to be within a few meters. However, field measurements need to be conducted to achieve higher accuracy than visual interpretation can provide.

Figure 4.10.: Satellite image of mast EH-MAS-023826 compared to the extracted GPS location of the same mast from recorded data spring and autumn 2020. Image obtained from Gule Sider [2]

To conduct field measurements, the following setup, detailed in Figure 4.11, is proposed.

Position 3 marks the assumed position of the passing train at minima or maxima measured stagger and is the GPS position desired to verify. Here, it is assumed that the GPS sensor is mounted at the same place as the stagger sensor. Deviations from this assumption can lead to a significant shift, depending on which of the three GPS sensors onboard Roger 1000 are utilized, see Figure 2.1. Due to the safety constraint, measurements can neither be conducted on the track, i.e., at position 3 directly, nor at the mast foot. Therefore, position 3 needs to be calculated based on measurements taken from a safe distance. When obtained, the distance between the position extracted from the data set and the field-derived position can be computed to determine the GPS accuracy from the measurement vehicle.

Utilizing the coordinate computation method described in Section 2.4.1, position 3 can be derived if the coordinates at position 1 and position 2 in Figure 4.11 are measured, in addition to the distance between position 2 and position 3. The utilized method requires that the line connecting position 1 and position 2 is parallel with the line connecting position 2 and position 3. Due to the safety precaution, the distance between position 2 and position 3 cannot be measured directly. However, in the field, distance from position 2 to the mast foot is measurable, i.e., dist. 2 in Figure 4.11. The distance from the mast foot to the track center line, i.e., dist. 3 in Figure 4.11, can be extracted from record. The sum of these distances gives the distance between position 2 and position 3. If, additionally, the distance between position 1 and position 2 is measured, i.e., dist. 1 in Figure 4.11, this measurement can be utilized to select the distance formula, as proposed later in this section.

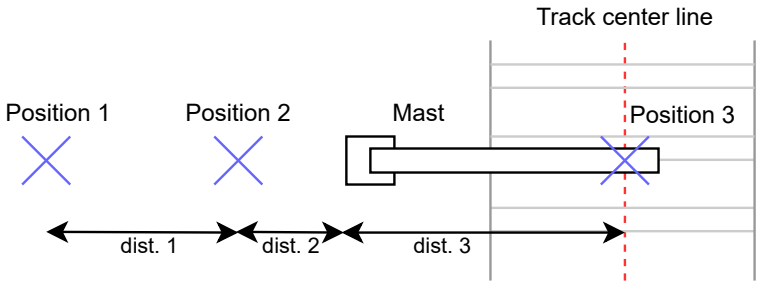

Figure 4.11.: Field measurement setup. The goal is to derive position 3 based on the field-measured location at position 2. A second position, position 1, is measured in the field to compute bearing.

With the proposed setup, coordinate and distance measurements are conducted in the field at the selected masts. The distance between position 2 and the mast foot and between position 1 and position 2 are measured utilizing measurement tape. Coordinate measurements are collected utilizing a Leica Viva GS16 GNSS Smart antenna selecting the WGS-84 reference frame, equivalent to the reference frame utilized by the measurement vehicle. The GNSS antenna delivers coordinate measurements with a maximum inaccuracy of 3 centimeters. Figure 4.12 illustrates collection of measurements in field at position 2 for mast EH-MAS-023281.

Measurements are retrieved from the Leica Viva GS16 GNSS antenna in the Degrees-

Figure 4.12.: Field measurement at mast EH-MAS-023281. Measuring coordinates at position 2 with the GNSS antenna and the distance from the position to the mast foot utilizing measurement tape.

Minutes-Seconds format, see Section 2.4.1. These are converted into Decimal Degrees utilizing Equation 2.10a to acquire the same format as the coordinates extracted from the measurement series. The obtained field measurements are detailed in Table 4.2.

Table 4.2.: Field measurements are obtained at the pre-selected masts following the setup described in Figure 4.11.

Mast object	dist. 1 (m)	dist. 2 (m)	Obtained coordinates from field	
			Position 1	Position 2
EH-MAS-022783	1.00	2.86	63.07723165° N, 10.25301848° E	63.07722829° N, 10.25300034° E
EH-MAS-023069	1.00	2.00	63.17344906° N, 10.30544301° E	63.17345231° N, 10.30542401° E
EH-MAS-023226	1.00	2.50	63.23294544° N, 10.28029656° E	63.23294959° N, 10.28031417° E
EH-MAS-023281	1.00	2.00	63.25414368° N, 10.28487143° E	63.25414604° N, 10.28485190° E
EH-MAS-023826	1.00	3.29	63.41064348° N, 10.38314179° E	63.41064261° N, 10.38316166° E

Further, to apply Equations 2.14 and 2.15, the coordinates in degrees are multiplied by $\frac{\pi}{180}$ to obtain radians. The equations are then applied, yielding position 3 listed in Table 4.3.

To evaluate the accuracy of the GPS mounted to the measurement vehicle, the distance between the field computed position and the position extracted from the measurement series can be computed. Based on the theory presented in Section 2.4.1 and the expected small magnitude in the distance to be computed, the Equirectangular approximation and the Haversine formula are relevant to consider. To select which of these formulas is the best-suited formula for this specific purpose, this study proposes evaluating both formulas utilizing coordinates for position 1 and position 2, as this closely resembles the distance computation to be conducted. As the distance between position 1 and position 2 is measured in the field, see Table 4.2, the most suited formula for this specific purpose can be determined based on the minimum deviation from this measured distance. Computation time is not relevant to consider due to the few calculations that are necessary to execute.

Table 4.3.: Derived coordinate position 3 for the selected masts, following the setup described in Figure 4.11.

Mast object	Derived position 3
EH-MAS-022783	63.07720884° N, 10.25289535° E
EH-MAS-023069	63.17346866° N, 10.30532842° E
EH-MAS-023226	63.23297290° N, 10.28041307° E
EH-MAS-023281	63.25415814° N, 10.28475173° E
EH-MAS-023826	63.41063691° N, 10.38329182° E

Calculating the distance with both formulas for all five selected masts yields identical accumulated and median deviation in distance compared to measured values, equal to 5.6 and 1.2 centimeters, respectively. As the distances measured in field are measured with measuring tape, it is more likely that this inaccuracy is due to inaccurate field measurements rather than inaccuracy in the utilized formulas.
Due to both methods yielding equivalent distance results on the test case, the Equirectangular approximation is selected based on its simpler mathematical form. The deviations between mast position extracted from the measurement recording and computed based on field measurements are presented in Section 5.2.1.

The proposed method for validating the GPS coordinates from the measurement vehicle relies on the potential error in the GPS coordinates from the measurement vehicle to be smaller than the distance between adjacent masts. Else, problems in extracting the correct mast from the recorded measurements occur. In such a case, stagger from record could be compared with measured stagger to ensure correct extraction. This would allow the potential error to at least be equal to the distance to the mast neighbor the adjacent mast. However, such comparison is not favorable as values for stagger form record have shown to be error-prone, see Section 3.2.2. Hence, given that the potential error in the GPS coordinates from the measurement vehicle is minor, this comparison is avoided to avert potentially inducing error.

Estimate of position uncertainty for the proposed method

This section aims to quantify and estimate the error caused by computing position in field as well as extracting GPS position from the recorded measurement series. These estimates are utilized in Section 5.2.1 to evaluate the obtained results. The errors are approximated for a single mast and based on the data from the five selected mast objects listed in Table 4.1.

The field computed positions are based on measurements conducted with measuring tape and GNSS antenna, and the mast distance from track center line extracted from the high voltage mast record. The computed position relies on parallel measurements in accordance with the proposed setup in Figure 4.11. The uncertainties in the field computed positions are impacted by inaccuracies in each of the listed measurements and their correct alignment.

The utilized GNSS antenna specifies an uncertainty of 3 centimeters. Since computations are performed on rather short distances, it is assumed that the utilized distances

formulas do not induce any error. Hence, the median deviation between computing distance 1 in Figure 4.11 based on field measured coordinates and measuring the same distance with measuring tape for the five selected masts, can be used as an indication of induced error by the measuring tape. This median deviation was found equal to 1.2 centimeters. Since distance 1 in Figure 4.11 is computed based on two field measured coordinates, each of these coordinate measurements contributes maximum with an additional error equal to 3 centimeters.

Without direct access to the track, the distance from the mast foot to the track center line, extracted from the high voltage mast record, cannot be verified with independent measurements. However, for the five masts studied, this distance is in the range 2.85 to 3.22 meters. Therefore, it is plausible to expect an error less than the range span of 37 centimeters.

Assuming that the measurements were conducted perpendicular to the mast foot and track center line, the potential effect of deviating from this setup can be analysed. Following Figure 4.11, position 1 for mast EH-MAS-023281 was in field measured to be 63.25414368° N, and 10.28487143° E. Moving this coordinate position 0.12 centimeters NE yields the new coordinates 63.25414369° N, and 10.28487144° E. This modified position is by assumption no longer perpendicular to the mast foot and track center line. Computing the new bearing based on this modified position 1 and utilizing the obtained bearing to compute a modified position 3 yields the coordinate 63.25415809° N, and 10.2847517° E, that deviates 0.58 centimeters from previously obtained position 3. Further modifications to position 1, for example by 3.48 centimeters NE yields 17.76 centimeters deviation in computed position. Hence, even small deviations in measured coordinate position propagate to greater deviations in computed coordinate position. A factor that, at least partly, explains this observation is the relatively short distance between position 1 and position 2, and hence even small changes in position cause significant impact on the computed bearing.

To summarize position uncertainty from field measurements, the following worst-case scenario is proposed. Assume a deviation in computing position 1 perpendicular to position 2, mast foot and track center line by 3.48 centimeters, an error in the GNSS measurement at position 2 equal to 3 centimeters, a 7.2-centimeter error in distance measured with measuring tape, and a 37 centimeters error in mast arm length extracted from the record. In this specific case, the total error equals 64.96 centimeters. This error is an estimated worst-case expected error for the field derived positions. Note that the error in field derived positions is dependent on correct execution of the field measurements and hence greater inaccuracy may occur dependent on execution.

Further, extracting GPS coordinate from the track geometry data set also induces uncertainties. Although positions are extracted based on minima or maxima local stagger, these minima or maxima values do not particularly stand out from neighbouring measurements. Using recorded stagger spring 2020 at mast EH-MAS-023281 as an example, depicted in Figure 4.13, the shaded area equal to 4.5 meters around maxima stagger shows small variation in stagger. Knowing that measured stagger is impacted by environmental conditions and wheel-to-rail movement, small disturbances can cause change to localized maxima. With measurements being conducted every 0.5 meters, false extraction can induce a noticeable error. Based on the measured stagger for EH-MAS-023281,

error from GPS coordinate extraction is estimated worst-case equal to 2 meters.

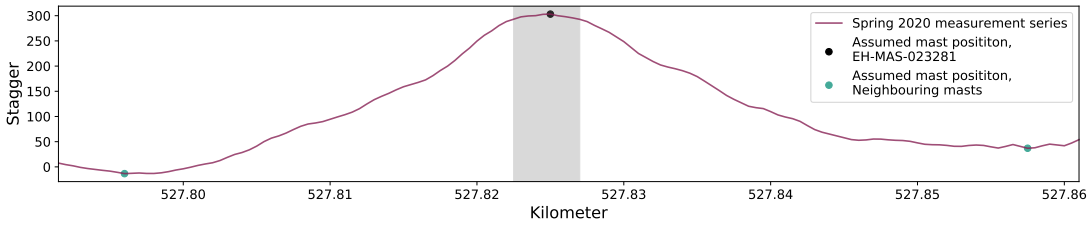

Figure 4.13.: Measured stagger spring 2020 passing mast EH-MAS-023281. Shaded area showing small variation in measured stagger close to local maxima.

Comparing the magnitude in potential error present in respectively the field computed position and extracted GPS position from the recorded measurements, the potential for error is greater for the latter.

4.2.2. Track object records

In Sections 3.2.1 and Section 3.2.2 data was constructed to enable alignment between track records and data from the measurement vehicle. This section evaluates which methods are feasible to apply to achieve such alignment.

Interpolated signals

Data construction through interpolation was shown feasible for curvature and cross-level values from the superstructure record and for curvature from the high voltage mast record. Recall that before alignment, recorded measurements and interpolated constructed data are mapped utilizing the assigned kilometer position value and index derived kilometer position. Absolute position alignment is necessary due to high inaccuracies in assigned kilometer values. Instead of utilizing kilometer values, the goal is to use other track data to map recorded data to stored records. Aligning the constructed signals to the recorded measurement series resembles the relative position alignment task. However, a more significant dissimilarity between the two signals is expected. This is because the interpolated signal is based on a relatively low frequency of data compared to the recorded measurements. Hence, only constant global shift alignment methods are relevant to consider, as other methods will strive to compensate for this difference through unwanted warping. This leaves only CCF.

To conduct the alignment, the constructed signals are segmented based on segmentation method 3. In this specific case, this is identical to aligning with segmentation method 2 as only the references series has measurements connected to speed. Under alignment, the spring 2020 measurement series is utilized as references and the max shift constraint is set equal to 150 meters, as proposed under relevant position alignment in Section 4.1.3.

An evaluation method needs to be employed to evaluate whether CCF successfully improves absolute positioning. Both the superstructure record and the high voltage mast record contain the positions of objects along the track. Although it is assumed that the records utilized are error-prone, as stated in Section 3.2, utilizing these objects to verify absolute position can indicate both the magnitude of error present and the success of

the alignment. Hence, the extracted GPS position of these objects from the measurement vehicle, before and after alignment, can be compared and verified through satellite images.

Superstructure record

For the data constructed based of the superstructure record, five bridge objects are selected from the superstructure record to be utilized in the proposed evaluation. Bridges are deliberately selected as they are clearly visible on satellite images, easing the evaluation. As in section Section 4.2.1, the measurement vehicle must pass these selected bridges at a speed above the defined speed limit for valid data, 40 km/h, and the bridges are desired to be evenly spread along the studied track section. Recall the latter is to ensure a better validation of the whole track section compared to selecting adjacent masts. This resulted in the selection of the bridge objects detailed in Table 4.4.

Table 4.4.: Selected bridge objects from record. Coordinate position obtained from the spring 2020 recording utilizing both kilometer position matching and based on index derived position.

Mast object in record	Kilometer position in recorded	Obtained coordinates from measurement series spring 2020	
		Extracted based on index derived position	Extracted based on kilometer position
Bridge A.	502.8000	63.06557220° N, 10.28635814° E	63.06543816° N, 10.28649667° E
Bridge B.	514.9200	63.15296148° N, 10.28235196° E	63.15273081° N, 10.28191013° E
Bridge C.	526.3850	63.24305682° N, 10.28055276° E	63.24264422° N, 10.28101554° E
Bridge D.	530.7835	63.27953566° N, 10.28304998° E	63.27910373° N, 10.28362231° E
Bridge E.	546.2830	63.38915543° N, 10.37199902° E	63.38875541° N, 10.37069174° E

Expected coordinate position of the selected bridge objects before alignment can be extracted from the recorded measurement series by comparing kilometer position. Recall that kilometer position for the measurement series can be defined in two separate ways, both based on index derived position and recorded millage value, see section 3.1.1. Hence, GPS coordinates can be extracted following both these conventions. Extracting GPS coordinates based on recorded kilometer position enables utilization of the manual corrected positions. However, alignment is conducted utilizing continuous measurement signal to archive the highest similarity between constructed and recorded data, thereby using the index derived kilometer position.

Extracting GPS coordinates from the measurement vehicle based on recorded kilometer position is simply done by extracting the coordinates from the measurement series corresponding to the kilometer position given in the record. For index derived kilometer position, Figure 4.14 visualises how coordinates are extracted for Bridge C. Since Bridge C has kilometer position 526.3850 in record, visualized by the black vertical line in Figure 4.14, the corresponding coordinate measurement at this point can be extracted from the spring 2020 recording. All extracted coordinates are listed in Table 4.4.

The extracted GPS positions for Bridge C are visualised in figure 4.15. Post alignment, the corrected position can be added to this comparison for evaluation, see Section 5.2.2.

High voltage mast record

For the high voltage mast record, the position location can be verified utilizing the field derived positions of the five selected masts in Section 4.2.1. Hence, for the extracted absolute positions, in addition to being verified visually, the deviation in meters can also

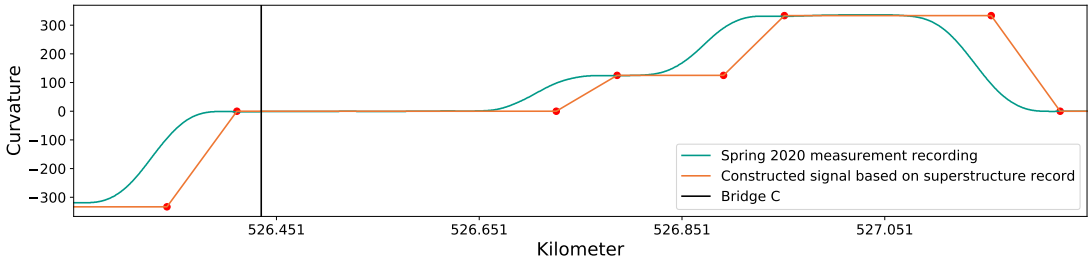

Figure 4.14.: Extracting coordinates for Bridge C in record utilizing spring 2020 measurement series with index based kilometer positioning.

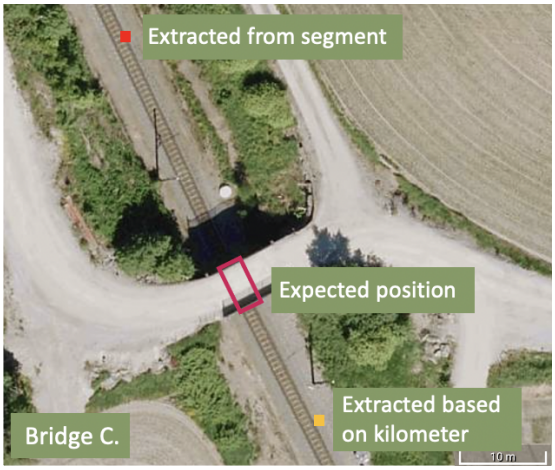

Figure 4.15.: Extracted GPS location of bridge object (yellow) through comparing assigned kilometer position in superstructure recorded and spring 2020 recorded measurements. The expected position range of the bridge object is marked with pink. Image obtained from Gule Sider [2]

be computed.

Stagger

In Section 3.2.2, assumed high voltage mast positions with corresponding stagger value were extracted for spring 2020 measurements. This section proposes a method to match the assumed mast position and kilometer position in the record. This method can be compared to the GPS verification method detailed in Section 4.2.1, where the method proposed here automates the manual mast selecting process. Through matching the two data sets, shift between the high voltage mast record and measurement series data can be determined. Hence, this method can also yield as an automated verification scheme for the GPS measurements extracted from the measurement vehicle, not only for determining absolute position.

The proposed method iterates through positions of all masts in the record and assumed mast positions, pairing masts where deviation in kilometer position is below 24 meters. This limit is set based on the findings in Section 3.2.2, where it was found that 95% of the mast in the data set have a span length to adjacent mast between 24 and 64 meters. By selecting the lowest span length within this interval, the chance of matching

two masts falsely is minimized, as it is below the usual minimum distance between two masts. Simultaneously, a lower limit is not desirable, to limit the method as little as possible in detecting shifts present. Applying a limit is necessary due to both missing and redundant masts present for the assumed high voltage mast positions extracted in Section 3.2.2.

An example of applying the proposed method is given in Figure 4.16. Figure 4.16a and 4.16b show high voltage mast positions with corresponding stagger and assumed high voltage mast position with corresponding stagger. Applying the proposed method results in the matched high voltage mast given in Figure 4.16c. Notice that there are significantly more masts in the record compared with the number of masts detected in the measurement series from spring 2020 for the studied 1 kilometer of track in Figure 4.16. The highest detected shifts for the studied 1 kilometer of track is 16.5 meters.

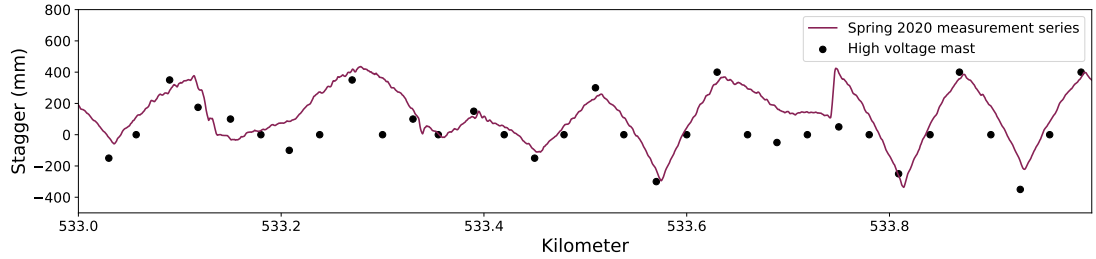

(a) High voltage mast with recorded stagger.

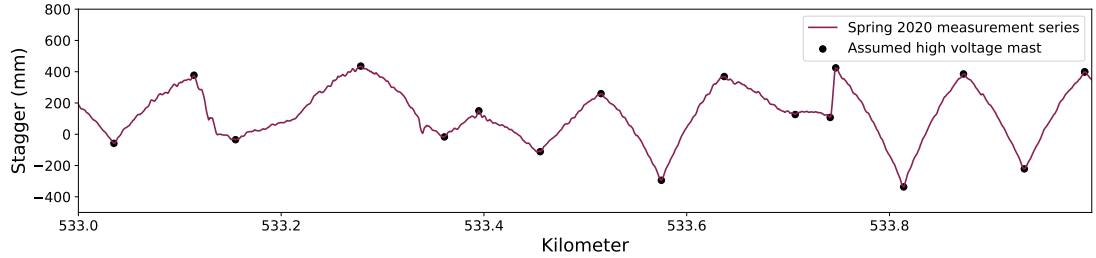

(b) Assumed high voltage mast position and stagger.

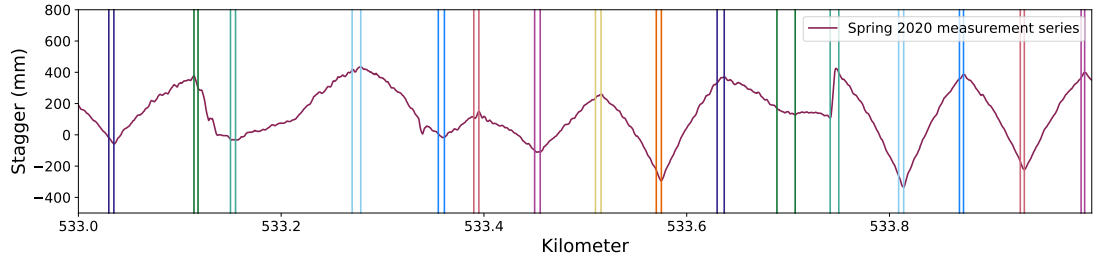

(c) Matched high voltage masts positions from recorded with assumed high voltage mast positions.

Figure 4.16.: Application of proposed matching method between high voltage masts from the record and assumed high voltage mast positions extracted from measured stagger spring 2020. A subsection of the track is studied between Melhus and Nypan stations.

The position location of the matched masts can be verified utilizing the field derived positions of the five selected masts in Section 4.2.1. A shortcoming of the proposed

method is its inability to detect shifts greater than the induced limit of 24 meters. Although the actual shift between the high voltage mast record and the measured stagger is unknown, detected shifts will indicate whether this poses as a limitation.

5. Results and Discussions

This chapter evaluates the proposed methods in Chapter 4 for both relative position alignment and absolute position determination. In Section 5.1, relative alignment with and without pre-alignment is assessed, and it is determined which alignment method is most suited to align the measurement series collected by Roger 1000. To evaluate the obtained results, simplicity value, peak factor, and warping effect are utilized. Further, in Section 5.2, the absolute positions of the recorded measurement series are determined by utilizing GPS sensor data and by comparing with values in both the high voltage mast record and the superstructure record. The obtained results are discussed, resulting in a proposed best practice.

5.1. Relative position alignment

In the related specialization project [21], alignment yielded the highest warping effect for RAFFT, followed by DTW, the combined method, and CCF. DTW scored highest when only considering the simplicity metric, followed by RAFFT and the combined method. Regarding peak factor, CCF, the combined method, RAFFT and COW scored highest. Further analysis showed that CCF was most suited to be utilized for alignment. This was due to its simpleness and shape perseverance ability, combined with the low degree of stretching and compression observed in the data set.

This section aims to evaluate the proposed improvements presented in Chapter 4. Note that scores achieved on the evaluation metric in the specialization project [21] cannot be compared with the results obtained here, recalling that a different measurement channel is utilized in the evaluation.

5.1.1. Results

Following the setup proposed in Section 4.1.3, warping effect is computed for alignment with and without pre-alignment, presented in Table 5.2 and Table 5.1 respectively. Independent of input, DTW scores the highest warping effect. DTW is followed by RAFFT, the combined method, and CCF without pre-alignment. With pre-alignment, RAFFT, the combined method, and COW follow DTW, and the latter two scorings are close to equal. Comparing alignment on the preprocessed data, i.e., Table 5.1, with further alignment on already pre-aligned data, i.e., Table 5.2, an increase in warping effect is achieved by all alignment methods. With alignment on pre-aligned data, all methods score higher, or equal, for both simplicity value and peak factor.

5.1.2. Discussion

The superior results achieved with pre-alignment utilizing CCF indicate an enhanced alignment performance when utilizing this method. Recall that CCF includes data from neighboring segments equaling the found shift. This is to resemble the reference as closely as possible, creating a trade-off between higher accuracy and potentially utilizing

Table 5.1.: Achieved alignment results with only preprocessed data as input.

Alignment Method	Simplicity value	Peak factor	Warping effect
CCF	0.88957	0.98985	1.87942
RAFFT	0.90208	0.98710	1.88918
DTW	0.96584	0.98804	1.95388
COW	0.74306	0.99847	1.74153
COMBINED method	0.89086	0.98977	1.88063

Table 5.2.: Achieved alignment results with both preprocessed and pre-aligned data as input.

Alignment Method	Simplicity value	Peak factor	Warping effect
CCF	0.88957	1.00000	1.88957
RAFFT	0.91300	0.99996	1.91297
DTW	0.97439	0.99431	1.96870
COW	0.90250	0.99991	1.90241
COMBINED method	0.90280	0.99991	1.90271

invalid data. In the following, the potential consequence of such inclusion is evaluated.

Accumulated over all segments, for all measurement series, CCF achieves alignment by executing a shift equivalent to 10.736 kilometers. Inclusion of data from neighboring segments results in utilizing 3.03% invalid data and 7.88% zero-values. The invalid data is gathered at speeds between 31.39 and 39.99 km/h. Hence, invalid data accounts only for a small portion of the data included, and the speed deviates at a maximum 8.61 km/h from the set speed validity limit. Knowing that data inclusion contributes to the superior results achieved with pre-alignment utilizing CCF and with a relatively low percentage of the included data being invalid, it is concluded that pre-alignment utilizing CCF is favorable. Hence, in the following, all analysis of the alignment methods is conducted on pre-aligned measurement series.

DTW achieves the highest score for the warping effect, scoring a superior simplicity value compared to the other alignment methods. The high simplicity value is at a minor cost of a lower peak factor. A performance benchmarking conducted by [1] showed that even a marginal difference in achieved score influenced alignment quality. Additionally, in the analysis of the results obtained in the underlying specialization project [21], it was uncovered that DTW extensively alternated the series it aligns to the reference, thereby removing essential differences caused by degradation. Recalling that the ultimate goal behind achieving relative alignment is enabling the data to be used for predictive maintenance, an investigation is conducted to examine if the slightly lower peak factor affects the obtained alignments.

Figure 5.1 compares measurements recorded autumn 2020 after pre-alignment with further alignment conducted utilizing DTW. Analyzing the DTW-aligned measurement series, it can be observed that the measurement recording extensively has been altered to achieve high similarity when compared with the reference. This is especially visible in the section shaded, where the recorded measurements have been extensively stretched

under alignment. Although the true alignment is unknown, it can immediately before the highlighted section be observed that the amplitude of the measurement recording follows the references relatively well. It is thus unlikely that measurements suddenly have been affected so extensively by stretching.

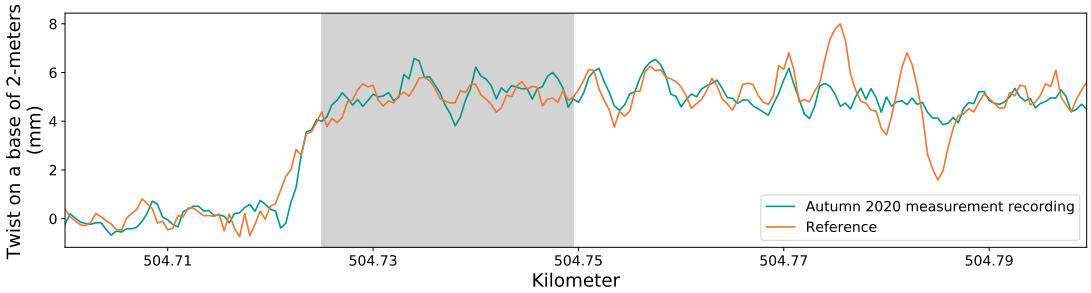

(a) Track measurements recorded autumn 2020 compared to the reference, after pre-alignment.

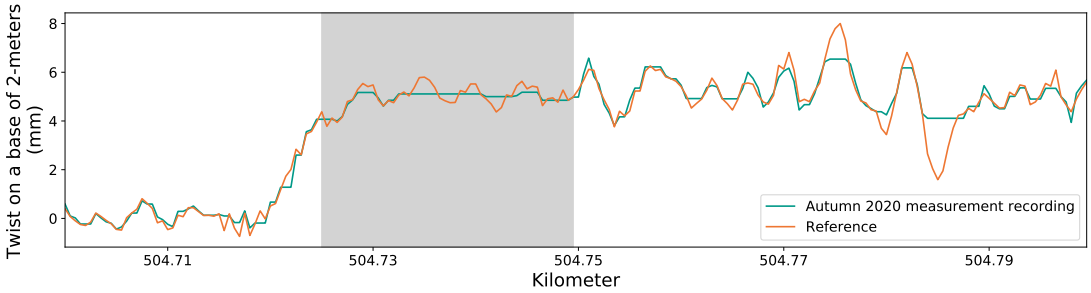

(b) Track measurements recorded autumn 2020 compared to the reference, further aligned with DTW.

Figure 5.1.: Autumn 2020 measurement recording after pre-alignment compared to further alignment with DTW. Observe how the autumn 2020 measurement recording is extensively altered post alignment with DTW.

Further, extensive alternation can also be observed in Figure 5.2. Analyzing the pre-aligned recording conducted autumn 2017, within the grey shaded area, a peak in twist can be observed at 503.38 kilometers. Alignment with DTW moves this peak to align with the left neighboring peak in the reference, thereby extensively compressing and stretching the autumn 2017 recorded data within the shaded area. To examine whether these extensive compression and stretching actually are present in the recording, or rather caused by the algorithm optimizing similarity, the found alignment is applied to another measurement channel. As measurements across different measurement channels are recorded simultaneously, it is expected that the potential compression and stretching have affected all measurement channels equally.

Figure 5.3 depicts the application of the found shift (found utilizing the twist on a base of 2-meters measurement channel) applied on the Gauge measurement channel. Comparing the areas shaded in Figure 5.2 and Figure 5.3, it can be observed that the compression and stretching applied to match the peaks in Figure 5.2, alternates the shape of the gauge measurements considerably. This implies that the induced compression and stretching by the algorithm do not compensate for compression and stretching during recording, but are rather introduced to achieve higher similarity.

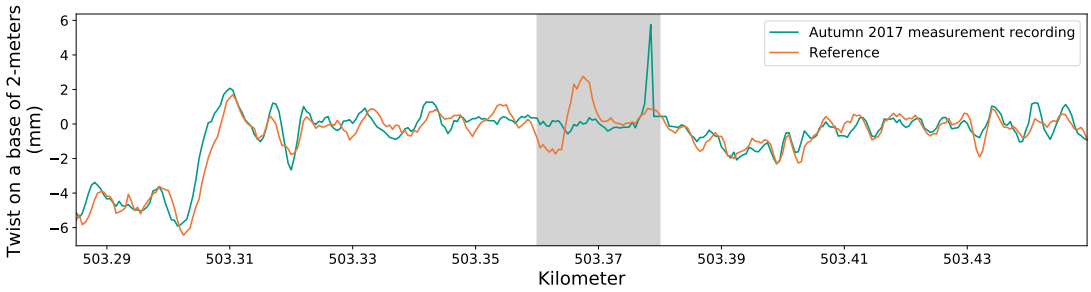

(a) Track measurements recorded autumn 2017 compared to the reference, after pre-alignment.

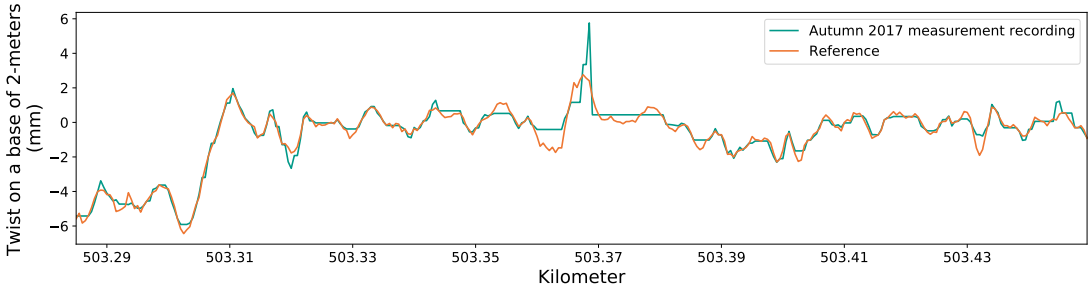

(b) Track measurements recorded autumn 2017 compared to the reference, further aligned with DTW.

Figure 5.2.: Autumn 2017 measurement recording after pre-alignment compared to further alignment with DTW. Within the grey shaded area, observe how the algorithm strives to pair neighbouring peaks.

The high degree of alternation causes loss of valuable information regarding track status. Differences between measurement recordings and the reference are expected and crucial to preserve. Hence, DTW is considered unfitted to perform this relative alignment task. This conclusion is in line with the results and conclusion presented by the authors in [1].

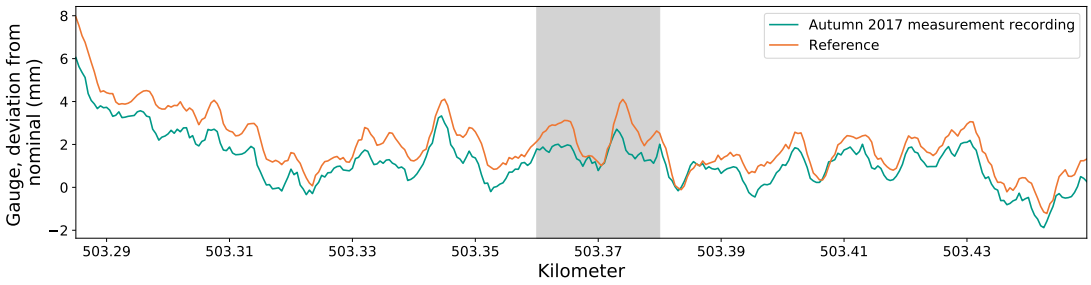

(a) Track measurements recorded autumn 2017 compared to the reference, after pre-alignment.

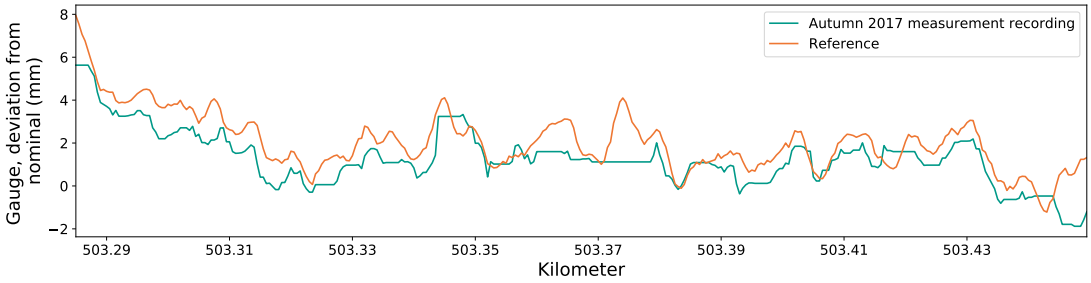

(b) Track measurements recorded autumn 2017 compared to the reference, further aligned with DTW.

Figure 5.3.: Autumn 2017 measurement recording after pre-alignment compared to further alignment with DTW, applied to the Gauge measurement channel. Within the grey area, observe how the applied shift, although achieving higher simplicity by matching the neighboring peaks in Figure 5.2, falsely stretches the gauge measurement in the same area.

The RAFFT alignment method scores second-highest warping effect and scores higher than DTW for peak factor. RAFFT performs recursive cross-correlation moving from a global to a local scale, giving the algorithm the capability to include a constant shift in the middle of a segment. Such inclusion allows the algorithm to compensate for potential stretching or compression. The algorithm exploits, for example, this property in Figure 5.4. Here, after pre-alignment, a small local shift is still presented between the measurement recording and the reference series, evident in the area highlighted with grey. RAFFT successfully applies a constant shift to this local part of the series, improving the alignment at this specific position.

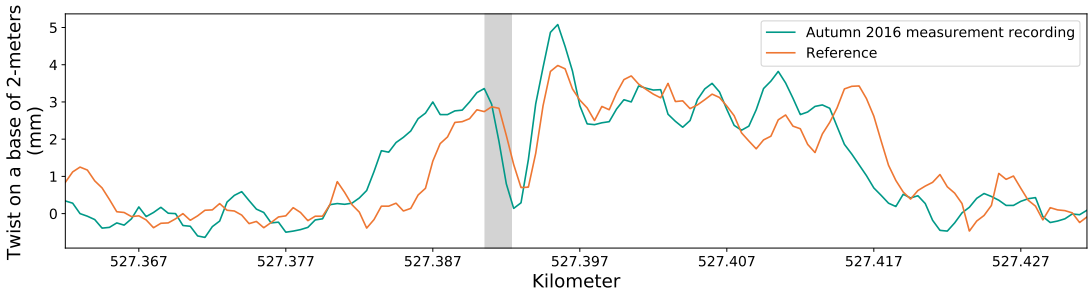

(a) Track measurements recorded autumn 2016 compared to the reference, after pre-alignment.

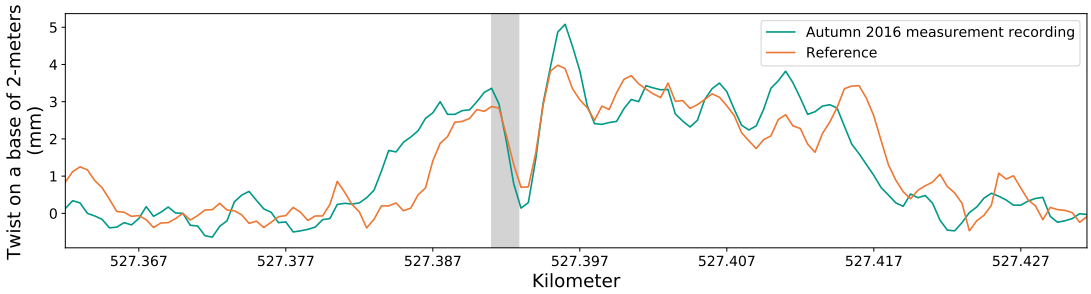

(b) Track measurements recorded autumn 2016 compared to the reference, further aligned with RAFFT.

Figure 5.4.: Autumn 2016 measurement recording after pre-alignment compared to further alignment with RAFFT. The Figure shows how RAFFT successfully applies a local shift, thereby improving the alignment.

In Figure 5.5, an adjacent section of track to the section studied in Figure 5.4 is addressed. The local shift addressed in the paragraph above still applies in the area highlighted with grey, yielding improved alignment. However, in the area highlighted with red, visual analysis shows that a more favorable alignment was achieved before applying the shift found with RAFFT. The algorithm has shifted its alignment between the area highlighted with red and blue, such that in the area highlighted in blue, RAFFT imposes the same shift as present after pre-alignment. Hence, a small degree of compression and stretching are present in the recording, which RAFFT partly successfully has corrected. The observation of compression and stretching present in the measurement recording is unexpected based on the findings in the underlying specialization project [21]. It is suspected that because the two-step alignment procedure conducted achieves higher accuracy, it is possible to discover the minor variations and, thereby, effects caused by compression and stretching. The observation of compression and stretching present in

the data is in line with observations done in related studies [1].

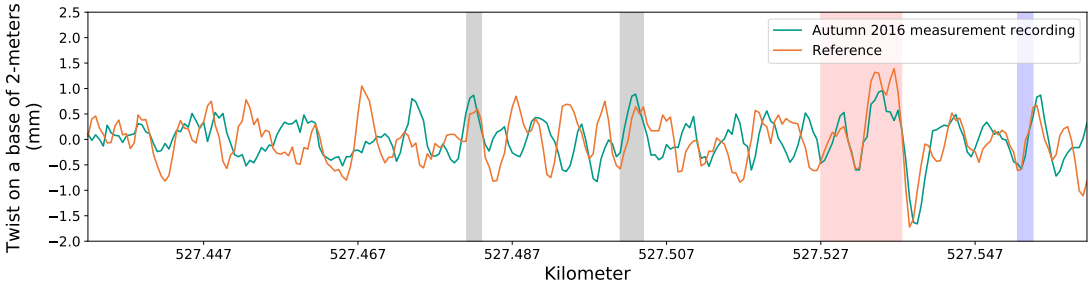

(a) Track measurements recorded autumn 2016 compared to the reference, after pre-alignment.

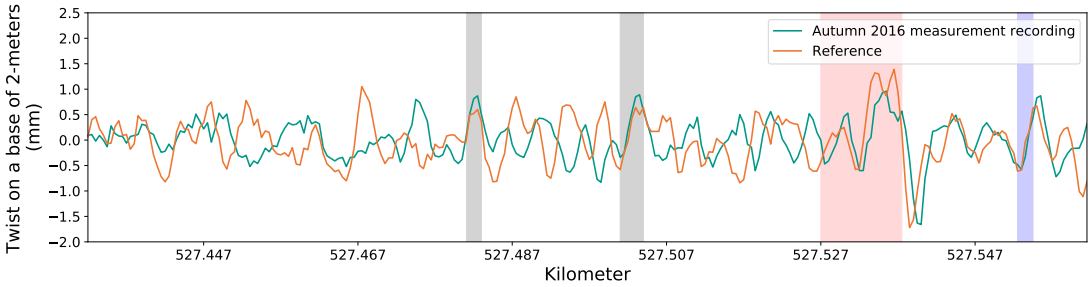

(b) Track measurements recorded autumn 2016 compared to the reference, further aligned with RAFFT.

Figure 5.5.: Autumn 2016 measurement recording after pre-alignment compared to further alignment with RAFFT. Observe how a small compression yields improved alignment in the grey shaded area at the expense of the worsened alignment in the red shaded area. No difference in shift is present in the area shaded in blue.

A high level of degradation yields more significant differences between the measurement series, causing the detection of the shift present to become more difficult. In Figure 5.4 and Figure 5.5 a sizable difference between the two measurement series can be observed, especially in subsections where the variation in amplitude is small. However, alignment is achievable through similarities in areas with greater amplitude. In Figure 5.6 however, no conclusive similarity is observable, even in areas with high amplitude, causing alignment difficulties. A result of such difficulties is over-fitting, as is assumed to be the case in Figure 5.6. Although true alignment is unknown, it is reasonable to assume that there is no local stretching with equivalent high magnitude to what is present in Figure 5.6, highlighted in grey. This finding is in line with what was observed in [1], where it was found that RAFFT may warp the aligned measurement series extremely at some locations. One solution to avoiding such undesired behavior is to apply a stricter max shift constraint on the pre-aligned data. Since pre-alignment successfully removes most of the initial shift present, further alignment optimization could be constrained with a smaller value for the max shift parameter, avoiding over-fitting. However, this becomes a trade-off between giving the algorithm flexibility to detect the true shifts present and avoiding over-fitting. To balance this trade-off, an additional manual analysis of the pre-aligned data is preferred. The latter however, results in the alignment method becoming more cumbersome.

COW and the combined method score close to equal warping effect, beaten by DTW and RAFFT. Although COW and the combined method score higher than DTW for peak factor, their results are slightly poorer than the peak factor obtained by RAFFT. However, the nature of the COW algorithm avoids extreme warping. The same does not apply for the combined method, recalling that the combined method utilizes RAFFT to align the start and end of the segment. With pre-alignment utilizing CCF and data inclusion, constant shifts applied by RAFFT are not desired. Therefore, alignment achieved by COW is further investigated in Figure 5.7, which reviews the same track section as studied in Figure 5.6. Observe how in Figure 5.7 no extreme warping is present, as the case was with the alignment achieved by RAFFT. For the studied section, COW proposes only minor shifts to compensate for compression or stretching, best visually observed in the sections highlighted in grey.

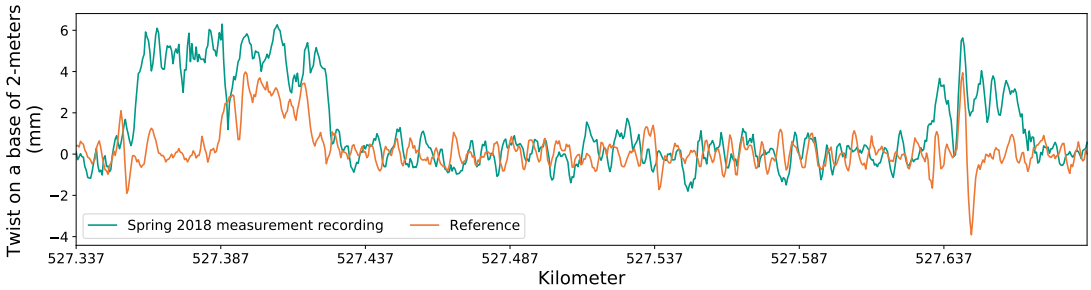

(a) Track measurements recorded spring 2018 compared to the reference, after pre-alignment.

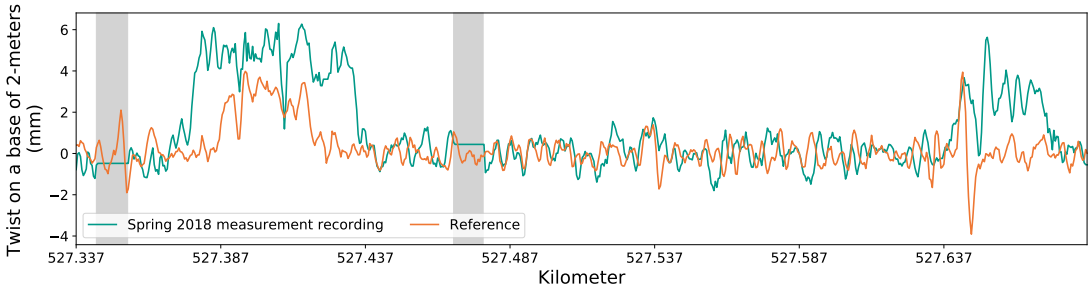

(b) Track measurements recorded spring 2018 compared to the reference, further aligned with RAFFT.

Figure 5.6.: Autumn 2018 measurement recording after pre-alignment compared to further alignment with RAFFT. Local extreme shifts of the aligned series shows over-fitting tendencies in situations where the amount of degradation is high.

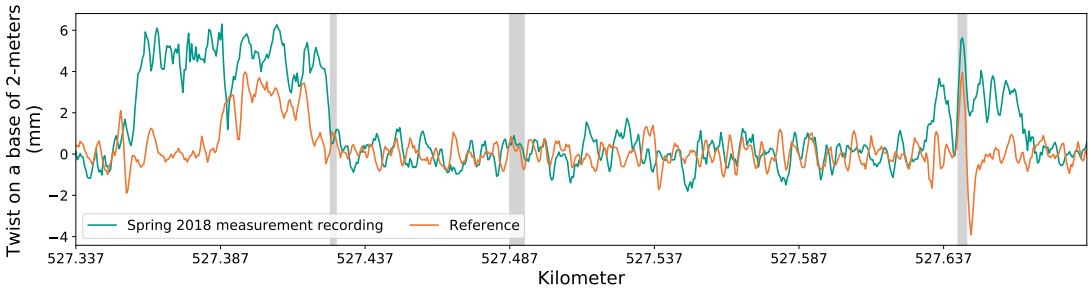

(a) Track measurements recorded spring 2018 compared to the reference, after pre-alignment.

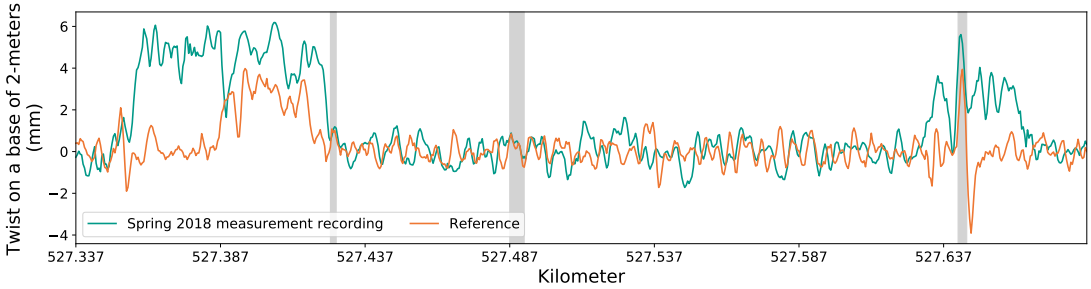

(b) Track measurements recorded spring 2018 compared to the reference, further aligned with COW.

Figure 5.7.: Autumn 2018 measurement recording after pre-alignment compared to further alignment with COW. Small shifts are applied by COW in an attempt to compensate for compression or stretching during recording, visible in the subsection highlighted in grey.

Without knowing the ground truth, the proposed alignment by applying COW in Figure 5.7 appears feasible and more accurate than both the alignment achieved after pre-alignment and by further alignment with RAFFT. However, in other subsections of the track, the alignment achieved by COW seems less favorable compared with RAFFT in regards to similarity. An example is shown in Figure 5.8, where the COW algorithm induces a shift in the opposite direction of what would be expected. Recall that the same section of track was aligned, assumed successfully, in Figure 5.4 utilizing RAFFT. This shows that different alignment methods can perform alternately favorably for different subsections of the track. Bearing the evaluation metric in mind where RAFFT overall scored higher for both simplicity value and factor compared to COW, it becomes a trade-off between potential local extreme shifts and lower simplicity value and peak factor. Hence the latter use of the alignment method becomes decisive.

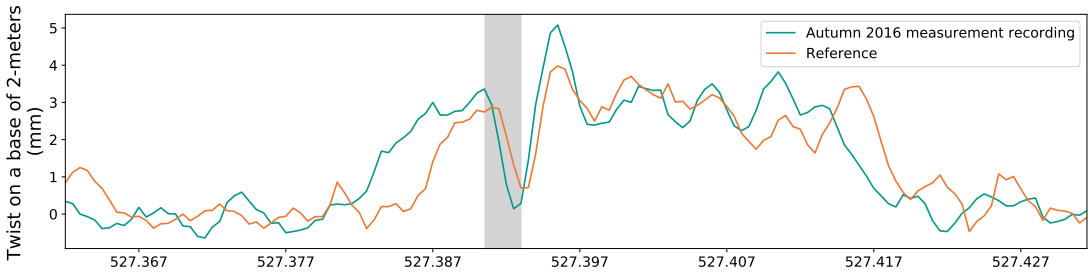

(a) Track measurements recorded autumn 2016 compared to the reference, after pre-alignment.

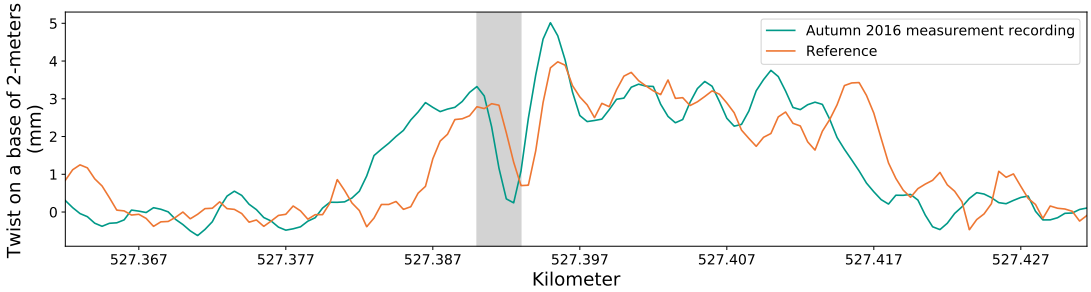

(b) Track measurements recorded autumn 2016 compared to the reference, further aligned with COW.

Figure 5.8.: Autumn 2016 measurement recording after pre-alignment compared to further alignment with COW. It is assumed that the algorithm induces a shift in the opposite direction of what would be expected as favorable.

To conclude, the proposed pre-alignment to reduce initial shift utilizing CCF gave superior results. Although some of the data included when applying this method was recorded below the set speed validity limit, the method is recommended. Further, alignment with DTW scored the highest warping effect at the cost of extensive alternation of the aligned measurement series. The latter is undesired when utilizing the measurement recordings in predictive maintenance, as information regarding degradation is lost. RAFFT scored the second-highest warping effect, achieving a higher peak factor score than DTW. However, for some locations, RAFFT warps the aligned measurement series extensively, causing unrealistic compression or stretching. COW avoids these potential local extreme shifts but scores slightly lower on all metrics compared to RAFFT. The

combined method utilizes RAFFT and is hence also impacted by possible extreme shifts in the start or end of the segment. CCF, scoring the lowest warping effect, cannot compensate for the compression and stretching observed present in the measurement series. Later use is considered due to a decisive trade-off between potential local extreme shifts and lower peak factor and simplicity value scoring. It is evaluated whether local extreme shifts are manageable in later utilization of the data and thereby acceptable. It is concluded that it is more favorable to avoid potential local extreme shifts, due to local extreme shifts resembling unrealistic compression and stretching. As extreme shifts locally account for a greater difference between the reference and measurement series, it is assumed to be more difficult to handle in the later application, e.g., in machine learning algorithms. Hence, based on the presented evaluation, COW is selected as the most suited algorithm to align the Bane NOR data set after pre-alignment. This results in the proposed setup for relative alignment depicted in Figure 5.9.

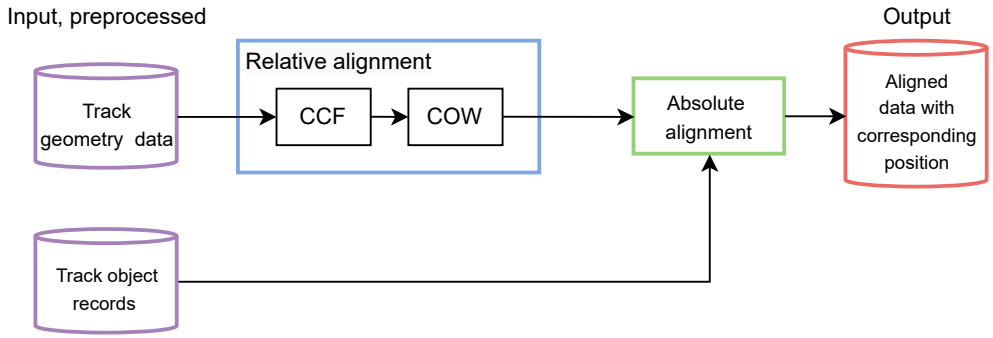

Figure 5.9.: Updated proposed structure for method to achieve aligned measurements series with established setup for relative alignment.

5.2. Absolute position determination

This section evaluates the proposed methods for determining absolute position to conclude on best practice. The goal is to map the measurement vehicle recorded data as closely as possible to their true positions, and hence the method minimizing positional error is favorable. As the track object records are in the process of being updated, their feasibility in producing absolute positioning is relevant to consider, bearing in mind that achieved accuracy may be misleading, see Section 3.2.

5.2.1. GPS

Results

Following the setup proposed in Section 4.2.1, deviations between coordinate positions extracted from the track geometry data set and the field computed positions for the five selected mast are computed. The found deviations are given in Figure 5.10. Accumulated, spring 2020 measurements deviate 8.21 meters while autumn 2020 measurements deviate 5.53 meters from the field computed positions. The median deviation from field computed positions for both measurement recordings is 0.96 meters.

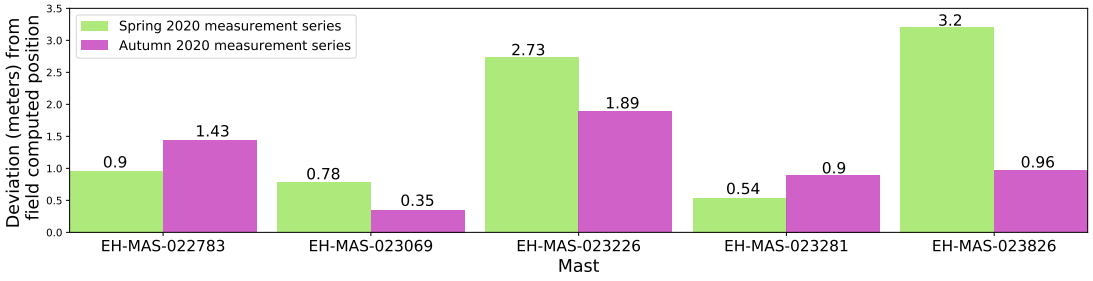

Figure 5.10.: Comparing deviation in meters between field computed position and position extracted from track geometry data set recorded spring and autumn 2020.

Figure 5.11 visualises field computed positions and positions extracted from the track geometry data set based on measured stagger. Studying this figure, all positions can be compared to what visually would be the expected position range of the mast. Recalling the measurement setup detailed in Figure 4.11, expected GPS position is on the track center line, perpendicular to the mast foot. From Figure 5.11 it can be observed that for all positions computed based on field measurements (pink), the derived position is within or on the boarder of the expected position range (crimson rectangle). The same applies to the GPS position extracted based on measured stagger autumn 2020 (purple). Extracted GPS position based on measured stagger spring 2020 (green) is within or on the boarder of the expected position range for all masts with the exception of mast EH-MAS-023826.

Discussion

To evaluate the results obtained for absolute positioning utilizing GPS coordinates from the measurement vehicle directly, the accuracy of these results needs to be considered. As measurements are recorded for every half meter, an object cannot be located with an accuracy surpassing this distance.

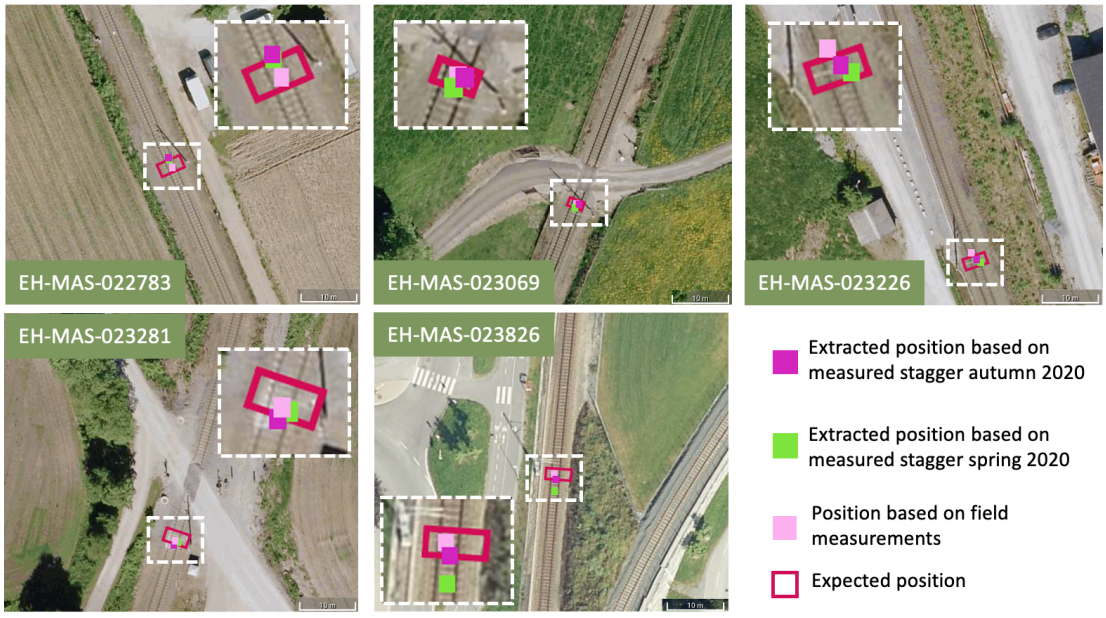

Figure 5.11.: Positions of the selected mast computed from field measurements and extracted from track geometry data set based on measured stagger value autumn and spring 2020 respectively. Computed and extracted positions are compared to the respectively expected positions. Satellite images extracted from Gule Sider [2].

In Section 4.2.1, worst-case errors for both computing position from field measurements and extracting position from the measurement recording were approximated. These errors were estimated to be 0.65 meters and 2 meters respectively. With deviation between measurements extracted from the measurement vehicle and computed positions based on field measurements varying from 0.35 to 3.21 meters, it is apparent that potential errors from both these measurements have a high risk of impacting the obtained result. In Figure 5.11, all computed positions are compared to what visually would be the equivalent expected position. Except for the extracted position from the spring 2020 measurement series at mast EH-MAS-023826, which is residing outside the expected position range, the potential position error is less than the approximated worst-case error. In the following, aspects of the results are analyzed in an attempt to distinguish between potential errors caused by the verification method and errors caused by the GPS sensor on the measurement vehicle.

Analyzing Figure 5.11, the most significant deviation in position between the extracted position from the spring and autumn measurement recording is for positioning mast EH-MAS-023826, for which the deviation between the extracted positions equals 0.99 meters. To analyze this deviation, Figure 5.12 compares the recorded stagger spring and autumn 2020 while passing this mast. Visually, the shape of the recorded stagger for both measurement series appears similar. Hence, it does not indicate that position extraction from the measured stagger is the cause of the observed deviation. However, there is a noticeable difference in amplitude when comparing the two measurement series. This can indicate an external factor, such as wind, impacting the recorded stagger

and thereby causing a difference in extracted position. Comparing the distance between the two adjacent masts extracted from the recording, see Figure 4.13, the distance is 60 meters under the autumn 2020 recording and 61 meters under the spring 2020 recording. In the high voltage mast record, the equivalent distance is specified to be 60 meters. These observations indicate that the deviation in position extracted from the two measurement series is due to the GPS verification method and not caused by an inaccuracy in the GPS sensor utilized onboard the measurement vehicle.

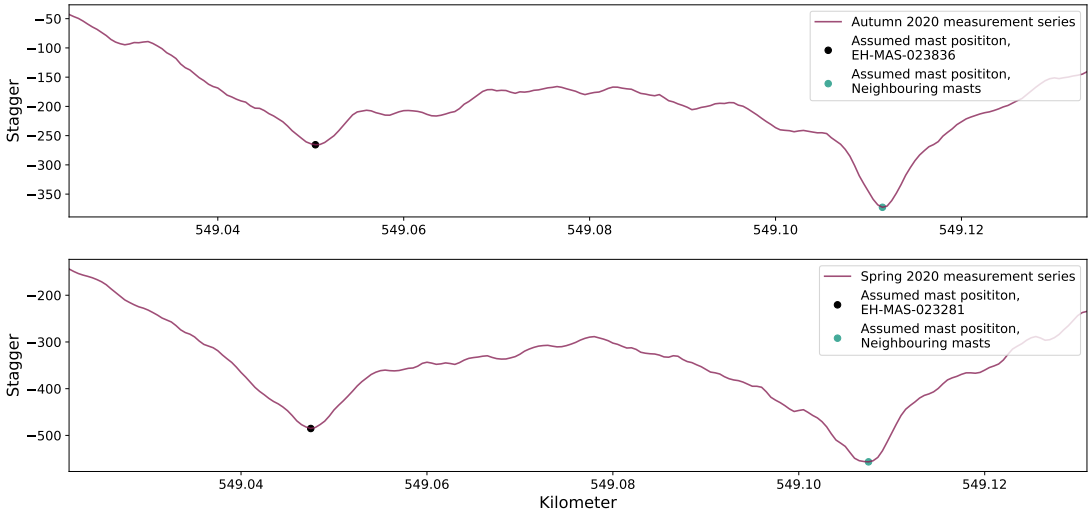

Figure 5.12.: Comparison in recorded stagger spring and autumn 2020 and assumed position of the mast EH-MAS-023836. The shape of the recorded stagger appears similar, but there is a noticeable difference in amplitude between the two recordings.

The smallest deviations between measurement series extracted position and computed position based on field measurements are obtained for mast EH-MAS-023069 and EH-MAS-023281. Closer inspection of EH-MAS-023069 in Figure 5.11 yields the observation that the extracted position from the autumn 2020 recording and the position computed based on field measurements are both perpendicular to the track center line. Hence, the deviation in position, i.e., 0.35 meters, is due to a difference in distance to the mast foot. This difference can be due to either error in the measured distances in the field, incorrectly retrieved mast arm length from record, or a mismatch between the GPS sensor's defined position in the GPS verification setup and its actual position on the measurement vehicle. Recall that the field computed position is placed on the track center line. If the GPS sensor mounted on the measurement vehicle is placed with an offset to the train's center line, this will cause a mismatch. However, perpendicular deviation in position to the train's driving direction has less impact regarding later use since the planning of maintenance activities is focused on knowing the position along the track in the train driving direction. However, in the computation of the deviations in position between field computed position and position extracted from the measurement recording, no consideration has been given to the direction of the deviation. Hence, both position errors influence the deviations obtained in Figure 5.10 equally. Taking this factor into account will either improve or result in the same position deviation as obtained in Figure 5.10. With the distance between the rails equal to 1.435 meters, this

is the maximum improvement in the deviation computation that can be expected.

When analysing the results visually in Figure 5.11, perpendicular deviations in position can be disregarded. In addition, positions from the measurement vehicle can be compared visually to the true position of the mast, eliminating potential errors in the field computed position. Such evaluation shows that the field computed position is closest or equally close to the expected mast position for four of the five studied masts, compared to the positions extracted from the recordings. Only for the mast EH-MAS-023226, the measurements extracted from the recordings are closer to the expected position. However, errors in the satellite images and scaling under extraction of the imaging can mislead and induce errors. The satellite images utilized are extracted from Gule Sider [2], where errors in image alignment were observed along the studied track section. Such an error in image alignment is common and was also observed by [71], where the position accuracy of Google Earth was addressed. Additionally, the angle at which the satellite image is taken can contribute to an incorrect perception. When comparing positioning between different images, these factors have a more significant effect than within the same image. Within only one image, potential error caused by the satellite image will have a more significant impact when comparing positions to the depicted mast than when comparing the derived positions to each other.

To summarize, it is difficult to differentiate between errors caused by the GPS verification method and the GPS sensor mounted to the measurement vehicle when determining the latter's accuracy. Without specifications regarding the type of GPS sensor mounted to the measurement vehicle, no information is available on accuracy from the enterprise manufacturing the sensor. However, the presented analysis indicates that the errors due to the verification method cause a more significant impact on the obtained result than the GPS sensor mounted to the measurement vehicle. Visual analysis indicates that the field computed positions are closest to the expected mast position for four of the five studied masts. Further, extracted coordinates from autumn 2020 measurements coincide with the expected positions for all five mast objects. Based on lowest accumulated deviation from the field computed positions, it is recommended to utilize coordinates obtained from the autumn 2020 measurement series. Hence, the strongest conclusion this study can propose is an expected upper limit for inaccuracy from the GPS sensor utilized autumn 2020 equal to 1.43 meters, as this is the maximum deviation observed from the field computed position when disregarding the assumed error-prone field computation for mast EH-MAS-023226.

5.2.2. Superstructure record

Results

Following the procedure detailed in Section 4.2.2, CCF was utilized to perform alignment between the spring 2020 measurement recording and the superstructure record. The coordinates obtained for the five selected bridges after conducting alignment are listed in Table 5.3 and visually shown in Figure 5.13. In Figure 5.13, it can be observed that for three of the five selected bridges, coordinate extraction after alignment successfully locates the bridges. In comparison, coordinate extraction from segments before alignment successfully locates one of the bridge objects while coordinate extraction based on kilometer match does not manage to locate any of the bridges.

Table 5.3.: Coordinates obtained for the five selected bridge objects after aligning the spring 2020 measurement recording to the constructed signal based on the superstructure record.

Bridge object in record	Kilometer position in record	Obtained coordinates after alignment with CCF Curvature	Cross-level
Bridge A.	502.8000	63.06557220° N, 10.28635814° E	63.06557220° N, 10.28635814° E
Bridge B.	514.9200	63.15274718° N, 10.28194348° E	63.15275712° N, 10.28196344° E
Bridge C.	526.3850	63.24279214° N, 10.28084980° E	63.24276024° N, 10.28088563° E
Bridge D.	530.7835	63.27953566° N, 10.28304998° E	63.27953566° N, 10.28304998° E
Bridge E.	546.2830	63.38873459° N, 10.37062640° E	63.38873459° N, 10.37062640° E

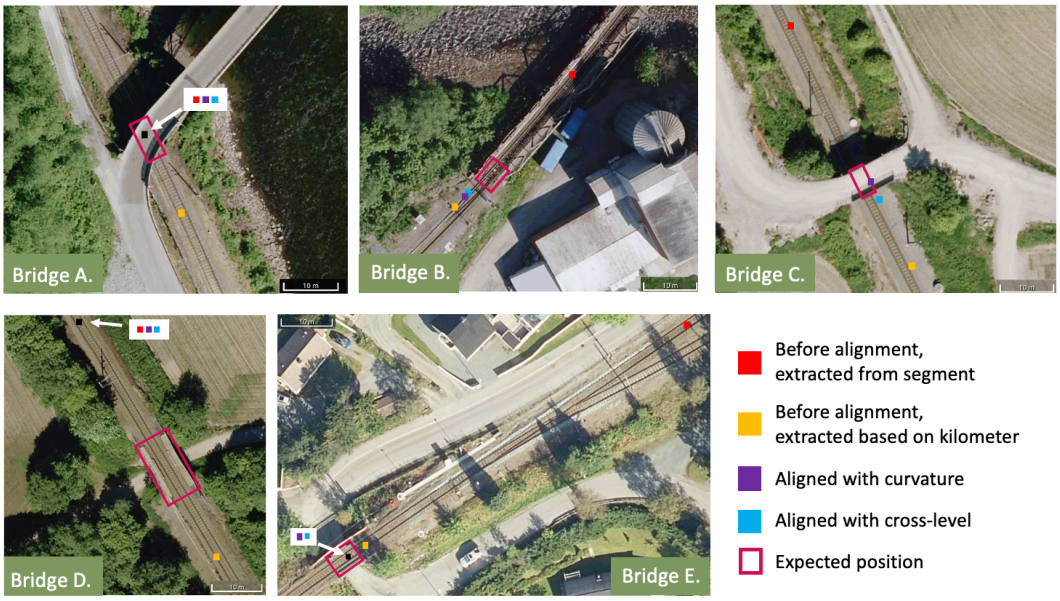

Figure 5.13.: Extracted positions of the bridge objects based on the superstructure record before and after alignment, compared to visually expected position of the bridge objects. Satellite images extracted from Gule Sider [2].

Discussion

An analysis is conducted to evaluate the results obtained from mapping the superstructure recorded to measurement vehicle recorded data. Three of the five bridges are selected for this analysis based on their obtained results, namely bridge C, D and E. Visual analysis of satellite images can potentially be misleading and thereby induce errors in the evaluation, see discussion in Section 5.2.1. The expected position of bridge B in Figure 5.13 is the starting point of the bridge, as it is this fixed point which is extracted from record.

For bridge C in Figure 5.13, it can be observed that alignment with curvature and cross-level results in expected and close to the expected positions of the selected bridge respectively. Further, analyzing the alignment that gave these results, Figure 5.14 depicts curvature measurements for the track segment where bridge C resides. In Figure 5.14, the subsection of the track is compared before and after alignment. Visually, it can be observed that the alignment between the constructed signal and spring 2020

measurement series is improved after applying the proposed shift. However, an even greater shift would be expected for optimal alignment. Expected optimal alignment is depicted in Figure 5.15, where the shift has been determined manually based on maximizing the similarity between the two series. CCF cannot locate this favorable shift due to too great a difference between the two series. While the values for curvature in the measurement recording transition smoothly between different values for curvature, the interpolated signal consists of abrupt angles. Hence, it would be more desirable for this specific alignment task to maximize correlation where the value in curvature changes. However, since this maximization is at the expense of achieved cross-correlation over the whole segment, the CCF algorithm employed does not locate the preferred shift.

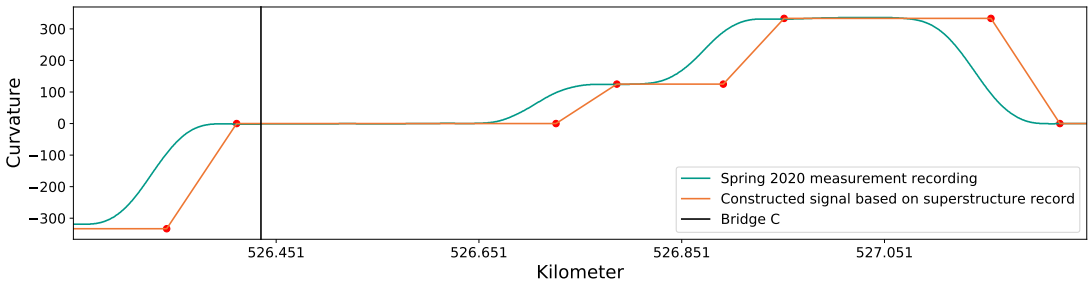

(a) Subsection of track at bridge C, before alignment.

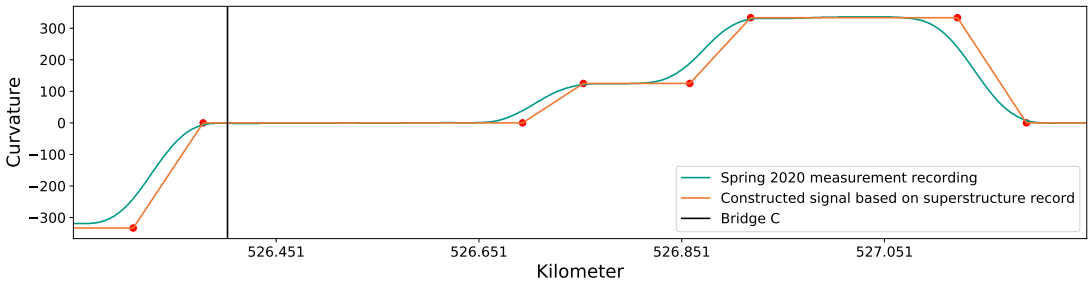

(b) Subsection of track at bridge C, after alignment.

Figure 5.14.: The constructed signal based on curvature values from the superstructure record and the spring 2020 measurement recording before and after applying the alignment proposed by CCF, i.e., a shift equal to 33.0 meters. However, visually, a greater shift is expected to achieve optimal alignment.

The CCF detected shift for the curvature measurement channel is equal to 33.0 meters, while the manual expected optimal shift is equal to 51.5 meters. This implies that applying the manual expected optimal shift results in position coordinates outside the expected position area, see Figure 5.16. Assuming that the manually determined shift is optimal, the position error is either due to an error in the measurement vehicle recorded GPS data or the utilized superstructure record. In Section 5.2.1 it was found that the deviation in GPS position from the utilized sensor onboard the measurement vehicle was expected to be below 1.43 meters and hence minimal compared to the position deviations obtained here. Therefore, it is more likely that the position error is due to errors in the superstructure record.

Further, alignment with cross-level for the same subsection of track is evaluated in Figure

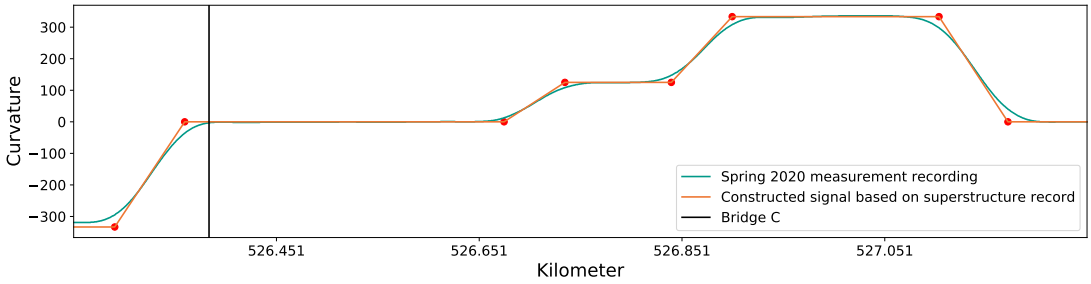

Figure 5.15.: Constructed signal based on curvature values in the superstructure record manually aligned to the spring 2020 measurement recording. The suggested shift is equal to 51.5 meters.

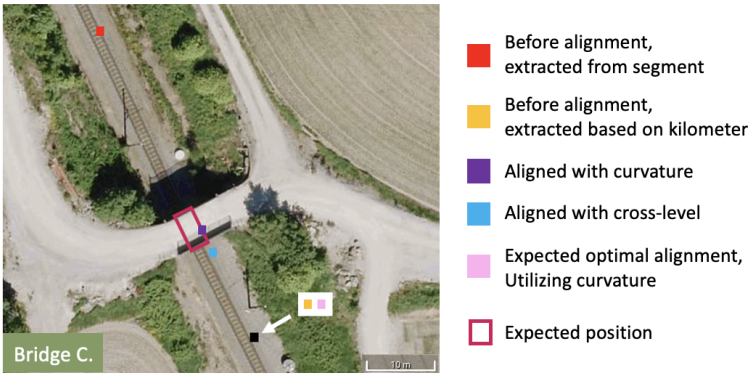

Figure 5.16.: Extracted coordinates, from the spring 2020 measurement recording, for bridge C based on the manual alignment between the superstructure record and measurement series. Observe how the position extracted from the measurement vehicle after assumed optimal alignment is outside the expected position range for the bridge object. Satellite image extracted from Gule Sider [2].

5.17. Like aligning with curvature measurements, CCF improves the alignment between the constructed signal and the spring 2020 measurement series but it does not detect the optimal shift. Here, the shift detected by CCF is equal to 37.0 meters, while the expected optimal shift is 51.5 meters. The expected optimal shift is independent of the measurement channel since both measurements were recorded simultaneously onboard the measurement vehicle. Hence, alignment conducted on the cross-level measurement channel is closer to the expected optimal alignment for this segment.

When comparing the recorded absolute[1] values for cross-level in Figure 5.17 with those obtained for curvature in Figure 5.14, it can be observed that measured cross-level at the start and end of the transition curve closer resembles the constructed signal. However, the cross-level measurements encounter more noise. Recall that the similarity between the constructed signal and measurement vehicle recorded data was compared in Section 3.2.1. Here, the lowest euclidean distance and hence highest similarity between the

[1]Recall from Section 3.2.1 that absolute values for recorded cross-level measurements are utilized due to difference in definition of cross-level between the recorded measurements and values from the superstructure record.

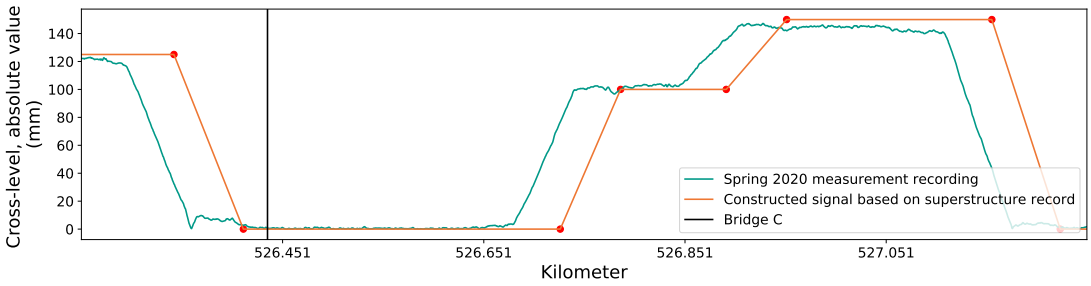

(a) Subsection of track at bridge C, before alignment.

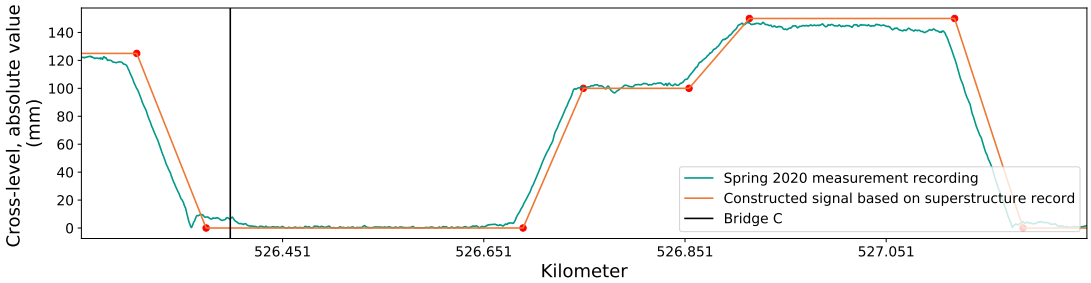

(b) Subsection of track at bridge C, after alignment.

Figure 5.17.: The constructed signal based on cross-level values from the superstructure record and the spring 2020 measurement recording before and after applying the alignment proposed by CCF, i.e., a shift equal to 37.0 meters. However, visually, a greater shift is expected to achieve optimal alignment.

constructed signal and the recorded data was obtained for the curvature measurement channel, when studying the whole track section between Støren and Trondheim.

For bridge E, it can be observed in Figure 5.13 that alignment with both curvature and cross-level yield expected coordinates of the bridge object. Figure 5.18 details the alignment on the curvature measurement channel for the track section where bridge E resides. From Figure 5.18, it can be observed that the alignment produced by CCF is close to the sought optimal alignment. The same applies for alignment with CCF on the cross-level measurement channel. Hence, in contradiction to bridge C, sought optimal alignment yields a coordinate position within the expected position range.

For bridge D, the extracted coordinates before and after alignment are identical, independent of the measurement channel used in alignment, see Figure 5.13. Figure 5.19 depicts detected alignment for the track section where bridge D resides. It can be observed that cross-level throughout the segment is equal to zero for the constructed signal and close to zero for the measurement vehicle recorded data. Recall from Section 4.1.2 that if no curvature (and therefore indirectly cross-level) is present within a segment, the shift will be impossible to detect. This is also the case for this alignment task, and hence the reason why no alignment is detected. For the studied track section between Støren and Trondheim, after prepossessing the spring 2020 recording, 5 of 52 segments contain railway track with no curvature.

To summarize, the optimal alignment between the superstructure record and measure-

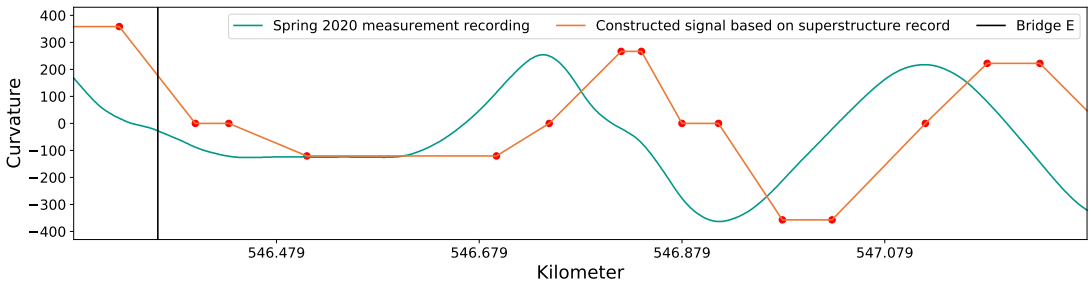

(a) Subsection of track at bridge E, before alignment.

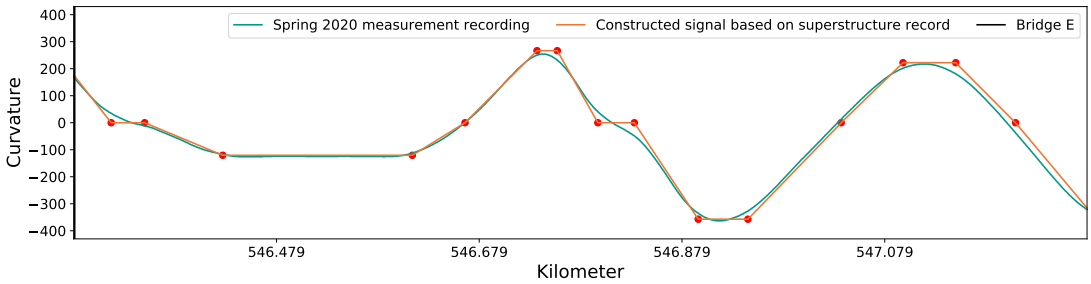

(b) Subsection of track at bridge E, after alignment.

Figure 5.18.: The constructed signal based on curvature values from the superstructure record and the spring 2020 measurement recording before and after applying the alignment proposed by CCF. Visually it can be observed that an optimal alignment is achieved by applying CCF.

ment series does not consequently yield the sought correct GPS position. With minor errors expected from the utilized GPS sensor on the measurement vehicle, it is assumed that the error in positioning is due to errors in the superstructure record. However, as stated in Section 3.2, the goal is to determine if it is possible to utilize this type of data to achieve absolute alignment, not to determine the method's accuracy. This is due to ongoing improvements to the utilized records that in the future potentially can compensate for the present lack of accuracy. Hence, it is assumed that optimal alignment yields the correct position in the following. Still, considerable differences between the constructed and recorded measurement series cause the utilized alignment method not to be capable of detecting the optimal shift for all segments. Hence, further investigation would be necessary to improve alignment. On straight tracks, alignment will still be impossible due to the lack of curvature and cross-level. Based on the euclidean distance computed between the constructed and measured series in Section 3.2.1, it is recommended to align the superstructure record utilizing curvature value.

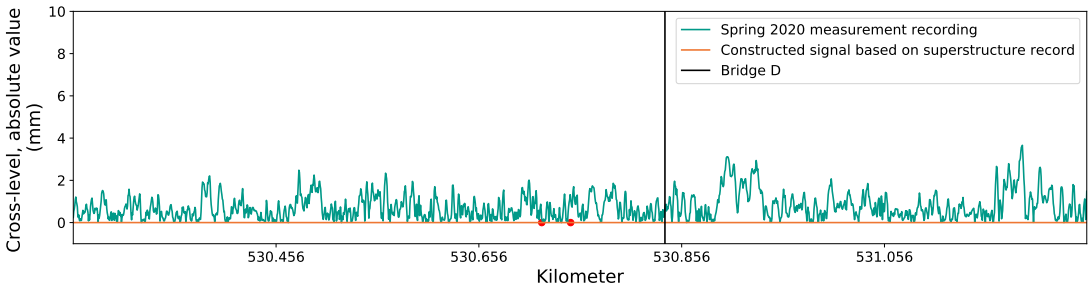

Figure 5.19.: Subsection of track at bridge D, before and after alignment. In the presence of curves, absolute values for cross-level reside between 0 mm and 170 mm. However, no cross-level is present for the displayed segment, making it impossible to detect shifts.

5.2.3. High voltage mast records

Following the procedure detailed in Section 4.2.2, the absolute position is determined both by aligning curvature data from the record to the reference measurement series and by matching mast objects based on kilometer position and stagger. These methods are in the following separately evaluated, as their approaches deviate substantially.

Results - Alignment of interpolated high voltage mast record

The coordinates obtained after aligning the interpolated curvature values from the high voltage mast record to the spring 2020 measurement recording are listed in Table 5.4. Table 5.4 also includes assumed mast positions based on matching kilometer values in record with measured kilometer values spring 2020. Notice that the latter is not the same as the proposed matching method, which utilizes the assumed mast position in the measurement series based on recorded stagger. The found deviations between retrieved positions based on comparing curvature and kilometer values, and the position computed based on field measurements are given in Figure 5.20. Accumulated positions based on curvature matching deviate with 226.21 meters, while positions based on kilometer matching deviate with 16.28 meters from the field computed positions.

Table 5.4.: Coordinate positions for the five selected mast objects after aligning the spring 2020 measurement curvature values to curvature values in the high voltage mast record and matching kilometer values in the recorded measurement series and record.

Mast object in record	Kilometer position in record	Obtained coordinates after aligning curvature with CCF	Obtained coordinates based on comparing kilometer value
EH-MAS-022783	505.216	63.07715057° N, 10.25295038° E	63.07721252° N, 10.25289146° E
EH-MAS-023069	517.595	63.17365118° N, 10.30548175° E	63.17346202° N, 10.30532359° E
EH-MAS-023226	525.262	63.23292188° N, 10.28047950° E	63.23291767° N, 10.28048305° E
EH-MAS-023281	527.822	63.25572404° N, 10.28563107° E	63.25414238° N, 10.28475180° E
EH-MAS-023826	549.055	63.41053562° N, 10.38328116° E	63.41069222° N, 10.38331222° E

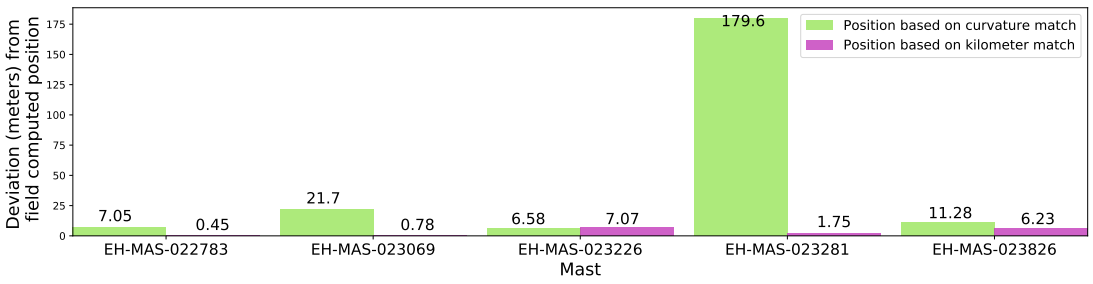

Figure 5.20.: Comparing deviation in meters between field derived position and position extracted based on aligning/matching curvature and kilometer values between high voltage mast record and spring 2020 recorded measurements.

Visual analysis of the obtained coordinates in Figure 5.21 shows that none of the obtained coordinates, after aligning curvature values (purple), manage to locate the mast objects correctly. Without alignment, matching the kilometer values of the mast objects in the record with the recorded kilometer values spring 2020 (yellow) yields the expected

position for three of the five mast objects, namely for mast EH-MAS-022783, EH-MAS-023069, and EH-MAS-023281.

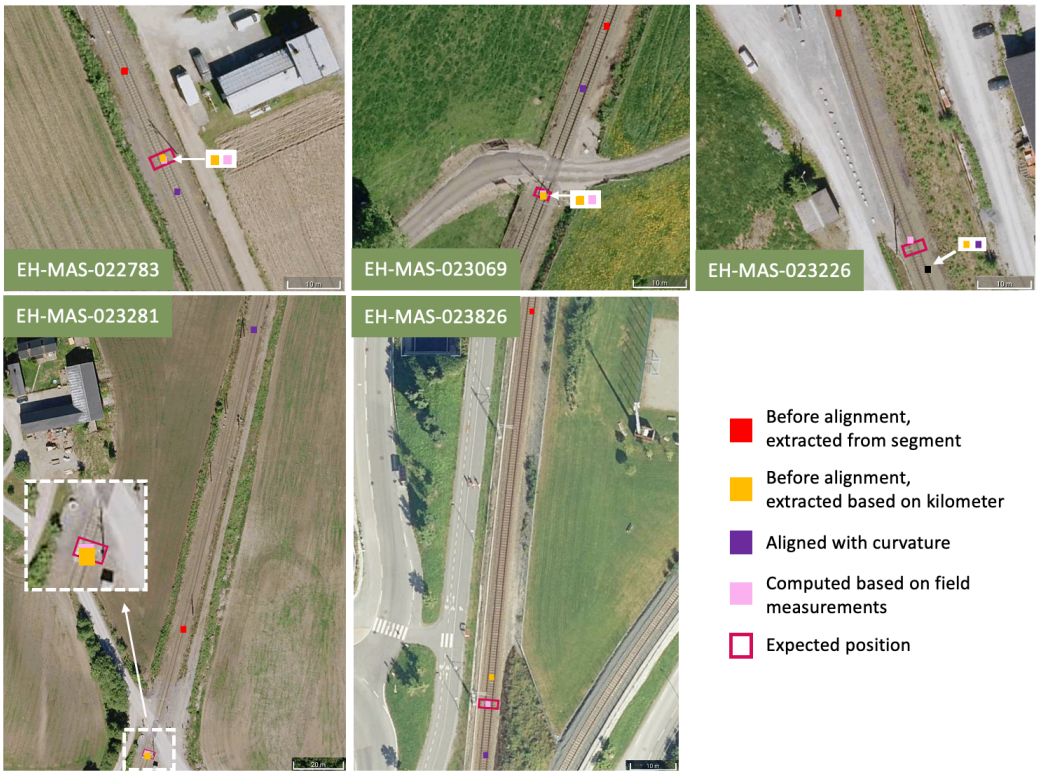

Figure 5.21.: Extracted positions for the mast objects based on the high voltage mast record, compared to the visually expected position of the mast objects. None of the extracted coordinate positions are within the expected position range with the proposed curvature alignment method. Satellite images extracted from Gule Sider [2].

Discussion - Alignment of interpolated high voltage mast record

To evaluate the obtained results and method, a further analysis is conducted. Key observations that are studied in detail, are the alignment methods' lack in correctly determining absolute position and the unexpected higher accuracy obtained by mapping solely based on kilometer values. Inaccuracies due to analysing positions in satellite maps was covered in Section 5.2.1 and apply equally here.

The position extracted after curvature alignment at mast EH-MAS-022783 deviates 7.05 meters from the position computed based on field measurements. Figure 5.22a depicts the subsection of track where mast EH-MAS-022783 is located before alignment. Further, Figure 5.22b depicts the CCF proposed alignment, showing an improvement in the alignment between the constructed signal based on curvature values in the record and the spring 2020 measurement recording. CCF applies a shift to the segment equal to 25.5 in the direction right, causing the specific mast object to end up just outside the depicted segment after alignment. Visually, the alignment achieved by CCF is equal to

the sought optimal alignment. Different from the transition curve events studied in Section 5.2.2, the masts are not located to coincide with the start or end of curves. Hence a more significant deviation between the constructed signal and recorded curvature is expected. However, assuming that the curvature recorded by the measurement vehicle is correct, the masts highlighted in grey in Figure 5.22b would be expected to have a curvature value different from zero to coincide with the recorded measurements. Hence, the extracted coordinates from the measurement vehicle deviate from the expected position, although the assumed optimal alignment is detected. This mismatch is assumed to be due to missing or incorrect curvature values in the record. Incorrect mast position data is less likely to cause the described mismatch due to low observed deviation between GPS position extracted from the measurement vehicle based on kilometer value and position computed based on field measurements.

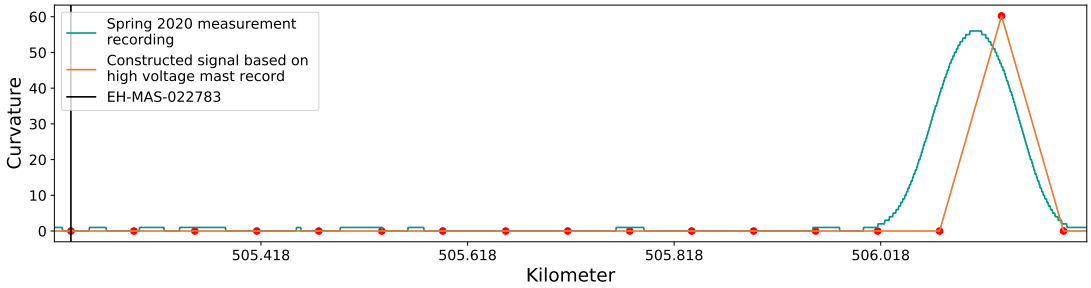

(a) Subsection of track at mast EH-MAS-022783, before alignment.

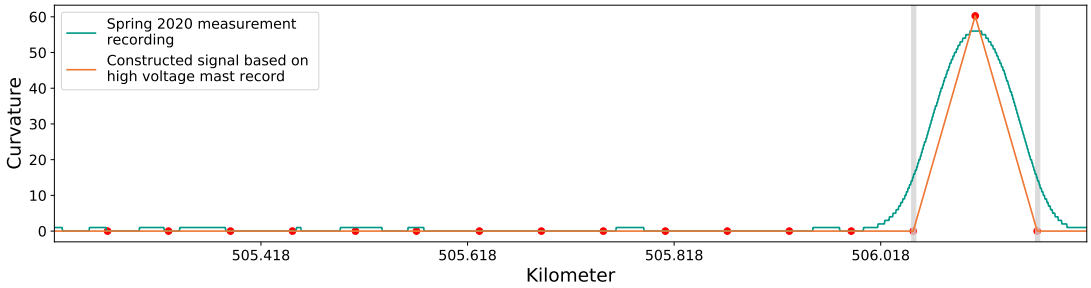

(b) Subsection of track at mast EH-MAS-022783, after alignment.

Figure 5.22.: The constructed signal based on curvature values from the high voltage mast record and spring 2020 measurement recording are compared before and after applying the alignment proposed by CCF. Visually the alignment detected by CCF is perceived to be optimal.

Further, Figure 5.23 depicts the alignment of curvature data for the subsection of track where mast EH-MAS-023281 is located. CCF applies a shift equal to 128.5 meters in the direction left. After aligning the curvature data, the extracted coordinates from the measurement vehicle deviate 179.6 meters from the positions computed based on field measurements. The substantial deviation in position can also be observed in Figure 5.21. Comparing the constructed signal based on curvature values and the spring 2020 measurement recording in Figure 5.23, a significant difference can be observed between the two series. Similar to the constructed signal studied in Figure 5.22 for mast EH-MAS-022783, it can be assumed that much of the disagreement is due to incorrect values for curvature for a significant amount of masts in the high voltage mast record.

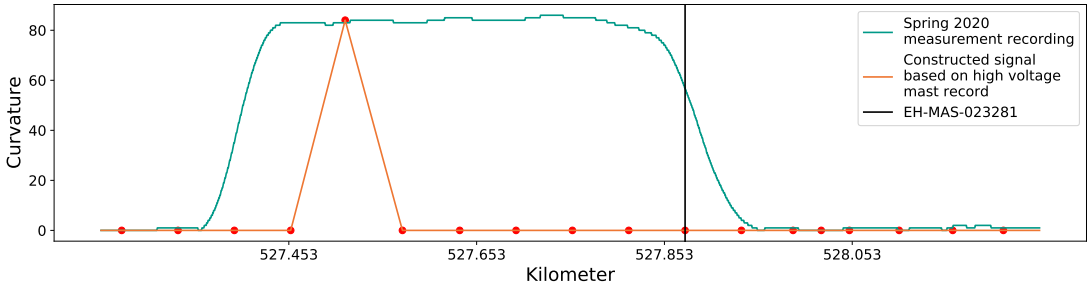

(a) Subsection of track at mast EH-MAS-023281, before alignment.

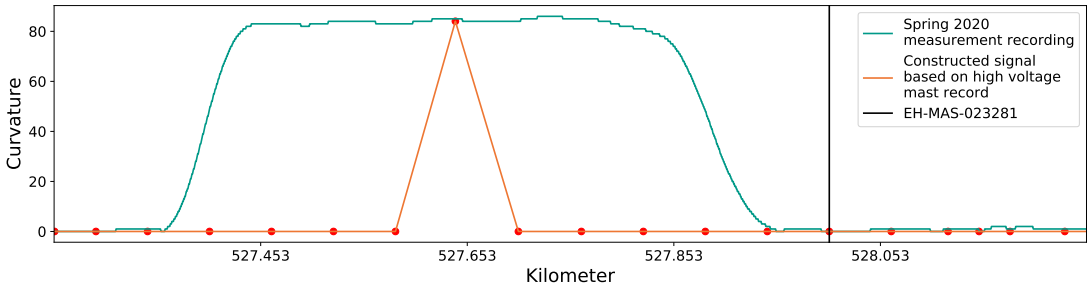

(b) Subsection of track at mast EH-MAS-023281, after alignment.

Figure 5.23.: The constructed signal based on curvature values from the high voltage mast record and spring 2020 measurement recording compared before and after applying the CCF proposed alignment. Observe how presumably curvature values are incorrect for a significant amount of mast in the high voltage mast record.

Extracting masts GPS positions from the spring 2020 recording solely based on comparing the recorded kilometer values and kilometer values in record yields surprisingly good results compared to aligning curvature, see Figure 5.20. By comparing kilometer values, this method benefits from the kilometer updates during recording, covered in Section 3.1.1. These position updates can be seen as a rough kilometer alignment during recording. As presumably the kilometer values in the high voltage mast record are precise, the matching yields substantially better results. The same kilometer matching method, when applied to the superstructure records in Section 5.2.2, did not yield any correct identification of the bridge objects. Hence, the alignment between the recorded kilometer position and the kilometer values in the superstructure record is less accurate. Since the recorded kilometer values coincide with the high voltage mast record, this indicates that the kilometer values in the superstructure recorded are inaccurate.

To summarise, incorrect and missing curvature values in the high voltage mast record prevent successful alignment between the constructed signal based on curvature values and recorded curvature. Even with correct values, the lack of similarity may pose a challenge when detecting alignment utilizing CCF. Less deviation in position from the field computed coordinates was achieved by matching kilometer values, where position updates during recording are exploited.

Results - Assumed mast position matching

For the five selected masts, matching the assumed mast position extracted from both spring and autumn 2020 measurement recordings yields the same coordinates as obtained for the GPS verification scheme. Hence, deviations between positions extracted from the measurement series and the field computed positions are detailed in Figure 5.10. The obtained coordinates are visualized in Figure 5.11.

Discussion - Assumed mast position matching

The accuracy of the obtained results was extensively discussed in Section 5.2.1 and is therefore not further discussed here. Instead, the method in itself is analyzed.

There are 964 masts along the detected driven track line, of which 733 and 739 are matched with a corresponding assumed mast position for the autumn and spring 2020 measurement series, respectively. Recall from Section 4.2.2 that there are significantly more masts in the record compared to the number of masts detected. Hence, a lower number of achieved matches is expected. However, suppose the lower number of assumed mast positions leads to matching masts that, in reality, do not correspond. In that case, an incorrect absolute position is determined. Figure 5.24 depicts a subsection of track between 506.5 and 507.0 kilometers. Observe that for both the autumn and spring 2020 recording in Figure 5.24, the masts EH-MAS-022806, EH-MAS-022808, EH-MAS-022813, are matched equally, despite differences between assumed mast position and mast position in the record. However, at ca. 506.8 kilometers for both the autumn and spring recording, there is no significant local maxima and minima in the recorded stagger, causing different locations to be selected as the assumed mast position. It can be observed that the spring recording in Figure 5.24c contains an additional assumed mast position compared to the autumn recording, which again is paired with an additional mast from the record in Figure 5.24d. Although it is not apparent which of these mast matches are correct, this shows a mismatch between the recorded measurements, which will further propagate into errors when extracting coordinates based on the achieved matches. Hence, this example displays how inaccuracy in stagger measurements causes incorrectly assumed mast position and hence falsely matched masts. For the five selected masts, the matching was successful. However, as shown, this is not the case for all masts, creating a drawback for this method.

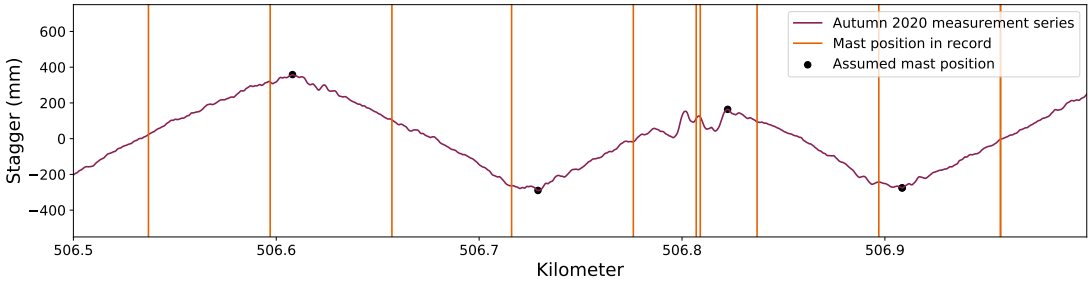

(a) All mast positions from record and assumed mast positions from autumn 2020 measurement recording.

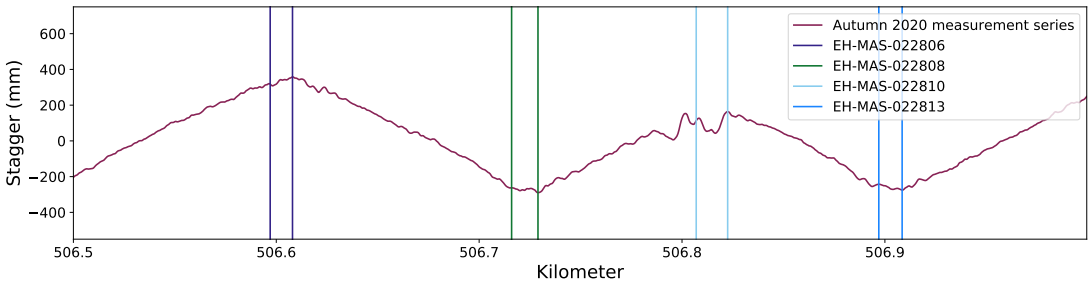

(b) Match mast positions from record with assumed mast positions autumn 2020.

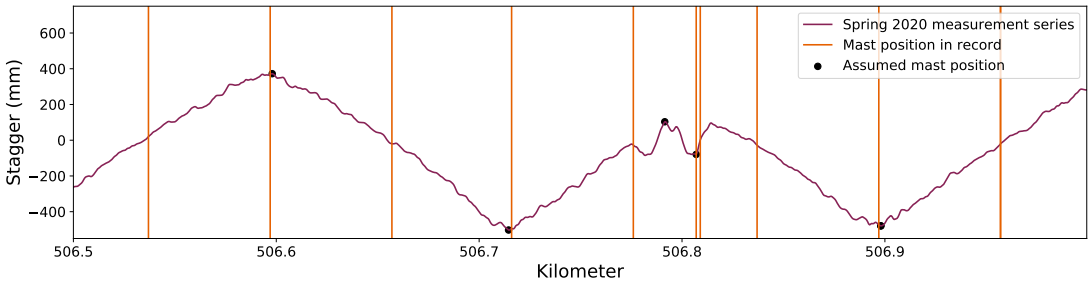

(c) All mast positions from record and assumed mast positions from spring 2020 measurement recording.

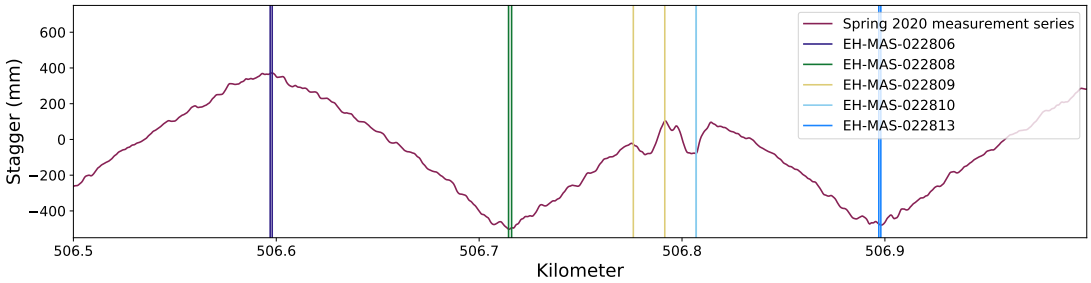

(d) Match mast positions from record with assumed mast positions spring 2020.

Figure 5.24.: Assumed mast positions and mast positions in record compared to the matched masts by applying the proposed method. Noise in recorded stagger causes different assumed mast positions and thereby different matches.

5.2.4. Summary and Further Discussion

The presented methods need to be compared and evaluated to determine the best practice for absolute positioning. As stated, the absolute position methods based on the superstructure and high voltage mast records have shown to be error-prone. Although these records are under ongoing improvements, they are evaluated based on their current state. Still, where relevant, the method's potential is emphasized.

The lowest deviation from expected position and hence highest accuracy was achieved by utilizing the GPS measurements from the measurement vehicle directly and determining absolute position through mast matching. Although not present for the studied masts, the latter method is exposed to noise in recorded stagger. However, an advantage with determining absolute position through mast matching is when the GPS signal is missing as the position is connected to physical objects. In tunnels, determining absolute position by utilizing the GPS measurements from the measurement vehicle directly is not possible. Due to stagger being substantially impacted by environmental conditions, utilizing GPS measurements from the measurement vehicle directly is more favorable. In the following, measures are presented to minimize the shortcomings of utilizing GPS measurements from the measurement vehicle directly.

For the methods determining position based on either the superstructure or high voltage mast record, positions can be verified based on physical objects. This is not evident when utilizing the GPS measurements from the measurement vehicle directly, recalling that the verification conducted in this study is based on a high degree of manual assistance. Although retrieved coordinates from the measurement vehicle can be verified through satellite images to check that the obtained coordinates follow the track line, this does not detect potential lag in the sensor. Therefore, GPS extracted coordinates from the measurement vehicle can be verified by pairing the method with a positioning method based on records. Determining absolute position through mast matching showed the highest accuracy compared to the other methods utilizing records. Therefore, utilizing this method as a verification method is the obvious choice. The drawback of potential incorrect matching is acceptable when only used for verification.

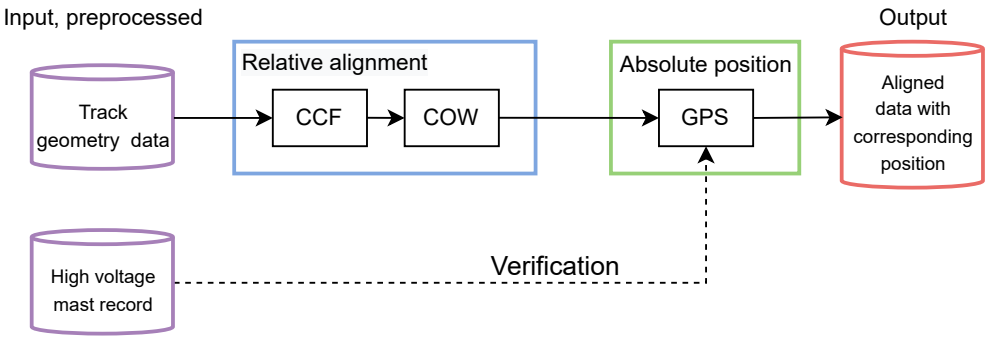

Figure 5.25.: Proposed structure to achieve aligned measurements series with corresponding absolute position.

When the GPS signal is missing, utilizing GPS measurements from the measurement vehicle directly cannot determine position. On the studied track section, missing GPS signal for more than two meters of track only occurs when passing tunnels. Position can then either be derived from the last known GPS position from the measurement vehicle

and recorded mileage or utilizing the high voltage mast record. The latter is proposed as mast are also present inside tunnels. If utilizing the high voltage mast record, mast matching is proposed rather than curvature matching based on the obtained results.

To summarize, this study proposes utilizing GPS measurements from the measurement vehicle directly to determine absolute position with the high voltage mast record as verification. This yields the alignment setup depict in Figure 5.25.

5.3. Lessons Learnt

With hindsight, one can always reflect and discover ways in which research could have been improved. Below are key improvements the author would have made if this work was to be repeated.

1. Significant uncertainty in the presented work was related to the lack of determining the accuracy of the utilized GPS sensor. Although field measurements were conducted to determine the error in the used sensor, the uncertainty in the field measurements themselves was too high to draw a firm conclusion. This uncertainty could have been reduced if position rather were measured on the track itself, with the proper allowance.

2. Uncertainties concerning the extraction of coordinates from the recorded measurements were observed, where noise and measured stagger errors could influence which coordinates were extracted. To minimize the possible effect of such error, it would be desirable to include more masts in the evaluation.

3. To quantify the results obtained in Section 5.2.2, it would have been valuable to conduct field measurements at the selected bridge object. This would have strengthened the comparison with the results obtained from utilizing the high voltage mast record.

6. Conclusion and Further Work

Within the railway domain, operators are struggling to sufficiently maintain all assets, resulting in frequent delays and cancellations. High spending and growing maintenance backlog are unfortunately characteristic across enterprises. Fortunately, with large amounts of data available and the rise of predictive modeling techniques, this trend can be changed. Predictive modeling techniques have already been presented in other studies capable of predicting location-specific defects along railway tracks. However, extensive research into methods for data preprocessing, relative alignment between measurement recordings, and determining the absolute position of the recorded data, especially gathered in complex terrain, is lacking. Complex terrain is characterized by tight curves, frequent low-speed limits, and tunnels, resulting in severe positional shifts and challenging absolute positioning.

This thesis proposes a pipeline of processing steps that transform recorded measurements into aligned measurement series with corresponding absolute positions. The resulting aligned measurement series can subsequently be utilized in predictive modeling. A wide variety of methods for all consecutive parts of the processing pipeline have been investigated and evaluated to obtain the most suitable and robust method, resulting in the pipeline detailed in Figure 6.1.

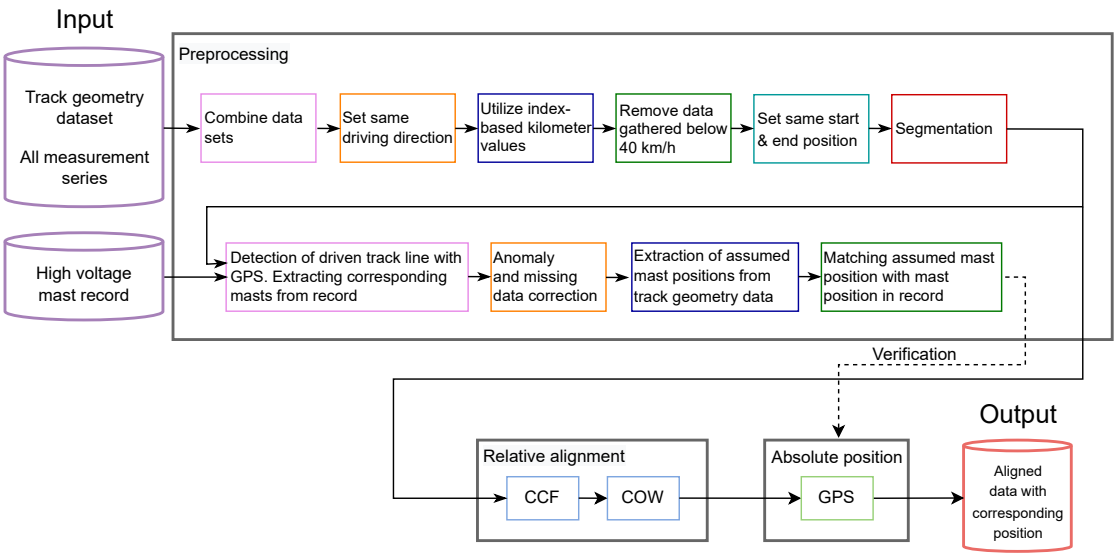

Figure 6.1.: The proposed pipeline transforming recorded measurements into aligned measurement series with corresponding absolute position.

Pre-aligning measurement series utilizing Cross-Correlation Function (CCF) is proposed to compensate for high initial shifts imposed partly by recording measurements in complex terrain. Comparing alignment achieved by applying CCF, Recursive Alignment by Fast Fourier Transform (RAFFT), Dynamic Time Warping (DTW), Correlation Opti-

mized Warping (COW), and a combined method consisting of both RAFFT and COW with pre-aligned measurement series as input, rather than utilizing the preprocessed measurement series directly, gives superior results. Alignment with pre-aligned measurement series as input scores higher on all metrics. Although 3.03% invalid data is included when applying pre-alignment, this method is recommended. Further, when comparing the different alignment algorithms on the pre-aligned measurement series, COW achieves the most satisfactory alignment. Although DTW and RAFFT score a higher warping effect, analysis shows that this is at the cost of unacceptable shape deformation. The latter also applies to the combined method as it includes RAFFT.

Utilizing GPS measurements from the measurement vehicle directly and determining absolute position through mast matching achieves the lowest deviation compared to expected position. As utilizing GPS measurements from the measurement vehicle directly does not rely on other sensor measurements for position determination, this method is recommended, with an expected upper limit for inaccuracy equal to 1.43 meters. However, with GPS signal occasionally missing and no automatic verification possibility, it is recommended to utilize high voltage mast records for sporadic verification of obtained coordinates and in case of missing GPS signal.

6.1. Further Work

In this thesis, a subset of relative alignment methods adapted from [1] have been evaluated. However, the characteristics of these methods are relatively similar, with all methods being both profile-based and pair-wise methods. As relative alignment is a key part of the proposed pipeline and without the possibility to compare with ground truth, it is appropriate to evaluate a broader selection of relative alignment methods. Such broader evaluation would strengthen the conclusion on best practice for relative alignment.

The utilized records are characterized by being prone to error. However, with the ongoing project to register the railway track's absolute position, it is highly relevant to re-evaluate the proposed methods when this process is completed. Such re-evaluation strengthens this work as with improved data quality firmer conclusions can be drawn. Additionally, simplifications have been performed to ease implementation. In Section 3.1, segmentation method three was chosen despite high data loss to determine whether absolute position mapping is possible. As this study shows that such mapping is feasible, it is proposed to minimize the data loss by rather applying alternative segmentation strategies detailed in Section 3.1.

The natural extension to the presented work is to apply predictive models to the obtained measurement series, thereby extending the proposed pipeline. Such extension will give insight into the quality of the obtained alignments and presumably lead to improvements to the proposed pipeline. Further, for industry applications, explainability is key. Hence, it is suggested to facilitate explainability throughout the pipeline so that operators can obtain predictions and justifications for the given predictions. Such justification includes how measurements are aligned and the degree of stretching and compression applied.

Bibliography

[1] M. Khosravi, I. Soleimanmeigouni, A. Ahmadi, and A. Nissen. Reducing the positional errors of railway track geometry measurements using alignment methods: A comparative case study. *Measurement*, 178, June 2021.

[2] Satellite image [Flyfoto], [cited 2022 Jun 2]. Available online at `https://www.gulesider.no`. Norwegian.

[3] Superstructure/maintenance/track adjustment and stabilization [Overbygning/vedlikehold/sporjustering og stabilisering], [updated 2021; cited 2022 Jan 10]. Available at `https://trv.banenor.no/wiki/Overbygning/Vedlikehold/Sporjustering_og_stabilisering`. Norwegian.

[4] Sixth report on monitoring development of the rail market. *European Commission*, feb 2019.

[5] Seventh monitoring report on the development of the rail market. *European Commission*, jan 2021.

[6] C. Kienzler, C. Lotz, and S. Stern. Using analytics to get european rail maintenance on track, [updated 2020 Jun 29; cited 2022 Mar 28]. Available online at `https://www.mckinsey.com/industries/public-and-social-sector/our-insights/using-analytics-to-get-european-rail-maintenance-on-track`.

[7] NTP: 2022-2033: More to maintenance and greater room for maneuver [NTP 2022-2033: Mer til vedlikehold og større handlingsrom], [updated 2021 Mar 19; cited 2022 Jan 23]. Available online at `https://www.banenor.no/Nyheter/Nyhetsarkiv/2021/ntp-2022-2033-mer-til-vedlikehold-og-storre-handlingsrom/`. Norwegian.

[8] Record high investment budget but still too little for renewal of existing railway in 2021 [Rekordstort investeringsbudsjett men fortsatt for lite til fornyelse på eksisterende jernbane i 2021], [updated 2020 Okt 7; cited 2022 Jan 23]. Available online at `https://www.banenor.no/Om-oss/nasjonal-transportplan/test-vare-prioriteringer/`.Norwegian.

[9] A. Consilvio, A. Di Febbraro, R. Meo, and N. Sacco. Risk-based optimal scheduling of maintenance activities in a railway network. *EURO Journal on Transportation and Logistics*, 8(5):435–465, 2019.

[10] J. Xie, J. Huang, C. Zeng, S. Jiang, and N. Podlich. Systematic literature review on data-driven models for predictive maintenance of railway track: Implications in geotechnical engineering. *Geosciences*, 10(11), 2020.

[11] J. Sadeghi. Development of railway track geometry indexes based on statistical distribution of geometry data. *J. Transport. Eng.*, 136(8):693–700, 2010.

[12] I. Cárdenas-Gallo, C. A. Sarmiento, G. A. Morales, M. A. Bolivar, and R. Akhavan-Tabatabaei. An ensemble classifier to predict track geometry degradation. *Reliability Engineering & System Safety*, 161:53–60, 2017.

[13] I. Soleimanmeigouni, A. Ahmadi, A. Nissen, and X. Xiao. Prediction of railway track geometry defects: a case study. *Structure and Infrastructure Engineering*, 16(7):987–1001, 2020.

[14] N. Alemazkoor, C. J. Ruppert, and H. Meidani. Survival analysis at multiple scales for the modeling of track geometry deterioration. *Proceedings of the Institution of Mechanical Engineers, Part F: Journal of Rail and Rapid Transit*, 232(3):842–850, 2018.

[15] N. R. Pedanekar. Methods for aligning measured data taken from specific tail track sections of a rail road with the correct geographic location of the sections, 2005. (Patent No. US205/080569A1), United States Patent Application Publication.

[16] Bentley. Railway maintenance decision support system, [updated 2009; cited 2022 Feb 9]. Available online at `https://prod-bentleycdn.azureedge.net/-/media/files/documents/product-data-sheet/pds_optram_ltr_en_hr.pdf?la=ru-ru&modified=20170711101520`.

[17] P. Xu, R. Liu, Q. Sun, and L. Jiang. Dynamic-time-warping-based measurement data alignment model for condition-based railroad track maintenance. *IEEE Transactions on Intelligent Transportation Systems*, 16(2):799–812, 2015.

[18] J. W. Palese, A. M. Zarembski, and N. O. Attoh-Okine. Methods for aligning near-continuous railway track inspection data. *Proceedings of the Institution of Mechanical Engineers, Part F: Journal of Rail and Rapid Transit*, 237(7):709–721, 2020.

[19] Y. Wang, P. Wang, X. Wang, and X. Liu. Position synchronization for track geometry inspection data via big-data fusion and incremental learning. *Transportation Research Part C: Emerging Technologies*, 93:544–565, August 2018.

[20] *Modeling Track Geometry Degradation Using Support Vector Machine Technique. Proceedings of the 2016 ASME/IEEE Joint Rail Conference*, Columbia, SC, 2016 Apr 12–15 2016.

[21] A. Eiken. Analysis of alignment methods for railway track geometry measurements. des 2021. Personalization project, not available online.

[22] A.F. Vikesland. Track geometry degradation cause identification and trend analysis. May 2019. NTNU, Master thesis.

[23] E. Berggren. *Dynamic track stiffness measurement: a new tool for condition monitoring of track substructure.* PhD thesis, KTH, Aeronautical and Vehicle Engineering, Stockholm,Sweden, 2005.

[24] H. Khajehei, A. Ahmadi, I. Soleimanmeigouni, M. Haddadzade, A. Nissen, and M.J.L. Jebelli. Prediction of track geometry degradation using artificial neural network: a case study. *International Journal of Rail Transportation*, 10(1), 2022.

[25] Civil Engineering Conference, editor. *Maintenance of track gauge guidelines*, volume 1. Heron Press, Birmingham, England, 2001.

[26] T.X. Wu and M.J. Brennan. Basic analytical study of pantograph-catenary system dynamics. *Vehicle System Dynamics*, 30(6):443–456, 1998.

[27] A. Lau. Compendium TBA4225 Railway Engineering, Basic course. 2022.

[28] T.N. Vu and K. Laukens. Getting your peaks in line: A review of alignment methods for NMR spectral data. *Metabolites*, 3(2):259–276, April 2013.

[29] T.R. Derrick and J.M. Thomas. *Time Series Analysis: the Cross-Correlation Function. In: Innovative Analyses of Human Movement. Stergiou, N.*, chapter 7, pages 189–205. Human Kinetics, Champaign, Illinois, 2004.

[30] J.W.H. Wong, C. Durante, and H.M. Cartwright. Application of fast fourier transform cross-correlation for the alignment of large chromatographic and spectral datasets. *Analytical Chemistry*, 77(17):5655–5661, August 2005.

[31] R. Korifi, Y.L. Dréau, and N. Dupuy. Comparative study of the alignment method on experimental and simulated chromatographic data. *Journal of Separation Science*, 37(22):3276–3291, November 2014.

[32] H.J. Ramaker, E.N.M. van Sprang, J.A. Westerhuis, and A.K. Smilde. Dynamic time warping of spectroscopic batch data. *Analytica Chimica Acta*, 498(1):133–153, November 15 2003.

[33] H. Sakoe and S. Chiba. Dynamic programming algorithm optimization for spoken word recognition. *IEEE Transactions on Acoustics, Speech, and Signal Processing*, 26(1):43–49, 1978.

[34] M. Huang, N.D. Shah, and L. Yao. Evaluating global and local sequence alignment methods for comparing patient medical records. *BMC Medical Informatics and Decision Making*, 19(263), December 19 2019.

[35] N.P.V. Nielsen, J.M. Carstensen, and J. Smedsgaard. Aligning of single and multiple wavelength chromatographic profiles for chemometric data analysis using correlation optimised warping. *Journal of Chromatography A*, 805:17–35, 1998.

[36] K.M. Pierce, J.L. Hope, K.J. Johnson, B.W. Wright, and R.E. Synovec. Classification of gasoline data obtained by gas chromatography using a piecewise alignment algorithm combined with feature selection and principal component analysis. *Journal of Chromatography A*, 1096(1):101–110, November 25 2005.

[37] P.H.C. Eilers. Parametric time warping. *Analytical Chemistry*, 76(2):404–411, 2004.

[38] W. Wu, M. Daszykowski, B. Walczak, B.C. Sweatman, Connor S.C., Haselden J.N., Crowther D.J., Gill R.W., and Lutz M.W. Peak alignment of urine NMR spectra using fuzzy warping. *Journal of Chemical Information and Modeling*, 46(2):863–875, 2006.

[39] P. Xu, Q. Sun, R. Liu, R.R. Souleyrette, and F. Wang. Optimizing the alignment of inspection data from track geometry cars. *Computer-aided civil and infrastructure engineering*, 30:19–35, 2014.

[40] B. Hoff, D.F.B. Koren, J.R. Pedersen, J. Bunes, and O.J.F. Bynke, M .and Martinsen. Utilizing measurement cart data for predictive maintenance [Å bruke målevogndata for prediktivt vedlikehold]. Norwegian, 2021.

[41] T. Skov, F.V.D. Berg, G. Tomasi, and Bro R. Automated alignment of chromatographic data. *Journal of Chemometrics*, 20:484–497, 2006.

[42] G.F. Giskeødegård, T.G. Bloemberg, G. Postma, B. Sitter, M.B. Tessem, I. S. Gribbestad, T.F. Bathen, and L.M.C. Buydens. Alignment of high resolution magic angle spinning magnetic resonance spectra using warping methods. *Analytica Chimica Acta*, 683:1–11, December 2012.

[43] W. Jiang, Z.M. Zhang, Y. Yun, D.J. Zhan, Y.B. Zheng, Y.Z. Liang, Z.Y. Yang, and L. Yu. Comparisons of five algorithms for chromatogram alignment. *Chromatographia*, 76:1067–1078, July 25 2013.

[44] T.G. Bloemberg, J. Gerretzen, A. Lunshof, R. Wehrens, and L.M.C. Buydens. Warping methods for spectroscopic and chromatographic signalalignment: A tutorial. *Analytica Chimica Acta*, 781:14–32, June 5 2013.

[45] B. Hofmann-Wellenhof, H. Lichtenegger, and E. Wasle. *GNSS - Global Navigation Satellite Systems: GPS, GLONASS, Galileo, and more.* SpringerWienNewYork, Vienna, Austria, 2008.

[46] E.D. Kaplan and C.J. Hegarty. *Understanding GPS/GNSS: Principles and applications*, volume 3. Artech House, Norwood, MA, 2017.

[47] J. A. Slater and S. Malys. *WGS 84-Past in Present and Future in Advances in Positioning and Reference Frames*, pages 1–7. Springer, 1998.

[48] T. Monawar, S. B. Mahmud, and A. Hira. Anti-theft vehicle tracking and regaining system with automatic police notifying using haversine formula. *International Conference on Advances in Electrical Engineering*, 4, September 2017.

[49] N.R. Chopde and M.K. Nichat. Landmark based shortest path detection by using a* and haversine formula. *International Journal of Innovative Research in Computer and Communication Engineering*, 1, April 2013.

[50] K. Yeom. Kinematic and dynamic controller design for autonomous driving of car-like mobile robot. *International Journal of Mechanical Engineering and Robotics Research*, 9(7), July 2020.

[51] J. Lewitowicz, S. Michalak, A. Szelmanowski, K. Sajda, Z. Jakielaszek, and P. Rogala. Selected aspects of implementing the requirements of wgs-84 standard in land navigation for precise determination of a railway vehicle route. *European Navigation Conference (ENC)*, pages 1–10, 2019.

[52] O.G. Esenbuga, C. Emre, B. Varol, and B. Erol. Comparison of principal geodetic distance calculation methods for automated province assignment in turkey. *International Multidisciplinary Scientific GeoConference SGEM2016*, June 2016.

[53] M. Kennedy. *Equirectangular in Understanding Map Projections*, chapter 4, page 61. Environmental Systems Research Institute, Inc., 1994.

[54] W. Gellert, S. Gottwald, M. Hellwich, H. Kästner, and H. Künstner. *Spherical Trigonometry in VNR Concise Encyclopedia of Mathematics*, volume 2, chapter 12, pages 261–282. Van Nostrand Reinhold, New York, 1989.

[55] M. A. Hoque, X. Hong, and B. Dixon. Analysis of mobility patterns for urban taxi cabs. *International Conference on Computing, Networking and Communications (ICNC)*, pages 756–760, 2012.

[56] T. Narock, V. Yoon, and S. March. A provenance-based approach to semantic web service description and discovery. *Decision Support Systems*, 64:90–99, 2014.

[57] S. Dabiri and K. Heaslip. Inferring transportation modes from gps trajectories using a convolutional neural network. *Transportation Research Part C: Emerging Technologies*, 86:360–371, January 2018.

[58] E.F. Burkholder. *The 3-D global spatial data model : foundation of the spatial data infrastructure*. CRC Press/Taylor & Francis, Boca Raton, 2008.

[59] J. Han, J. Kamber, and J. Pei. *Data Mining: Concepts and Techniques*. Elsevier Inc, Waltham, USA, 3 edition, 2012.

[60] S. Kappal. Data Normalization using Median & Median Absolute Deviation (MMAD) based Z-Score for Robust Predictions vs. Min – Max Normalization. *London Journal of Research in Science: Natural and Formal*, 19(4), 2019.

[61] J.K. Steffensen. *Interpolation*. Dover Publications Inc, New York, USA, 2 edition, 2006.

[62] C.K. Chan, W.P. Loh, and I. Abd Rahim. Data Elimination cum Interpolation for Imputation: A Robust Preprocessing Concept for Human Motion Data. *Procedia - Social and Behavioral Sciences*, 91:140–149, oct 2013.

[63] P. Xu, Q. Sun, R. Liu, and R.R. Souleyrette. Optimal match method for milepoint postprocessing of track condition data from subway track geometry cars. *Journal of Transportation Engineering*, 142(8), August 2016.

[64] I. Soleimanmeigouni, A. Ahmadi, I.A. Khouy, and C. Letot. Evaluation of the effect of tamping on the track geometry condition: A case study. *Proceedings of the Institution of Mechanical Engineers, Part F: Journal of Rail and Rapid Transit*, 232(2):408–420, February 2018.

[65] A.R. Andrade and P.F. Teixeira. Statistical modelling of railway track geometry degradation using hierarchical bayesian models. *Reliability Engineering & System Safety*, 142:169–183, October 2015.

[66] Track layout/Track geometry [Sporets trasé/sporgeometri], [updated 2021 Apr 15; cited 2022 May 18]. Available online at `https://www.jernbanekompetanse.no/wiki/Sporets_trase/Sporgeometri`. Norwegian.

[67] P. Virtanen, R. Gommers, T. E. Oliphant, M. Haberland, T. Reddy, D. Cournapeau, E. Burovski, P. Peterson, W. Weckesser, J. Bright, S. J. van der Walt, M. Brett, J. Wilson, K. J. Millman, N. Mayorov, A. R. J. Nelson, E. Jones, R. Kern, E. Larson, C. J. Carey, I. Polat, Y. Feng, E. W. Moore, J. VanderPlas, D. Laxalde, J. Perktold, R. Cimrman, I. Henriksen, E. A. Quintero, C. R. Harris, A. M. Archibald, A. H. Ribeiro, F. Pedregosa, P. van Mulbregt, and SciPy 1.0 Contributors. SciPy 1.0: Fundamental Algorithms for Scientific Computing in Python. *Nature Methods*, 17:261–272, 2020.

[68] University of New South Wales [Internet]. *SpecAlign - processing and alignment of spectral datasets*, [updated 2021; cited 2022 Mar 12]. Available online at `https://powcs.med.unsw.edu.au/research/adult-cancer-program/services-resources/specalign`.

[69] G. Tomasi, F.W.J. Berg, and C.A. Andersson. Correlation optimized warping and dynamic time warping as preprocessing methods for chromatographic data. *Journal of Journal of Chemometrics*, 18(5):231–241, May 2004.

[70] Dynamic time warping (dtw) and correlation optimized warping (cow), [cited 2022 Mar 12]. Available online at `http://www.models.life.ku.dk/DTW_COW`.

[71] D. Potere. Horizontal positional accuracy of google earth's high-resolution imagery archive. *Sensors*, 8(12):7973–7981, 2008.

A. Appendix

A.1. Limits specifying track class and allowed deviation

Table A.1.: Defect limits for deviation in longitudinal level for each rail, relative to allowed speed (adapted based on [3]).

Quality class	Speed (km/h)	Unevenness in longitudinal level for each rail (mm)			
		New track	Alert limit	Intervention limit	Immediate action limit
K0	145-	+/-2	+/-6	+/-9	+/-16
K1	125-140	+/-2	+/-6	+/-10	+/-23
K2	105-120	+/-2	+/-7	+/-12	+/-26
K3	75-100	+/-4	+/-10	+/-16	+/-26
K4	45-70	+/-5	+/-13	+/-21	+/-28
K5	-40	+/-6	+/-17	+/-27	+/-28

Table A.2.: Defect limits for deviation in gauge relative to allowed speed (adapted based on [3]).

Quality class	Speed (km/h)	Deviation in gauge (mm)			
		New track	Alert limit	Intervention limit	Immediate action limit
K0	145-	+4/-0	+5/-3	+15/-5	+28/-7
K1	125-140	+4/-0	+7/-3	+20/-5	+35/-8
K2	105-120	+4/-0	+7/-3	+20/-5	+35/-9
K3	75-100	+4/-3	+15/-5	+30/-8	+35/-9
K4	45-70	+4/-4	+15/-5	+30/-8	+35/-9
K5	-40	+5/-5	+15/-5	+30/-8	+35/-9

Table A.3.: Defect limits for deviation in gauge over a 10 meter track section relative to allowed speed (adapted based on [3]).

Quality class	Speed (km/h)	Deviation in gauge over 10 meters (mm)	
		Alert limit	Intervention limit
K0	145-	+/-7	+/-10
K1	125-140	+/-8	+/-12
K2	105-120	+/-9	+/-15
K3	75-100	+/-10	+/-18
K4	45-70	+/-12	+/-21
K5	-40	+/-15	+/-25

Table A.4.: Defect limits for unintended deviation in cross-level relative to allowed speed (adapted based on [3]).

Quality class	Speed (km/h)	Deviation in cross-level (mm)		
		New track	Alert limit	Intervention limit
K0	145-	+/- 2	+/- 4	+/- 6
K1	125-140	+/- 2	+/- 4	+/- 7
K2	105-120	+/- 2	+/- 5	+/- 8
K3	75-100	+/- 3	+/- 7	+/- 10
K4	45-70	+/- 4	+/- 10	+/- 13
K5	-40	+/- 5	+/- 12	+/- 16

Table A.5.: Defect limits for deviation in twist over 2 meter measure basis (adapted based on [3]).

Quality class	Speed (km/h)	Deviation in twist over 2 meter measure basis (mm)				
		New track	Alert limit	Intervention limit	Immediate action limit	
					R $\geq$ 400m	R < 400m
K0	145-	+/- 2	+/- 7	+/- 10	14	12
K1	125-140	+/- 2	+/- 7	+/- 10	14	12
K2	105-120	+/- 2	+/- 7	+/- 10	14	12
K3	75-100	+/- 3	+/- 7	+/- 10	14	12
K4	45-70	+/- 4	+/- 7	+/- 10	14	12
K5	-40	+/- 5	+/- 7	+/- 10	14	12

Table A.6.: Defect limits for deviation in twist over 9 meter measure basis (adapted based on [3]).

Quality class	Speed (km/h)	Deviation in twist over 9 meter measure basis (mm)				
		New track	Alert limit	Intervention limit	Immediate action limit	
					R $\geq$ 400m	R < 400m
K0	145-	+/- 6	+/- 24	+/- 31	43	34
K1	125-140	+/- 6	+/- 24	+/- 31	43	34
K2	105-120	+/- 6	+/- 24	+/- 31	43	34
K3	75-100	+/- 9	+/- 24	+/- 31	43	34
K4	45-70	+/- 12	+/- 24	+/- 31	43	34
K5	-40	+/- 15	+/- 24	+/- 31	43	34

A.2. Non-incremental position updates

Table A.7 details all manual position updates conducted on the utilized data set.

Table A.7.: Manual position corrections during measurements recording.

Year	Season	Position of correction	Length of correction, in meters	Direction of correction
2020	Autumn	505.0000	17.0	Forwards
2020	Autumn	510.0000	1.0	Forwards
2020	Autumn	523.0000	9.0	Forwards
2020	Autumn	530.0000	14.5	Forwards
2020	Autumn	540.0000	17.0	Forwards
2020	Autumn	552.8445	1	Backwards
2020	Spring	502.0000	3.0	Backwards
2020	Spring	510.0000	18.0	Forwards
2020	Spring	520.0000	18.0	Forwards
2020	Spring	530.0000	5.0	Forwards
2020	Spring	540.0000	23.5	Forwards
2020	Spring	550.0000	24.0	Forwards
2019	Autumn	513.9430	57.5	Backwards
2019	Autumn	551.9935	7.0	Backwards
2019	Spring	510.0000	3.5	Forwards
2018	Autumn	501.0000	14.5	Forwards
2018	Autumn	510.0000	15.5	Backwards
2018	Spring	508.0000	48.0	Backwards
2017	Autumn	551.9575	43.0	Backwards
2017	Spring	502.0000	14.0	Forwards
2017	Spring	524.0000	36.5	Forwards
2017	Spring	545.0000	21.5	Forwards
2016	Autumn	503.0000	15.5	Forwards
2016	Autumn	539.0000	49.0	Backwards
2016	Autumn	550.0000	9.0	Backwards
2016	Spring	504.0000	12.0	Forwards

Anne Willkommen Eiken

Position Alignment and Geographical Location Determination of Railway Track Condition Monitoring Data

NTNU
Norwegian University of
Science and Technology